INFORMATION TO USERS

This manuscript has been reproduced from the microfilm master. UMI films the text directly from the original or copy submitted. Thus, some thesis and dissertation copies are in typewriter face, while others may be from any type of computer printer.

The quality of this reproduction is dependent upon the quality of the copy submitted. Broken or indistinct print, colored or poor quality illustrations and photographs, print bleedthrough, substandard margins, and improper alignment can adversely affect reproduction.

In the unlikely event that the author did not send UMI a complete manuscript and there are missing pages, these will be noted. Also, if unauthorized copyright material had to be removed, a note will indicate the deletion.

Oversize materials (e.g., maps, drawings, charts) are reproduced by sectioning the original, beginning at the upper left-hand corner and continuing from left to right in equal sections with small overlaps.

ProQuest Information and Learning
300 North Zeeb Road, Ann Arbor, MI 48106-1346 USA
800-521-0600

DETERMINATION OF THE OPTICAL PROPERTIES OF TWO-LAYER TURBID MEDIA FROM SPATIALLY RESOLVED REFLECTANCE MEASUREMENTS IN THE FREQUENCY DOMAIN

by

GEORGE ALEXANDRAKIS , M.Sc., B.Sc. Hon.

A Thesis

Submitted to the School of Graduate Studies

in Partial Fulfilment of the Requirements

for the Degree

Doctor of Philosophy

McMaster University

DETERMINATION OF TWO-LAYER TURBID MEDIA OPTICAL PROPERTIES

DOCTOR OF PHILOSOPHY (2000) McMaster University

(Medical Physics) Hamilton, Ontario

TITLE: Determination of the Optical Properties of Two-Layer Turbid Media from Spatially Resolved Reflectance Measurements in the Frequency Domain

AUTHOR: GEORGE ALEXANDRAKIS , M.Sc. (McMaster University)

SUPERVISOR: Professor M.S. Patterson

NUMBER OF PAGES: xii, 181

to my parents

Acknowledgements

I am thankful to McMaster University for allowing me the possibility of pursuing my doctoral research in affiliation with the Hamilton Regional Cancer Center (HRCC).

I am grateful to my supervisor Dr. Michael Patterson and to Dr. Thomas Farrell for their guidance and support throughout my doctoral work. Their mentorship has helped me become an independent thinker and also establish a firm footing in the field of biomedical optics. My supervisor's generosity has allowed me to attend and present my work at several international conferences. I owe most of my knowledge of radiation physics to Dr. William Prestwich whose insights have improved the quality of my thesis work.

I feel very fortunate to have established a collaboration with Dr. Gregory Faris of SRI International. His exceptional experimental skills and the hard work of his year 2000 summer student, David Busch, have contributed towards elucidating the practical feasibility and some limitations of the methods explored in my thesis work. Experimental work at HRCC could not have been done without the untiring help and advice by Jody Bruulsema, the diligent work of Jeff Carter, and the animal handling expertise of Eric Seidlitz. Technical support from Alan Hazelhurst and William Olson, of the HRCC and SRI International machine shops respectively, was critical to the successful completion of my experimental work. I could not be forgiven if I forgot to thank the secretaries at HRCC, Donna Laking and Karen Dougherty, for helping me fight through paperwork and bureaucracy innumerable times and also for being caring towards all students. I should also thank my fellow graduate students who have made my work environment pleasant and stimulating. At the risk of forgetting some: Rob Hunter, Markus Hermann, Kevin Diamond, Jonathan Dysart, and Dragana Stasic.

During the six years of my stay in Hamilton I've had the good fortune of making some good friends with whom I've had a multitude of interesting discussions on and

off science. The names of Alwin Kienle, Gordon Chan, Marcel Marcu, Jose Brito, and Thanassis Kassidas are foremost in my mind. I don't have enough words to thank Marie-Claude Asselin for untold psychological support, and for pushing me to expand my horizons geographically, culturally, and scientifically. Finally, I am indebted to my family who have always been there for me.

Abstract

Quantification of the optical properties of superficial biological tissue (e.g. skin on muscle) from spatially resolved reflectance measurements can yield important physiological information. Some examples include the non-invasive measurement of chemotherapy drugs or exogenous chromophores used for photodynamic cancer treatment and the assessment of hemoglobin oxygenation in tissue. Superficial tissue is a multilayered structure with each component having different macroscopic absorption and scattering coefficients, as well as different vascularization and exogenous chromophore pharmacokinetics. A layered model of photon transport is therefore required to match theoretical predictions with experimental measurements. Once a photon transport model is developed, it defines the forward calculation used in the inverse problem of determining the set of tissue optical properties that gives the best fit to experimental data. In the present work the frequency domain (FD) method is employed to probe a two-layer turbid medium. The goal is to improve quantification of superficial tissue optical properties relative to current methods assuming tissue homogeneity.

Chapter 2 introduces simulated annealing as a robust method of exploring the

limits of a two-layer pure diffusion model in determining the optical properties of a two-layer turbid medium. The inadequacies of pure diffusive transport lead to inaccurate optical property estimates for the top layer. To improve on these estimates a hybrid Monte Carlo (MC) - diffusion model for FD photon transport was developed and presented in Chapter 3. The hybrid model was shown to accurately model MC simulated reflectance data for all optical properties in the physiological range. In Chapter 4 an efficient hybrid simplex - simulated annealing global optimization algorithm was introduced to demonstrate that the hybrid transport model can, in principle, accurately determine all optical properties of a two-layer turbid medium. The practical feasibility of the method was tested with high accuracy FD experimental measurements. Some preliminary results and future directions towards the *in vivo* implementation of the method are discussed.

Contents

List of Figures

Chapter 1

Introduction

The interaction of light with biological tissue can yield important information about its structure and physiological function. Tissue is not transparent to light in the optical and near-infrared wavelength ranges, but rather is a turbid medium. Physically this means that incident light is multiply scattered and absorbed as it travels through tissue. The fraction of light that escapes from the tissue surface as diffuse reflectance carries diagnostic information about the tissue volume through which it has traveled. Light transport in tissue is characterized by the macroscopic scattering (μ_s) and absorption (μ_a) interaction coefficients, which will be referred to as the tissue optical properties. The former is the probability per unit length of an elastic scattering interaction caused by microscopic variations in refractive index of cellular components. The latter is the probability per unit length of a photon being totally absorbed. Scattering can give information about tissue structure and

may help quantify tissue glucose concentration *in vivo*[1]. Quantification of absorption changes resulting from exogenous chromophores can find applications in many pharmacokinetic studies[2] and is an essential part of photodynamic therapy (PDT) dosimetry for the treatment of cancer[3, 4]. Another important application is the *in vivo* assessment of the oxygenation status of tissue[5, 6]. Simultaneous determination of (μ_s) and (μ_a) can also provide knowledge of the light fluence distribution in tissue which is required for PDT and other therapeutic applications of light.

Physiologically, superficial tissue is a layered structure [7]. Each layer has a different structural composition, level of blood perfusion and, possibly, specific chromophores (e.g. melanin). The implications of these variations on the development of models for light transport through tissue can be illustrated by considering the case where light is used to probe the pharmocokinetics of an exogenous chromophore. Different tissue layers would scatter differently, which would also affect the amount of time photons spend in each layer. Differences in blood perfusion and chromophore tissue retention would result in different pharmacokinetics in each layer and therefore, to variable amounts of light absorption. Hence, a theoretical model of light transport that explicitly takes into account the layered nature of superficial tissue is required to best match experimental measurements of the spatio-temporal distribution of photons escaping tissue. It is also clear that absorption and scattering are intricately related in the light transport process.

Much work in the last two decades has been devoted on modeling light

transport[8, 9, 10] and determining the optical properties of tissue[12], by assuming it to be a homogeneous semi-infinite medium. Clearly, the optical property values obtained in this manner are some kind of "average" of those for the different layers and depend on the tissue volume probed. Such estimates are therefore biased and preclude accurate quantification of the true tissue optical properties. On the other hand, the field of optical tomography that has emerged in recent years[13] offers the promise of recovering quantitative optical property maps as a function of depth from the tissue's surface with a spatial resolution of a few millimeters (mm). Though the practical implementation of such a method is one of the ultimate goals of optical imaging, the deduction of optical property maps from surface measurements only is a severely ill-posed problem[14]. It thus remains to be seen whether optical tomography will become a quantitative method.

In this thesis a crude two-layer model of tissue structure is assumed, where a thin layer of skin lies on top of a homogeneous semi-infinite medium that can be fat or muscle. Hence in the context of the present work, the problem of deducing the optical properties of superficial tissue is reduced to determining the optical properties of an idealized two-layer turbid medium. The assumption of a two-layer geometry aims at reducing the biases in the estimates of the true optical properties introduced by assuming a semi-infinite geometry. At the same time, the question of whether one can obtain quantitative estimates for all optical properties characterizing an ideal two-layer medium can be addressed. The process of determining the optical properties of

a two-layer turbid medium, as for any medium geometry, has two components; the forward problem and the inverse one.

The forward problem consists of developing a light transport model that accurately simulates the interaction of light with tissue. The information that the model provides comes in the form of spatially resolved reflectance. This is defined as the fraction of incident photons that escapes the medium, per unit area as a function of distance **r** from the point of incidence of the beam. For a vertically incident beam on a sideways infinite medium, as is the case for the semi-infinite and two-layer geometries, spatially resolved reflectance is cylindrically symmetric and thus defined in terms of a radial coordinate ρ. There exist three different ways of interrogating a tissue volume depending on the temporal profile of the incident beam:

(i) Continuous Wave (CW): The incident light intensity is invariant with respect to time. Thus, the only experimental data type obtained with this method is the steady-state spatially resolved reflectance ($R_{DC}(\rho)$).

(ii) Frequency Domain (FD): The incident beam is intensity modulated sinusoidally in time at a circular frequency ω. The average time that photons spend in tissue before exiting at a distance ρ results in a phase delay with respect to the incident beam. Hence, the two experimental data types that the FD method offers are the amplitude of the spatially resolved reflectance ($R_{AC}(\omega, \rho)$), and the phase delay ($\phi(\omega, \rho)$).

(iii) Time Domain (TD): A train of pulses (usually fempto- or picoseconds in duration) defines the incident beam. Multiple scattering and absorption distort each pulse whose exit fraction as a function of time delay can be measured at different ρ and define the spatio-temporally resolved reflectance amplitude $R(t, \rho)$.

In this work the FD method of interrogating tissue is utilized. The TD and FD techniques yield are related to each other by means of a Fourier transform in time.

The inverse problem consists of finding the combination of tissue optical properties that minimizes the difference between the forward model predictions and the experimental measurements in a least-squares sense. The process usually involves iterative evaluations of the forward model with the optical properties used in each iteration being updated according to a particular parameter search startegy until some predefined search termination criteria have been met.

Given the above considerations, the light transport simulation techniques utilized in the forward model 1.1, as well as the optical property estimation techniques utilized in the inverse problem 1.2, merit some detailed discussion.

1.1 Models of light transport in tissue

1.1.1 Stochastic models

In the stochastic approach photon migration is modelled by brute force simulation of the photon histories (Monte Carlo), or by calculating transition or passage probabilities for a photon through a space-time point in tissue (Random walk, Markov model).

1.1.1.1 Monte Carlo (MC)

The basis of the method is the explicit simulation of the histories of photons as they travel through, and possibly exit, tissue. The method can, within stochastic limits, give exact predictions of spatially resolved reflectance for all source-detector distances and tissue geometries. It can also provide information about aspects of photon migration inside tissue that are not measurable experimentally from the surface. The only prerequisite is the accurate knowledge of tissue geometry and the probability distribution functions (PDFs) for all relevant photon interactions. The latter could be scattering and its angular dependence, absorption, specular reflection at boundaries etc. Each of these PDFs, defined as the indefinite integral $F(y) = \int^y p(y')\,\mathrm{d}y'$ of the corresponding probability density function $p(y)$, is sampled in an unbiased manner by a uniform deviate x in $[0, 1)$. The key to sampling a PDF is the one to one correspondence between a value of x and $F(y)$, because $\int_{-\infty}^{\infty} p(y)\,\mathrm{d}y = 1$. For any interaction

a random number generator provides a value of x which is equal to the fraction of area under the probability curve $F(y)$, which in turn corresponds to a unique value for y[15].

As the sampling of PDFs and the corresponding evolution of a photon history is statistical in nature, a large number of photon histories needs to be tracked in order to obtain precise estimates of spatially resolved reflectance and other photon migration attributes of interest. The resulting computational burden of MCs renders them impractical as the forward model in an iterative optical property estimation regime. On the other hand, a MC simulation run for a large number of photon histories can provide 'gold standard' synthetic data sets. These can be used to test the validity of predictions of other more computationally efficient, but approximate forward models. Since the optical properties with which the MC data sets were created are known *a priori* the performance of different optical property search strategies can be assesed. Also, the "ideal" nature of MC data can help identify potential problems associated with real physical measurements.

1.1.1.2 Random walk models

Photons are constrained to move on a cubic lattice with equal probability of visiting any of their nearest neighbours, and those neighbours only. The lattice spacing is inversely proportional to μ_s for the medium. At each lattice site visited, each photon loses a fraction of its weight which is proportional to μ_a. Expressions for the average

photon visit probability at any lattice point and the spatially resolved reflectance have been derived for the semi-infinite[16] and two-layer[17] geometries. Though this model provides an accurate description of multiply scattered light, its inherent limitation in incorporating anisotropic transport and the difficulty of its generalization to more complicated geometries have limited its widespread use.

1.1.1.3 Markov models

This is a generalized method of computing the stochastic transition probabilities of photons travelling on a grid of uniform spacing, simulating the tissue medium[18]. Though this approach provides exact photon escape probabilities at the grid boundary, its inability to incorporate noisy data and anisotropy in tissue geometry and photon transport limits its practical utility.

1.1.2 Deterministic models

At the core of all deterministic models for photon transport is the bookkeeping task of accounting for all photons passing through, interacting, or being created within a given volume element of tissue. This is formally expressed as the Boltzmann equation, which is a continuum model ignoring the wave nature of light. Of the many notations with which it has appeared in the literature, the most pertinent form to the current work is[8]:

$$\frac{1}{c}\frac{\partial I}{\partial t} + \hat{\mathbf{s}} \cdot \nabla I(\mathbf{r}, t, \hat{\mathbf{s}}) + (\mu_a + \mu_s) I(\mathbf{r}, t, \hat{\mathbf{s}})$$
$$= \mu_s \int_{4\pi} f(\hat{\mathbf{s}}, \hat{\mathbf{s}}') I(\mathbf{r}, t, \hat{\mathbf{s}}') \mathrm{d}^2\hat{\mathbf{s}}' + q(\mathbf{r}, t, \hat{\mathbf{s}}) \quad (1.1)$$

where c is the speed of light in the medium and $I(\mathbf{r}, t, \hat{\mathbf{s}})$, in units of W/m^2sr describes the radiance in position $\mathbf{r}$, time t, and direction $\hat{\mathbf{s}}$. The scattering and absorption coefficients, μ_s and μ_a, are the inverse mean free paths for each of these interactions to occur. The function $f(\hat{\mathbf{s}}, \hat{\mathbf{s}}')$ is known as the scattering phase function and describes the probability of a photon moving in direction $\hat{\mathbf{s}}'$ to be scattered into direction $\hat{\mathbf{s}}$. The photon source $q(\mathbf{r}, t, \hat{\mathbf{s}})$ defines the nature of the time dependence of the solution $I(\mathbf{r}, t, \hat{\mathbf{s}})$ to eq.(1.1). The existence of the scattering integral, expressing the multiply scattered nature of light transport, creates computational difficulties. Numerous approximations to eq.(1.1) have thus been attempted to make the problem more tractable. First and foremost among these has been the diffusion approximation.

1.1.2.1 The diffusion equation and the P_1 approximation

All directionally dependent terms in eq.(1.1) can be expanded in terms of spherical harmonics, which are defined as an orthogonal set involving increasing orders ℓ of Legendre polynomials P_ℓ. In the P_1 approximation only the zeroth and first order ($\ell = 0, 1$) terms of that expansion are retained which represent the isotropic and dipole-like

anisotropic components respectively. One can then derive the P_1 equation[13]:

$$\frac{1}{c}\frac{\partial\Phi(\mathbf{r},t)}{\partial t} - \nabla\cdot\mathbf{J} + \mu_a(\mathbf{r})\Phi(\mathbf{r},t) = q_0(\mathbf{r},t) \tag{1.2}$$

where Φ is the fluence rate

$$\Phi(\mathbf{r},t) = \int_{4\pi} I(\mathbf{r},t,\hat{\mathbf{s}})\mathrm{d}^2\hat{\mathbf{s}} \tag{1.3}$$

and J is the current

$$\mathbf{J}(\mathbf{r},t) = \int_{4\pi} \hat{\mathbf{s}} I(\mathbf{r},t,\hat{\mathbf{s}})\mathrm{d}^2\hat{\mathbf{s}} \tag{1.4}$$

To get to eq.(1.2) from eq.(1.1) an expansion of I and $f(\hat{\mathbf{s}},\hat{\mathbf{s}}')$ to first order and q to zeroth order was implemented, and the temporal variation of J was ignored[13]. It can be shown that the latter can be equivalently expressed as[12]:

$$\mathbf{J}(\mathbf{r},t) = -D(\mathbf{r})\nabla\Phi(\mathbf{r},t) \tag{1.5}$$

which is known as Fick's law. $D(\mathbf{r})$ is a spatially varying diffusion coefficient that can be defined as:

$$D(\mathbf{r}) = \frac{1}{3((1-g)\mu_s + \mu_a)} \tag{1.6}$$

where g is the average value of the cosine of the angle for a single scatter, as deduced from the first order expansion of $f(\hat{\mathbf{s}},\hat{\mathbf{s}}')$. The appropriate definition of D consistent with eq.(1.1) and the inclusion of μ_a in eq.(1.6) has been a topic of recent debate[19, 20, 21]. It is important to note that in eq.(1.6) the term $\mu_s(1-g)$ appears, which defines an effective isotropic scattering coefficient $\mu_s{}'$. This leads to the concept

of solution similarity, as all media with the same product of μ_s and $(1-g)$ will produce identical reflectance profiles in the P_1 approximation[11]. In the case of FD photon migration the sinusoidal intensity variation of the incident beam at a circular frequency ω, $\exp(i\omega t)$ in complex notation, induces all time dependent quantities in eq.(1.2) to vary at the same frequency. This results in a simplification of eq.(1.2) to an effective time-independent equation with complex coefficients:

$$\nabla \cdot D(\mathbf{r})\nabla\Phi(\mathbf{r},\omega) - (\mu_a(\mathbf{r}) + i\frac{\omega}{c})\Phi(\mathbf{r},\omega) = -q_0(\mathbf{r},\omega) \tag{1.7}$$

where Φ is now a complex quantity.

The simplest geometries used to model diffusive photon migration in tissue are the infinite and semi-infinite. In both geometries μ_a, μ_s and therefore D, are spatially invariant. However, in the semi-infinite case the diffusion solution cannot satisfy exactly the boundary condition (b.c.). For example, in the case of refractive index matched b.c.'s there is no light coming in from outside the tissue boundary other than the incident light. A review paper by Haskell *et al* [12] provides an excellent review of the possible diffusive transport solutions in the infinite and semi-infinite geometries for CW, FD and TD illuminations. In that review, an account of the possible approximations for the b.c. consistent with diffusion and the resulting solutions are presented.

The next more complicated tissue geometry is the two-layer one. For a definition of the two-layer diffusion equation in the FD and its method of solution, the reader is referred to Chapter 2. An account of previous work on two-layer diffusion models in

CW, FD, and TD leading up to the work presented in this thesis is given in Chapter 3.

No matter how simple or complicated a tissue geometry is, a diffusive description of photon transport will inherently not be able to take into account the propagation of ballistic and few scatter, or snake, photons. Another limitation of diffusion is that absorption will always have to be small compared to scattering[8]. In the case of FD photon migration the inverse of the modulation frequency of the incident light will have to be much larger than the time it takes light to travel between two sequential interaction events for diffuse transport to be meaningfull[12]. All of the above shortcomings of diffusion theory limit the amount of information that can be extracted from the interaction of light with tissue using this model. Hence, motivation exists for the development of more accurate approximations to the Boltzmann equation albeit at the cost of increased computational overhead.

1.1.2.2 More accurate approximations to the Boltzmann equation

1.1.2.2.1 The telegrapher's equation and the P_n approximation Going back to the transition from Boltzmann to the diffusion equation, if the first order anisotropy of the source and the time variation of **J** are not ignored, one arrives at the telegrapher's equation[13]. Strictly speaking, this equation is the proper definition of the P_1 approximation. In contrast to eq.(1.2) which predicts a reflectance solution instantaneously after photons have been injected in tissue, the telegrapher's equation does not violate causality. On the other hand, it is a more cumbersome equation to

solve. It has not enjoyed widespread use because of this, and also because, for the high-scattering regimes and modulation frequencies encountered in tissue optics, the differences in reflectance predictions from those of eq.(1.2) are negligible[13].

One can include a larger number of spherical harmonics when expanding the Boltzmann equation in such terms. Keeping the first n harmonics is known as the P_n approximation. The expansion results in a set of n coupled differential equations that can be solved by standard methods[22]. The higher order harmonics offer, in principle, the possibility of modelling the anisotropic transport of photons and overcoming all of the other P_1 limitations mentioned above. However, the scattering of light in tissue is strongly forward peaked, frequently having g-values between 0.9 and 0.96[11]. This makes the number of Legendre polynomials needed in the expansion to model accurately anisotropic light transport very large. This renders the method computationally impractical in most circumstances.

1.1.2.2.2 Path integrals Photons are considered as classical mechanics particles that have a certain collision frequency resulting in a mean deflection in trajectory per collision. The summation over all possible individual photon steps and all possible trajectories in tissue define a path integral[23]. The method is tailored to modelling efficiently the transport of ballistic and snake photons and has given some encouraging results for the semi-infinite tissue geometry[24]. On the downside, the method is mathematically involved and difficult to generalize to more complex tissue geometries.

1.1.2.2.3 Discrete ordinates In a spirit similar to that of the P_n approximation, the Boltzmann equation is expanded to a set of n coupled equations, only this time the radiance $I(\mathbf{r}, t, \hat{\mathbf{s}})$ is discretized in n predetermined directions, or ordinates, $\hat{\mathbf{s}}_\mathbf{n}$. The spatial discretization of the medium defines a grid of volume elements $\mathbf{k}$ through which $I(\mathbf{r}_\mathbf{k}, t, \hat{\mathbf{s}}_\mathbf{n})$ is propagated in a manner dictated by the interaction coefficients of the medium. The multiple scattering of light in tissue results in an iteration of the radiance propagation through all volume elements until its value everywhere has converged to a predetermined tolerance[25]. The method can be as accurate as a MC simulation even in circumstances that the P_1 approximation is inadequate and promises to be one of the future models of choice for optical tomography. The method has so far been developed for CW illumination only[26]. It is computationally expensive though, which makes its current use as the forward model in an iterative optical property estimation algorithm impractical.

1.1.3 Hybrid stochastic-deterministic models

The idea of using a restricted MC simulation to compensate for the inadequacy of diffusion at short source-detector distances has existed for some time[27]. Wang and Jacques were the first to propose a model that naturally incorporates the accuracy of MC close to the source with the computational efficiency of diffusion at larger distances[28]. The essence of their model is the definition of a critical depth $z_c = 1/(\mu_s' + \mu_a)$ inside the medium. Above z_c photon transport is modelled by MC, but

below it photons are assumed to have become isotropic sources and their locations are scored on a predefined grid. Multiple photon histories thus define a distributed photon source below z_c that is further propagated by the diffusion solution for the appropriate geometry. They reported that for a semi-infinite medium and CW illumination the hybrid model was approximately 7 times faster than pure MC and within 6% of the latter. A corresponding model for a slab geometry was subsequently reported[29]. Chapter 3 is devoted to the expansion of the above idea to the two-layer geometry and FD illumination. The reader is referred to that chapter for a detailed description of the model and its method of solution[30].

1.2 Optimization and optical property estimation techniques

Once a forward model of photon migration is developed to model experimental reflectance data, a question arises: What is the appropriate combination of tissue optical property values that the forward model can use to best match experimental data? This question is the gist of the inverse problem and it is one of optimization. As the solution of the forward model has a non-linear dependence on tissue optical properties, the resolution of the inverse problem calls for non-linear optimization methods. A large variety of such methods exists in the literature, but each is appropriate for solving efficiently a specific type of inverse problem. A review of opti-

mization methods used in optical tomography is given in ref.[13]. Only the methods appropriate to determining tissue optical properties for a two-layer geometry will be briefly discussed here. In all cases, the object function to be minimized was χ^2. If there are $i = 1, N$ reflectamce measurements y_i, each with standard deviation σ_i, and corresponding model-based relectance calculations yc_i then χ^2 is defined as:

$$\chi^2 = \sum_{i=1}^{N} \frac{(y_i - yc_i)^2}{\sigma_i^2} \tag{1.8}$$

As was the case for the forward models, parameter search methods can be classified as deterministic or stochastic. The former search parameter space with a well-defined predetermined strategy. The latter sample parameter space initially in a random manner, and later focus on promising search areas by keeping a memory of the best parameter sets found in their search history. For deterministic methods the routines' convergence to a global minimum is strongly dependent on the starting, or initial, optical property guesses. Stochastic methods are more robust to recovering an approximate global minimum at the price of substantially increased computational overhead. In all methods the search is terminated within the first few occasions that χ^2 decreases by a small, predetermined tolerance.

1.2.1 A stochastic method

1.2.1.1 Simulated annealing (SA)

The method of SA has proved to be a powerful global optimization tool for a wide variety of problems unrelated to biomedical optics[15, 31]. At the heart of the SA algorithm is the parallel drawn with the cooling of a material from, say, the liquid to its solid state. In the liquid state the molecules move around relatively independent of each other. As the material cools down, molecular motion decreases and the material crystalizes. Slow cooling results in a uniform lattice structure, but rapid cooling results in a more amorphous one. The process of slow cooling is referred to as annealing and the uniform crystal lattice represents the global energy minimum of the system. Rapid cooling results in quenching which is only a local energy minimum for the molecular ensemble.

In the analogy to the SA method, the molecules are the sets of optical properties $\mathbf{a}$ and the current energy E of the system is represented by χ^2. The range of optical property values searched is determined by the maximum possible energy state that can be reached by the molecules at the current temperature T. A random number generator is used to create random changes in the current optical property set $\mathbf{a_{cur}}$ and redefine it as the next set, $\mathbf{a_{next}}$, whose χ^2 value is to be found. One can thus define a Boltzmann-like probability distribution $p(\Delta E)$:

$$p(\Delta E) = \exp\left(\frac{-\Delta E}{T}\right) \tag{1.9}$$

where $\Delta E = E_2 - E_1$ is the difference between the energy (or χ^2) value resulting from the $\mathbf{a_{next}}$ and $\mathbf{a_{cur}}$ forward model evaluations. If $E_2 < E_1$ then $p(\Delta E) > 1$ in which case, the value of $p(\Delta E)$ is redefined to unity and a downhill move in χ^2 space is always accepted. However, an uphill move ($E_2 > E_1$) will also be accepted if the random number generator gives a real number in $[0, 1)$ that is greater than $p(\Delta E)$. Clearly if T is high, $p(\Delta E)$ will be close to zero and many uphill moves will be accepted. This helps the parameter search to escape from local minima. As the temperature cools down, in a predetermined manner called the annealing schedule, essentially all of the allowed moves will be downhill. Hopefully the global minimum has been reached if the search was allowed to anneal slowly. The above method of deciding on uphill or downhill moves in χ^2 space is known as the Metropolis criterion[15]. Simulated annealing can in principle obtain a local minimum in a complicated multi-dimensional χ^2 landscape, which deterministic methods cannot. The downside is the substantially increased number of forward calculations.

1.2.2 Deterministic methods

1.2.2.1 The Marquardt-Levenberg method

To explain the principle of the method it is necessary to introduce the concept of the partial derivative of χ^2 with respect to the set of optical properties $\mathbf{a}$ characterizing the medium. The search for the next optical property set to be tried $\mathbf{a_{next}}$ can be visualized as a vector of a given magnitude in a direction where the simultaneous

incremental change of the elements of the current set $\mathbf{a_{cur}}$ will result in a forward calculation that maximally reduces the current value of χ^2. This is considered to be a downhill move in χ^2 space in the direction of steepest descent and can be formally written as[15]:

$$\mathbf{a_{next}} = \mathbf{a_{cur}} - constant \times \nabla\chi^2(\mathbf{a_{cur}}) \tag{1.10}$$

It is also necessary to introduce the concept of second order partial derivative of χ^2 with respect to the elements of $\mathbf{a_{cur}}$. This is known as the Hessian, or curvature, matrix as it expresses the degree of χ^2 space smoothness in the vicinity of $\chi^2(\mathbf{a_{cur}})$. Once the region of a minimum is found, knowledge of the curvature information accelerates the convergence to a minimum if one is close enough to start with. The inverse of the Hessian matrix is the covariance matrix of the fitted parameters. The Marquardt-Levenberg method searches parameter space by varying smoothly between the methods of inverse Hessian and the steepest descent. The latter method is used far from the minimum, switching continuously to the former as the minimum is approached[15]. The Marquardt-Levenberg method is one of the standards of non-linear least-squares routines.

1.2.2.2 The simplex method

A simplex is a polygon in χ^2 space with each of its vertices corresponding to a particular value of χ^2 resulting from the evaluation of a forward model for given tissue geometry characterized by a set of optical properties a[15]. The dimensionality of the

simplex, or polygon, always exceeds that of **a** by one. For example, in a semi-infinite medium μ_a and μ_s' are the only two fitting parameters defining a two-dimensional χ^2 space. In this case, the simplex is a triangle that can in principle engulf the coordinates of the sought minimum in χ^2 space. The algorithm is deterministic because it systematically goes through a predetermined set of moves to search parameter space. The simplex goes through reflections, expansions, and contractions to reach the nearest local minimum which it finally engulfs to a predetermined tolerance in χ^2 differences among all the vertices. The method does not require calculation of χ^2 derivatives with respect to the elements of **a**, but that makes it less efficient in converging to a minimum compared to Marquardt-Levenberg.

1.2.3 A hybrid stochastic-deterministic method

1.2.3.1 The hybrid simplex-simulated annealing method

The SA method samples discrete points in parameter space. Moreover, its requirement to anneal slowly results in many potentially unnecessary forward calculations in the valley around the eventual minimum found. The number of these evaluations could be reduced if a pure downhill deterministic algorithm became the search method once that valley was reached. These considerations point to the need for a hybrid stochastic-deterministic optimization algorithm. Combining the stochastic and deterministic components seamlessly in a single algorithm is non-trivial. A hybrid simplex-simulated annealing algorithm has been recently proposed to achieve

this task[15]. In this method the vertices of the simplex, as defined in Section 1.2.2.2, are perturbed by thermal fluctuations. For large T each vertex of the simplex moves in a random manner through parameter space. The thermal fluctuations of the vertices are controlled by an annealing schedule, and the decisions on uphill moves are based on the Metropolis criterion. As T cools towards zero the method reduces to the pure downhill moving simplex. In effect, the parameter search can be visualized as a fuzzy polygon roaming through parameter space. Its SA attributes allow its vertices to escape local minima, while its downhill simplex character accelerates the search towards a minimum. The algorithm promises to be as robust, but much more computationally efficient in obtaining a global minimum than pure SA. The hybrid search algorithm's performance as applied to the determination of the optical properties of a two-layer turbid medium from FD data will be presented in Chapter 4.

1.3 Experimental methods

The ultimate purpose of any theoretical model of photon migration is to predict as accurately as possible the experimental measurements for the corresponding tissue geometry and temporal dependence of the incident light illumination. A large variety of techniques have been developed for use in tissue optics and have recently been summarized by Hebden *et al*[32]. Only the experimental methods pertinent to the current work will be discussed here. In all FD measurements the intensity of the light was modulated at a frequency $f = \omega/2\pi = 100MHz$. The light signal thus consisted

of a certain DC baseline signal on which an rf modulation depth was superimposed. Light was both delivered and collected from the surface of the medium being probed with optical fibers. The fibers are vertically imbedded into a flat, rigid piece of black nylon material , to be referred to as a face plate, with their light collection ends flush with the plate's lower surface. The plate filled the space between fibers and absorbed most of the light escaping the medium's surface that was not collected by them. This ensured the uniformity of the boundary condition which was equivalent to a light sink everywhere at the medium's surface. The face plate also stabilized the relative distance between different fibers which helped improve measurement reproducibility. The collected light was focussed into a photomultiplier tube (PMT) which converted it to an electronic signal for subsequent processing. There exist two methods of extracting the modulation amplitude ($R_{AC}(\omega, \rho)$), and the phase delay ($\phi(\omega, \rho)$) from the spatially resolved reflectance measurement signal. They are known as homodyne and heterodyne detection, and both were employed in this work.

In the case of homodyne detection, the measured reflectance is separated into its DC and rf components by a bias tee. The rf component, oscillating at $100MHz$, is then filtered for noise, amplified and demodulated by an I/Q-demodulator. R_{AC} and ϕ can then be deduced from the two quadrature components of the rf signal, I and Q. If higher rf harmonics happen to exist, they will also contribute to the measured signal and will therefore introduce a measurement bias.

In the case of heterodyne detection, the $100MHz$ intensity modulated light is

detected by a PMT whose gain was modulated at $100.0001MHz$. A lock-in amplifier was employed to isolate the measured signal at the beat frequency of $100Hz$. This frequency contains the sought after amplitude and phase delay information. Thus R_{AC} and ϕ can be determined from a signal oscillating at $100Hz$ which is much easier to process electronically than achieving the same thing at $100MHz$. In contrast to homodyning, if higher order harmonics exist they are eliminated from the measured rf signal. Heterodyning results in a somewhat more complicated experimental setup with more components whose performance need to be optimized.

FD measurements were performed on tissue-simulating phantoms and *in vivo*. For a detailed discussion of phantom construction the reader is referred to Chapter 4. For both the semi-infinite and two-layer geometries liquid phantoms were used. The experimental methods employed for *in vivo* measurements on New Zealand rabbits are described in Chapter 5. The technical details of the implementation of the homodyning technique can be found in Chapter 4 and those for the heterodyne method in Chapter 5.

1.4 Thesis Proposal

The diffusion model of light transport in the semi-infinite medium geometry is well understood. Considerable research has been published over the last decade based on this model. The P_1 approximation for CW illumination in the semi-infinite geometry was first applied to tissue optics by Reynolds *et al*[22]. The TD version of the equation

for a pencil incident beam was solved by Patterson *et al*[10]. Shortly after, the same group published the corresponding FD solution[33]. Improved solutions have appeared since[34, 35]. Haskell *et al*[12] have provided a comprehensive review of all solutions to date. The semi-infinite diffusion model has enjoyed widespread use because it affords an analytical solution. This makes it a fast and computationally easy to implement forward model for an iterative fitting algorithm. The fact that there are usually only two unknowns being fitted, μ_a and μ_s', makes the model robust to real world noisy data. As previously discussed, its downside is the inadequate quantitative information it can extract due to the averaging of information obtained over an inhomogeneous tissue volume. To this end, a two-layer model of superficial tissue structure may help improve quantification.

For a brief account of previous work on two-layer medium diffusion models leading up to the work presented in this thesis, the reader is referred to the Introduction section of PaperII presented in Chapter 3. An outline of the thesis contents, including the author's contributions is listed here:

Chapter (ii) (PaperI): The details of the most accurate two-layer diffusion model known at the beginning of this work[36] are presented. The simulated annealing (SA) algorithm was introduced to the field. It was shown to be a more robust global minimum search method for determining the optical properties of a two-layer medium compared to the standard Marquardt-Levenberg method. The use of SA allowed the exploration of the ultimate limits of two-layer diffusion

to determine all the optical properties of a two-layer turbid medium. This was achieved by using two-layer MC simulated data as ideal FD experimental measurements. It was suggested that the inherent limitation of diffusion in describing accurately light transport close to the incident beam limited the accuracy of the optical property estimates, especially for the top layer.

Chapter (iii) (PaperII): Based on the idea initially proposed by Wang and Jacques[28], a FD two-layer MC-diffusion hybrid model was developed. It was shown to give reflectance predictions in good agreement with MC data for both close and far distances from the incident light beam.

Chapter (iv) (PaperIII): The limits of the inverse problem of determining the optical properties of a two-layer medium when the hybrid model is used as the forward calculation were explored. Since the hybrid model is computationally intensive, a global optimization algorithm that is substantially more efficient than SA is required to make the iterative fitting of the former feasible. A hybrid simplex-SA algorithm that was adapted to the two-layer problem achieved just that goal. The hybrid model's performance was tested against that of pure diffusion. For ideal, MC simulated, FD data it was shown that the hybrid model can accurately determine all optical properties of a two-layer medium. The additional experimental limitations encountered from high accuracy FD measurements on two-layer liquid phantoms were analyzed.

Chapter (v) (Some in vivo data): Some preliminary *in vivo* results on following the pharmacokinetics of an injected chromophore ($CuPcS_4$) in New Zealand rabbits are presented. The additional experimental difficulties in going from phantom measurements to the *in vivo* setting, and their impact on quantitative measurements, are discussed.

Chapter (vi) (Conclusions): The thesis results are summarized and, based on them, suggestions are made for the possible directions of future work.

Chapter 2

Paper *I*

2.0.1 Introduction to Paper *I*

The following paper examines the extent to which one can determine accurately all of the optical properties characterizing a two-layer turbid medium from spatially resolved reflectance measurements in the frequency domain (FD). The two-layer geometry is a more realistic model of superficial tissue relative to the semi-infinite one assumed by most researchers. The effect of spatial averaging on tissue optical property estimates when assuming a semi-infinite geometry impairs quantitative measurements *in vivo*. Previous work in our group [Kienle et al., Appl. Opt. **37,** 1958 (1998)] led to a forward model for the diffuse spatially resolved FD reflectance from a two-layer medium. However, it was not clear how much information one can extract from this model. The present paper addresses that question by introducing a global optimization technique. The results presented are specific to skin on top of fat in the presence

of an exogenous chromophore. Only Monte Carlo simulated reflectance measurements are considered.

The work in this paper was performed by me under the supervision of Dr. Patterson. Dr. Farrell had many good suggestions, especially on how to calculate scaling factors when reflectance data are fitted as relative measurements. The manuscript was written by me and was edited by both Drs. Patterson and Farrell.

2.0.2 Contents of Paper *I*

Accuracy of the diffusion approximation in determining the optical properties of a two-layer turbid medium.

George Alexandrakis, Thomas J. Farrell, and Michael S. Patterson

Department of Medical Physics, Hamilton Regional Cancer Centre and McMaster University,

699 Concession Street, Hamilton, Ontario, Canada, L8V 5C2.

Applied Optics, Vol. 37, No. 31, 1 November 1998

Abstract

We have examined the possibility of determining the optical properties of a two-layer medium using a diffusion approximation radiation transport model [Appl. Opt. **37,** 779 (1998)]. Continuous-wave and frequency domain (FD) low noise Monte Carlo (MC) data were fitted to the model. Marquardt-Levenberg and a simulated annealing algorithm were used and compared as optimization techniques. Our particular choice of optical properties for the two-layer model was consistent with skin and underlying fat in the presence of an exogenous chromophore [Appl. Opt. **37,** 1958 (1998)]. The results are therefore specific to this set of optical properties. It was found that the cw diffusion solution could never estimate all optical properties reliably. The combined cw and FD solutions could not be used to estimate some of the top-layer optical properties to an accuracy better than 10%, although the absorption and transport scattering coefficients of the bottom layer could be estimated to within 7% and 0.5% respectively. No improvement was found from simultaneously fitting MC data at three different modulation frequencies. These results point to the need for a more accurate radiation transfer model at small source-detector separations.

OCIS codes: 170.3660, 170.40909,290.1990, 290.7050

1. Introduction

Optical reflectance measurements offer the potential to gain diagnostic information about biological tissue by determination of the absorption and scattering coefficients. The absorption coefficient depends on the concentration of endogenous chromophores such as hemoglobin and may reflect the physiological status of the tissue.[1] Pharmacokinetic information about exogenous chromophores can also be obtained in this manner.[2] The scattering coefficient has been exploited as an indicator of tissue structure[3] and the relative indices of refraction of tissue components.[4] Estimation of the absolute absorption (μ_a) and scattering (μ_s) coefficients requires a model of light propagation between the light source and detectors on the tissue surface. To date, most *in vivo* applications of these models have relied on the diffusion approximation of light transport and on the assumption that the tissue is macroscopically uniform.[1] This made μ_a and μ_s spatially invariant, while the preferential forward scattering of photons was equivalently described by an isotropic transport scattering coefficient μ_s'.

It is clear that in most situations the tissue itself is optically inhomogeneous or physiological changes occur in only one tissue component. For example, in a recent paper[2] we attempted to measure the uptake of a photosensitizing dye in rabbit skin by measuring the reflectance at source-detector distances ranging from 1 to 10 mm. Analysis of excised tissue samples showed that the uptake of the dye in skin was about an order of magnitude higher than that in the underlying muscle or fat. We

have also shown that the optical properties of the dermis are quite different from fat or muscle.[5] The result of these differences was that it was not possible to apply a model of light propagation in a homogeneous medium to the analysis of reflectance on the skin surface and gain meaningful data about the dye concentration in the tissue. Such an analysis lead to estimates of drug concentration which were lower than the actual value in either tissue layer.[2] The goal of this paper was to determine whether it is possible in principle to estimate the optical properties of two tissue layers (skin and underlying fat) from fitting an appropriate two-layer diffusion approximation model to Monte Carlo (MC) generated calculations of surface reflectance so that the drug concentration in each layer can be determined. We recognize that even this is a simplification, in that the skin itself consists of three distinct layers,[6] but there is much to be gained from examining the simpler case. We also assume that the thickness of the upper layer is not known *a priori* although such information might be provided by ultrasound imaging or other techniques. The basic approach is to find a set of five diffusive transport parameters (μ_a, μ_s' in both layers and the thickness of the top layer) which provides the best agreement with the measured, or in this case, MC simulated reflectance. Because the optimal set is found by iterative methods, it is necessary to have a model which provides a rapid forward calculation of the reflectance for a two-layer medium.

Kienle *at al.*[7] have developed a solution based on the diffusion approximation which is similar to that proposed by Dayan *et al.*[8] but which is more accurate and

accounts for a mismatch in the index of refraction at the tissue surface. Kienle *et al.*[7] presented preliminary results showing that the optical properties of two layers could be approximately recovered under some conditions (e.g., top layer thickness known). We decided to apply this model to the specific problem of estimating the five parameters listed in Table 1 (True column), which represent a skin layer containing a relatively high concentration of a light absorbing dye and a fat layer with a much lower content. These optical properties were estimated from the baseline values for skin and fat at 750 nm.[5] The MC simulated true reflectance calculation assumed a point source which was either continuous (CW) or intensity modulated at a frequency f. The simulation provided the absolute cw reflectance or the amplitude and phase of the ac (i.e., intensity modulated) reflectance. The same information is provided by the diffusion calculation. Marquardt-Levenberg and simulated annealing algorithms were used to find the parameters which provided the best agreement between the diffusion calculations and the MC simulations. To test the sensitivity of the fitting algorithms to the initial values of the parameters, we used various initial guesses. One was the set of true values; another, also shown in Table 1, consisted of similar coefficients in both layers and a thickness about double the true value. This represents a realistic but stringent test of the fitting algorithms and will be used to illustrate their performance.

Experimentally it is possible to measure the cw reflectance,[9] the ac reflectance, and/or the phase.[10] These quantities may be measured absolutely or relatively. There-

fore we examined the potential of various combinations of data types. In addition, we

Table 1. True Set of Optical Properties with which all MC Runs were Performed All Fitting Routines[a]

Parameters	True	False
μ_{a1} / mm^{-1}	7.75×10^{-2}	7.75×10^{-2}
μ_{s1}' / mm^{-1}	1.49	1.0
μ_{a2} / mm^{-1}	7.0×10^{-3}	1.3×10^{-2}
μ_{s2}' / mm^{-1}	1.0	1.1
ℓ / mm	1.5	3.5

[a]Parameter definitions in text.

also investigated whether fitting data at multiple modulation frequencies improved the estimates of the optical properties.

2. Methods

A. Two-Layer Diffusion Approximation

The radiation transport model used for fitting the MC data was the diffusion approximation for a two-layer medium, as reported by Kienle *et al.*[7]. Only the salient features of the problem definition, and its solution are being reproduced here to assist the reader:

A beam of light enters the top layer of the medium along the z direction. It

is assumed that all photons scatter at one transport mean free path length $z_0 = 1/(\mu_{s1'} + \mu_{a1})$ into the top layer. In reality, each photon would travel a different distance along the z axis until it scattered for the first time. However, assuming a single source at z_0 has been shown to be a good approximation for the calculations of diffuse reflectance in a semi-infinite medium.[11] It is also implicitly assumed that the top layer thickness ℓ is greater than z_0. The two-layer medium diffusion equations for the fluence rates ($mm^{-2}s^{-1}$) due to the intensity modulated source are then given by

$$D_1\nabla^2\Phi_1(r,\omega) - \left(\mu_{a1} + j\frac{\omega}{c_m}\right)\Phi_1(r,\omega) = -\delta(x,y,z-z_0)exp\left(j\frac{\omega}{c_m}r\right), \quad 0 \le z \le \ell\ , \tag{1}$$

$$D_2\nabla^2\Phi_2(r,\omega) - \left(\mu_{a2} + j\frac{\omega}{c_m}\right)\Phi_2(r,\omega) = 0\ , \qquad \ell \le z\ , \tag{2}$$

where, given the radial symmetry of the problem, $r = (x^2 + y^2 + z^2)^{1/2}$. Also, $D_i = (1/3)(\mu_{ai} + \mu_{si}')^{-1}$ are the diffusion constants and Φ_i are the fluence rates for layers $i = 1$ and 2 respectively. The intensity modulation frequency of the incident light is $\omega = 2\pi f$ ($\omega = 0$ for cw), c_m is the speed of light in the medium, and $j = \sqrt{-1}$. The boundary conditions are as follows:

(1) Zero fluence rate at the extrapolated boundary ($z = -z_b$):

$$\Phi_1(z = -z_b, r) = 0\ . \tag{3}$$

(2) Finite photon fluence rate:

$$\Phi_2(r \to \infty) = 0 \ . \tag{4}$$

(3) Continuity of fluence rate and flux at the boundary between the two layers, assuming matched refractive indices for the two layers, is:

$$\Phi_1(\ell) = \Phi_2(\ell) \ , \tag{5}$$

$$D_1 \frac{\partial \Phi_1(z)}{\partial z}\bigg|_{z=\ell^-} = D_2 \frac{\partial \Phi_2(z)}{\partial z}\bigg|_{z=\ell^+} \ . \tag{6}$$

In our study it was assumed that the medium and the surface probe were refractive index matched, making the fraction of internally reflected photons at the surface R_{eff} equal to zero. This made the extrapolated boundary length[12]

$$z_b = 2D_1 \ . \tag{7}$$

It was shown by Kienle *et al.* that the fluence rate at the surface ($z = 0$) can be obtained by a spatial Fourier inversion of Eq. (1), giving

$$\Phi_1(\rho, z = 0) = \frac{1}{2\pi} \int_0^\infty \phi_1(s, z, \omega) s I_o(s\rho)\, ds \ , \tag{8}$$

where

$$\begin{aligned} \phi_1(z = 0) \ = \ & \frac{\sinh(\alpha_1(z_b + z_o))}{D_1\alpha_1} \frac{D_1\alpha_1 \cosh(\alpha_1(\ell - z)) + D_2\alpha_2 \sinh(\alpha_1(\ell - z))}{D_1\alpha_1 \cosh(\alpha_1(\ell + z_b)) + D_2\alpha_2 \sinh(\alpha_1(\ell + z_b))} \\ & - \frac{\sinh(\alpha_1(z_o - z))}{D_1\alpha_1} \ , \end{aligned} \tag{9}$$

$\rho = (x^2 + y^2)^{1/2}$, s is a spatial-frequency dummy variable, $I_o(s\rho)$ is the zeroth order Bessel function, and $\alpha_i = (D_i s^2 + \mu_{a_i} + j\frac{\omega}{c_m})/D_i$, $(i = 1, 2)$. For a refractive index-matched-boundary, the reflectance is given by

$$R(\rho,\omega) = \frac{1}{4}\Phi_1(\rho, z = 0, \omega) + \frac{1}{2}D_1 \left.\frac{\partial\Phi_1(\rho, z, \omega)}{\partial z}\right|_{z=0} . \tag{10}$$

Since Eq. (9) and its analytical derivative converge to zero as differences between two large numbers, appropriate limiting expressions were found in order to eliminate any problems with the numerical integration of Eq. (8).

In the frequency domain (FD), the phase of the detected light signal relative to the source was calculated as

$$\theta(\rho,\omega) = \tan^{-1}\frac{Im[R(\rho,\omega)]}{Re[R(\rho,\omega)]} \tag{11}$$

and the AC reflectance as

$$ACR(\rho,\omega) = (\{Im[R(\rho,\omega)]\}^2 + \{Re[R(\rho,\omega)]\}^2)^{1/2} . \tag{12}$$

B. Fitting Algorithms

Two very different optimization algorithms were compared for their accuracy in estimating the true optical properties which had been used to generate the two-layer medium reflectance MC data:

1. Marquardt-Levenberg Method

The method is described in detail in Ref. 13, and variants have been used by several authors (e.g., Refs. 5 and 7) as a standard method for parameter estimation.

Briefly, the algorithm switches continuously from the inverse Hessian method far from the minimum, to the steepest descent method as the minimum is approached.

2. Simulated Annealing

This is a global optimization method that has been successfully used in fields other than biomedical optics.[14] It was designed to find approximate global minima of complicated multi-dimensional functions with built-in system noise. The algorithm relies on an analogy between optimization and the process of annealing of a hot material. The energy E function of the system is the one in which we seek a global minimum (χ^2 in this case). The temperature parameter T is related to the magnitude of a downhill (or uphill) move in χ^2 space depending on whether a real number $\in [0, 1)$ is greater (less) than the current value of the quantity $exp - (E/T)$ (Metropolis criterion). For every specified number of function evaluations, T is reduced by a temperature reduction factor $RT \in (0, 1)$. Hence, as the temperature of the system is lowered the algorithm focuses on the most promising volume of parameter space. A low initial T, or a low RT value cause the system to quench or converge prematurely to a local minimum. High RT values greatly increase the chances of attaining an approximate global minimum, at the price of a very large function-call overhead.

An initial T of 5 and RT values in the range of 0.85-0.96 were found to be adequate for simulated annealing to reach an approximate global minimum in most cases. When the last five χ^2_{min}'s found did not differ by more than an absolute value of 0.1, the fitting program was terminated. For runs that exceeded 100,000 function evaluations,

convergence was deemed satisfactory when no new global minimum had been found in the last 10,000 function evaluations, and the search steps for each parameter were less than 1% of the current optimal parameter magnitudes.

C. Monte Carlo Simulations

A two-layer MC code[5] was run for a single set of optical properties (Table 1, True column). Continuous-wave and intensity modulated perpendicularly incident beams were used as light sources. As the code employed reduced variance schemes, several runs were made using the same set of optical properties to obtain reliable estimates of statistical uncertainty for all data, to as far as $\rho = 20$ mm away from the source. A total of 50 million photon histories were acquired. For cw data and $\rho < 5$ mm, the noise was less than 0.1%, increasing to $\sim$2% at $\rho = 20$ mm. For FD reflectance data similar values were observed for the relative noise in phase and ac signal. A low-noise MC reflectance calculation for a two-layer medium with known optical properties was used as a tool to test how much information the cw and FD two-layer medium diffusion approximation solutions could extract under ideal circumstances. Experimental uncertainties in these quantities could be larger, and may not have the same relative variation with source-detector distance as the noise in the MC simulations.

D. Absolute versus Relative Measurements

In a relative reflectance measurement, the intensity of scattered light measured at

different source-detector distances is only known relative to the other measurements. However, if the measured intensity is known relative to the light source intensity, a reflectance measurement is absolute. Similarly, for a relative phase measurement, the phase of intensity modulated scattered light is known only relative to the other measurements, whereas in an absolute measurement the phase is known relative to that of the incident beam. A reflectance scaling factor q_r, and an additive phase constant p_{ph}, can be used to match the relative measurements with the absolute ones, as predicted by the diffusion approximation. For absolute reflectance and phase fittings, $q_r = 1$, and $q_{ph} = 0$, respectively. It should be mentioned that our MC results were in fact equivalent to absolute measurements, but q_r and q_{ph} were allowed to vary as extra degrees of freedom to emulate possible forms of experimental data.

Assume that for a set of source-detector distances $(\rho_i, i = 1, N)$, there is a set of cw (or ac) reflectance measurements $[y(\rho_i)]$ each of standard deviation σ_i, both known from the MC data, and a corresponding set of diffusion-calculated values $[yc(\rho_i)]$. Then there is a scaling factor q_r that minimizes χ^2:

$$\chi^2_{min(R)} = \left\{ \sum_{i=1}^{N} \left[\frac{y(\rho_i) - q_r yc(\rho_i)}{\sigma_i} \right]^2 \right\}_{min} , \tag{13}$$

where

$$q_r = \frac{\sum_{i=1}^{N} \frac{y(\rho_i) yc(\rho_i)}{\sigma_i^2}}{\sum_{i=1}^{N} \frac{yc(\rho_i)}{\sigma_i^2}} . \tag{14}$$

In a similar manner it is found that for a set of phase measurements $[yp(\rho_i), i = 1, N]$, each of standard deviation σ_i, and a corresponding set of diffusion-calculated phases

$[ypc(\rho_i)]$, there is an additive constant q_{ph} that minimzes χ^2:

$$\chi^2_{min(ph)} = \left(\sum_{i=1}^{N} \left\{ \frac{yp(\rho_i) - [ypc(\rho_i) + q_{ph}]}{\sigma_i} \right\}^2 \right)_{min} , \tag{15}$$

where

$$q_{ph} = \frac{\sum_{i=1}^{N} \frac{yp(\rho_i) - ypc(\rho_i)}{\sigma_i^2}}{\sum_{i=1}^{N} \frac{1}{\sigma_i^2}} . \tag{16}$$

3. Results and Discussion

The accuracy to which all five parameters $(\mu_{a1}, \mu_{s1}', \mu_{a2}, \mu_{s2}', \ell)$ of a two-layer medium could be predicted by the cw and FD solutions of Eqs. (1) and (2) was examined. As the magnitude of the reflectance $[R(\rho)]$ decreased rapidly with ρ, it was plotted as $ln[\rho^2 R(\rho)]$ to compress the scale of the data, and help visualize more clearly differences between reflectance curves at small ρ.

The cw reflectance as calculated in the diffusion approximation for a two-layer medium, is represented by the solid curve in Fig. 1. The open circles are the MC results for the same optical properties (Table 1, True column), and the filled circles are the MC results for a semi-infinite with the optical properties of the top layer. The diffusion solution for a semi-infinite medium having the same optical properties as those of the top layer in the two-layer medium case, is represented by the dashed curve. The semi-infinite medium solution for the bottom-layer optical properties is represented by the dash-dot-dot curve in Fig. 1. It can be seen that for $\rho < 2$ mm, the diffusion solution for the two-layer case is nearly identical for a semi-infinite medium

with the optical properties of the top layer. Similarly, for $\rho < 2$ mm, the two-layer MC results were found to be in good agreement with those for a semi-infinite medium having the optical properties of the top layer. These results are expected, since in the two-layer case photons which escape close to the source travel mostly through the top layer. However, for the same range of distances, the diffusion solutions are not in good agreement with the MC results because differences as great as 17% are observed. For $\rho > 6$ mm, the slope of the two-layer reflectance curve becomes equal to that computed for a semi-infinite medium having the optical properties of the bottom layer. Again this is expected, because photons that exit the medium at large ρ have spent the greatest proportion of their path in the bottom layer. In this region there is very good agreement between the diffusion calculations and MC results for both two-layer and semi-infinite media.

Very similar characteristics were observed for the ac reflectance versus radial distance for modulated incident light (Fig. 2, $f = 195MHz$). The only difference was that the ac reflectance dropped faster with ρ. As the modulation frequency increased, the slopes of the two-layer and semi-infinite medium reflectance curves increased, thus reducing even further the ac amplitude for a given ρ. The phase of the ac reflectance as calculated by the two-layer diffusion approximation also appeared to be close to the corresponding MC results (Fig. 3, $f = 195MHz$). The diffusion solution consistently underestimated the MC results, less so for larger ρ. The discrepancy was $\sim$4.5% for $\rho < 1$ mm, reducing to $\sim$1.5% at $\rho = 10$ mm. It is interesting to note that

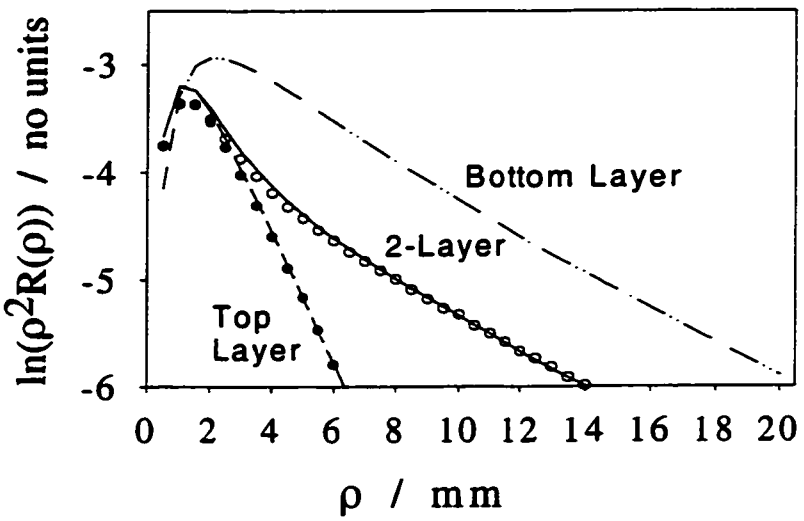

Fig. 1 The two-layer medium cw diffusion solution of Eqs. (1) and (2) (solid curve) compares well with the corresponding MC results (open circles) for $\rho > 6$ mm. The optical properties used for both are shown in Table 1, True column. Similarly, the semi-infinite medium solution for the top layer optical properties (dashed curve) agrees well with the corresponding MC results (filled circles) for $\rho > 4$ mm. The semi-infinite medium diffusion solution for the bottom-layer optical properties (dash-dot-dot curve) is also shown.

for $\rho > 3$ mm, the two-layer phase delay was larger than that for either of the two semi-infinite medium solutions. For increasing modulation frequencies, similar trends were observed with increasing phase for a given ρ for all curves. However, the discrepancy between diffusion and MC results increased.

It can be seen from Figs. 1-3, that the two-layer medium diffusion solution, both in cw and FD, contains features which differ from the semi-infinite solutions for the

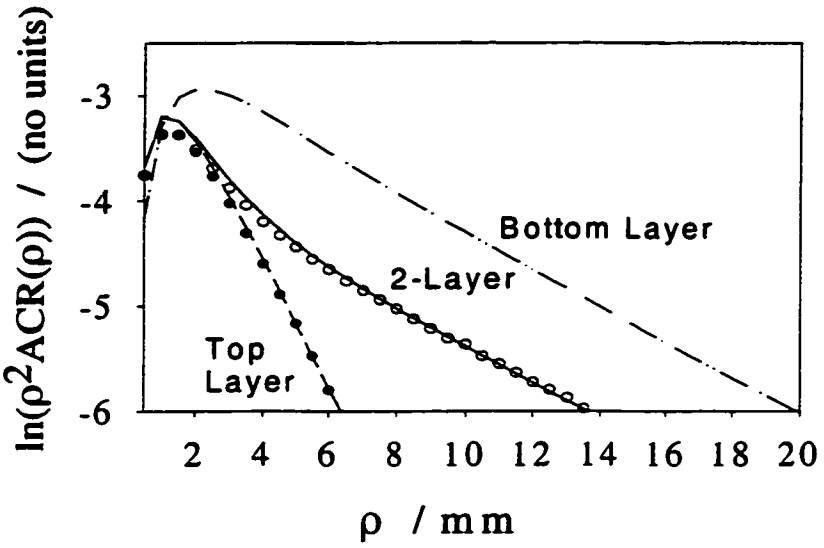

Fig. 2 As in Fig. 1, but for the ac reflectance (ACR) of an intensity-modulated incident beam. Notice the steeper drop of ac reflectance with radial distance compared to the cw case in Fig. 1.

two media that compose it. This difference was the motivation for determining how informative these solutions can be.

MC data were generated using the optical properties shown in Table 1, True column. They were then fitted as absolute or relative measurements to the appropriate two-layer diffusion approximation. Results from Marquardt-Levenberg fittings using the true parameters as an initial guess are indicated as Marqrt-t, and those using a false initial guess (Table 1, False column) are indicated as Mrqrt-f. Though several different sets of false initial guesses were tested, only one set is shown, representative of the trends for all fitting procedures. Similarly, results from simulated annealing

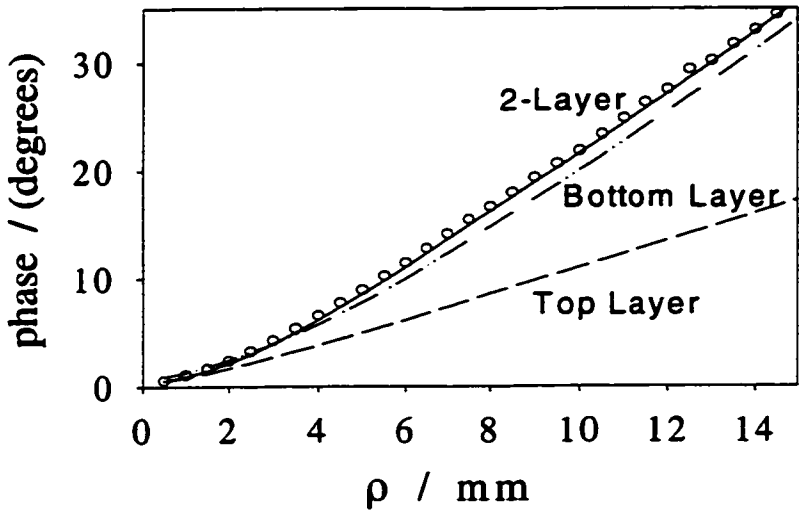

Fig. 3 The two-layer diffusion solution of Eqs. (1) and (2) for the phase of the ac one (open circles), with increasing discrepancies at small radial distances ($\rho < 2$ mm). For larger ρ, the two-layer phase is greater than the phase calculated from the individual semi-infinite solutions for the top (dashed curve) and bottom (dash-dot-dot curve) layer optical properties.

fittings are indicated as SA-t or SA-f depending on whether the initial guesses are true or false, respectively. Whenever the SA-t fitted parameters are not shown, they are in close agreement with SA-f. The percentage error in each parameter, relative to the corresponding true value, is shown in adjacent columns. The number of data points used for all fittings was 12, at radial distances $\rho = 6$, 8-16(increment 1), 18, and 20 mm. Including data points for $\rho < 6$mm only reduced the quality of fit without improving the accuracy of the fitted optical properties, for reasons to be discussed

below.

A. Continuous-Wave Reflectance

The results of Mrqrt-t, Mrqrt-f, and SA-f are shown in Table 2. It can be observed that the Marquardt method was sensitive to the initial parameter guess, and was trapped at local minima close to it. It can also be seen that even with the true initial guesses as a starting point, one of the parameters (μ_{a2}) had an error considerably larger than our goal of 10%. However, it appears that Marqrt-t had also found a local minimum, since SA-f was able to find an even lower χ^2_{min}, where all fitted parameters had errors larger than 10%. The χ^2 that the true parameters themselves gave [$\chi^2(t)$] was 21.6. This was much higher than any of the χ^2_{min} values produced by the different fitting methods. Note that SA required almost 100 times as many function evaluations for χ^2_{min} to be found. The execution time for a SA fitting procedure employing 300,000 function evaluations was ~2 h on an Ultrasparc 1 and was relatively independent of the initial parameter guesses.

When absolute reflectances were fitted for the same data points, the accuracy to which all optical parameters could be estimated did not improve. As shown in Table 3, a very small difference in χ^2_{min} between Marqrt-t and SA-f corresponded to wildly different optical properties. Mrqrt-f failed to converge. Also, note the very high number of function evaluations that SA had to employ to find an approximate

Table 2. Estimates of Optical Properties Obtained by Fitting MC Data for Relative cw Reflectance Measurements, by Marquardt-Levenberg and a True Initial Guess (Mrqrt-t), a False Initial Guess (Marqrt-f), and Simulated Annealing with a False Initial Guess (SA-f)[a]

Parameters	Mrqrt-t	Error (%)	Mrqrt-f	Error (%)	SA-f	Error (%)
μ_{a1} / mm^{-1}	7.425	4.20	2.537	99.67	6.517	15.91
	$\times 10^{-2}$		$\times 10^{-4}$		$\times 10^{-2}$	
μ_{s1}' / mm^{-1}	1.552	4.16	1.111	37.94	1.198	19.60
μ_{a2} / mm^{-1}	8.674	-23.91	9.780	39.71	1.160	-65.67
	$\times 10^{-3}$		$\times 10^{-3}$		$\times 10^{-2}$	
μ_{s2}' / mm^{-1}	0.8850	11.50	0.8753	12.48	0.6909	30.91
ℓ / mm	1.476	1.61	2.327	-55.13	1.654	-10.29
q_r/no units	0.9897		0.3547		0.7260	
χ^2_{min}	2.30		2.42		2.29	
Evaluations	660		2112		16,501	

[a]The χ^2 of the true parameters was $\chi^2(t) = 21.6$. Parameters are defined in the text.

global minimum, which implied a high density of very different solutions all giving similar χ^2_{min} values. The uncertainty in the fitted parameters can be estimated from the curvature of χ^2 space around the minimum.[13] The calculated uncertainties for all five optical properties were greater than 300%, and were even larger for the case of relative measurements. These results strongly suggest that the use of the cw diffusion

Table 3. Estimates of Optical Properties Obtained by Fitting MC Data for Absolute cw Reflectance Measurements ($q_r = 1.0$) by Mrqrt-t, and SA-f where $\chi^2(t) = 23.3$[a]

Parameters	Mrqrt-t	Error (%)	SA-f	Error (%)
μ_{a1} / mm^{-1}	7.377 $\times 10^{-2}$	4.81	0.1680	-116.77
μ_{s1}' / mm^{-1}	1.550	-4.05	0.7710	48.26
μ_{a2} / mm^{-1}	8.805 $\times 10^{-3}$	-25.71	1.674 $\times 10^{-2}$	-139.14
μ_{s2}' / mm^{-1}	0.8766	12.35	0.4600	54.00
ℓ / mm	1.494	0.43	1.625	-8.33
χ^2_{min}	2.30		2.29	
Evaluations	924		300,001	

[a]Mrqrt-f failed to converge.

equation to estimate all optical properties of a two-layer medium from corresponding MC data is not a well-posed problem.

B. Continuous-Wave Reflectance and Frequency-Domain Phase

From an experimental point of view, it is easier to acquire relative rather than absolute measurements. Continuous-wave and FD data generated for the same optical properties as in the cw case alone (Table 1, True column), were fitted as relative steady-state reflectances and phase measurements, as explained in the Subsection 2D. Table 4 shows the results of the Mrqrt-t, SA-t, and SA-f fits of the MC data.

Table 4. Estimates of Optical Properties Obtained by Fitting MC Data for Relative Phase and cw Reflectance Measurements by Mrqrt-t, SA-t, and SA-f[a]

Parameters	Mrqrt-t	Error (%)	SA-t	Error (%)	SA-f	Error (%)
μ_{a1} / mm^{-1}	6.764	12.72	6.621	14.57	6.447	16.82
	$\times 10^{-2}$		$\times 10^{-2}$		$\times 10^{-2}$	
μ_{s1}' / mm^{-1}	1.686	-13.18	1.473	1.17	2.085	-39.94
μ_{a2} / mm^{-1}	7.399	-5.51	6.793	2.96	7.932	-13.32
	$\times 10^{-3}$		$\times 10^{-3}$		$\times 10^{-3}$	
μ_{s2}' / mm^{-1}	1.000	0.0	1.023	2.29	1.020	2.03
ℓ / mm	1.439	4.07	0.8833	41.11	1.631	-8.73
q_r/no units	0.9955		0.5343		1.595	
q_{ph}/deg	-2.691		-7.997		1.821	
	$\times 10^{-3}$		$\times 10^{-3}$		$\times 10^{-2}$	
χ^2_{min}	3.83		3.69		3.14	
Evaluations	3642		109,001		194,001	

[a]The true parameters gave $\chi^2(t) = 24.3$.

As before, Mrqrt-t converged to a local minimum close to the true initial guesses. Similarly, Mrqrt-f converged to a local minimum close to the false initial guess (results not shown). On the other hand, SA-t and SA-f converged to similar χ^2_{min} values but to top-layer optical properties that were quite different. This is attributed to the

ability of the of the steady-state reflectance scaling factor [q_r, Eq.(14)] to assume values other than unity. Hence, a very large number of function evaluations must be employed by SA to avoid being trapped at local minima that produce similar values of χ^2, but correspond to very different sets of optical properties. The χ^2_{min} of both fits was far from the true $\chi^2(t) = 24.3$. The percentage uncertainties in the estimated parameters were 48.19% for μ_{a1}, 6.29% for $\mu_{s1}{}'$, 5.21% for μ_{a2}, 2.45% for $\mu_{s2}{}'$, and 5.46% for ℓ. These uncertainties imply that even with low noise data, we cannot retrieve the top-layer true optical properties with good accuracy by fitting relative phase and cw reflectance measurements.

The most informative, yet most difficult to obtain experimentally, are absolute measurements. The same MC data were fit as absolute phase and cw reflectance measurements. Table 5 shows the 'Mrqrt-f, SA-t, and SA-f fitting results to the MC data. This time the local minimum to which Mrqrt-t converged was almost identical to the approximate global minimum that SA-t and SA-f found. Notice the high number of function evaluations employed in SA-f to avoid a local minimum. Once again, $\chi^2(t) = 52.5$ was much higher than the χ^2_{min} values at the minima found. The percentage uncertainties in the estimated parameters were 17.16% for μ_{a1}, 4.04% for $\mu_{s1}{}'$, 3.72% for μ_{a2}, 1.71% for $\mu_{s2}{}'$, and 11.39% for ℓ. These results show that absolute measurements are somewhat more informative, allowing retrieval of the true optical properties to a better accuracy than relative measurements. However, the errors in μ_{a1} and $\mu_{s1}{}'$ still exceed 10% (11% and 14% respectively).

Table 5. Estimates of Optical Properties Obtained by Fitting MC Data for Absolute Phase and cw Reflectance Measurements ($q_r = 1.0$, $q_{ph} = 0.0$) by Mrqrt-t, SA-t, and SA-f[a]

Parameters	Mrqrt-t	Error (%)	Mrqrt-f	Error (%)	SA-f	Error (%)
μ_{a1} / mm^{-1}	6.893 $\times 10^{-2}$	11.06	6.901 $\times 10^{-2}$	10.95	6.894 $\times 10^{-2}$	11.05
μ_{s1}' / mm^{-1}	1.698	-13.93	1.696	-13.83	1.698	-13.95
μ_{a2} / mm^{-1}	7.400 $\times 10^{-3}$	-5.71	7.393 $\times 10^{-3}$	-5.61	7.401 $\times 10^{-2}$	-5.72
μ_{s2}' / mm^{-1}	1.003	-0.32	1.003	-0.32	1.003	-0.32
ℓ / mm	1.419	5.42	1.419	5.39	1.418	5.44
χ^2_{min}	3.78		3.78		3.78	
Evaluations	660		46,501		300,001	

[a]The true parameters gave $\chi^2(t) = 52.5$.

Between the two extremes of all relative, or all absolute phase and cw reflectance data, lie two more possible combinations. Absolute phase and relative cw almost as bad as having both measurements relative, owing to the ability of q_r [Eq.(14)] to assume values far from unity. Absolute reflectance and relative phase, on the other hand, produced results almost as good as when both measurements were absolute, again with μ_{a1} and μ_{s1}' having errors slightly larger than 10% (results not shown).

C. Continuous-Wave and Alternating-Current Reflectance and Phase

Since fitting both phase and cw reflectance as absolute measurements didn't quite reach our target accuracy in parameter estimation, the absolute ac reflectance amplitude was added to the fitting procedures. Table 6 shows the results of Mrqrt-t, and SA-f fittings for a modulation frequency $f = 195MHz$. Both algorithms converged to the same χ^2_{min} which was much smaller than $\chi^2(t) = 80.3$. Once again, however, the errors in μ_{a1} and $\mu_{s1}{}'$ were slightly over 10%. It was found that including

Table 6. Estimates of Optical Properties Obtained by Fitting MC Data for Absolute cw, ac Reflectance, and Phase Measurements ($q_r = 1.0$, $q_{ph} = 0.0$) at a Modulation Frequency $f = 195MHz$[a]

Parameters	Mrqrt-t	Error (%)	SA-f	Error (%)
μ_{a1} / mm^{-1}	6.660×10^{-2}	14.07	6.663×10^{-2}	14.03
$\mu_{s1}{}'$ / mm^{-1}	1.698	-13.94	1.698	-13.94
μ_{a2} / mm^{-1}	7.418×10^{-3}	-5.97	7.412×10^{-3}	-5.96
$\mu_{s2}{}'$ / mm^{-1}	0.9985	0.16	0.9985	0.16
ℓ / mm	1.446	3.58	1.446	3.60
χ^2_{min}	7.39		7.39	
Evaluations	660		250,001	

[a]Mrqrt-t and SA-f converged to the identical minimum. The true parameters gave $\chi^2(t) = 80.3$.

the reflectance data at $\rho < 6$ mm in the fit decreased both the quality of the fit, and the accuracy of the estimated optical properties. This is demonstrated in Table 7. Despite the very large number of function evaluations, SA-t converged to a high

Table 7. Estimates of Optical Properties Obtained by Fitting MC Data for Mrqrt-t, Mrqrt-f, SA-f[a]

Parameters	SA-t	Error (%)
μ_{a1} / mm^{-1}	1.849 $\times 10^{-1}$	-138.50
μ_{s1}' / mm^{-1}	1.478	0.83
μ_{a2} / mm^{-1}	5.659 $\times 10^{-3}$	19.16
μ_{s2}' / mm^{-1}	1.220	-21.95
ℓ / mm	8.289 $\times 10^{-1}$	44.74
χ^2_{min}	2630	
Evaluations	1.04 $\times 10^{6}$	

[a]The number of reflectance measurements included in the fits was the same as in all other cases (12), but they were made at ρ = 1-6 (increment 1), 8-16 (increment 2), and 20 mm. Despite the large number of function evaluations, SA-t gave poor quality parameter estimates. The true parameters gave $\chi^2(t)$ = 19,400.

value of χ^2_{min}, which gave large errors for most optical properties, especially μ_{a1}. Increasing the number of data points offered no improvement in the quality of the fitted parameters.

Tables 8 and 9 show the fitting results for modulation frequencies $f = 300MHz$

and $1GHz$, respectively, for the usual set of radial distances defined at the end of Section 3. Table 8, SA-t is shown instead of SA-f as the latter ended up in local minima far from the global, although more than 200,000 function evaluations were employed. The approximate global minima found by both methods closely agreed. Given the faster drop of ac reflectance with distance at higher frequency, smaller radial distances [ρ = 4-15 (incr. 1) mm] were used for the $1 - GHz$ MC data fittings. It was also hoped that in this way more information about the top layer would be fed into the model. The radial distances used for the $f = 300MHz$ fittings were the same as those for the $f = 195MHz$ ac and cw reflectance, as specified at the beginning of this section. If, for comparison, the $\chi^2(t)$ for $f = 300MHz$ is evaluated for the same

Table 8. As in Table 6 but for a Modulation Frequency $f = 300MHz$ [$\chi^2(t) = 80.3$]

Parameters	Mrqrt-t	Error (%)	SA-f	Error (%)
μ_{a1} / mm^{-1}	6.843 $\times 10^{-2}$	11.70	6.999 $\times 10^{-2}$	9.69
μ_{s1}' / mm^{-1}	1.691	-13.46	1.692	-13.57
μ_{a2} / mm^{-1}	7.279 $\times 10^{-3}$	-3.98	7.256 $\times 10^{-3}$	-3.66
μ_{s2}' / mm^{-1}	1.005	-0.46	1.006	-0.64
ℓ / mm	1.433	4.47	1.414	5.73
χ^2_{min}	8.93		8.93	
Evaluations	1584		200,001	

Table 9. As in Table 6 but for a Modulation Frequency $f = 1GHz$ and SA-t Shown Instead of SA-f [$\chi^2(t) = 1010$]

Parameters	Mrqrt-t	Error (%)	SA-f	Error (%)
μ_{a1} / mm^{-1}	6.859 $\times 10^{-2}$	11.49	6.867 $\times 10^{-2}$	11.39
μ_{s1}' / mm^{-1}	1.695	-13.78	1.695	-13.76
μ_{a2} / mm^{-1}	7.511 $\times 10^{-3}$	-7.30	7.509 $\times 10^{-3}$	-7.27
μ_{s2}' / mm^{-1}	1.004	0.39	1.004	0.41
ℓ / mm	1.415	5.64	1.415	5.69
χ^2_{min}	22.5		22.5	
Evaluations	1320		58,001	

data points as for $f = 1GHz$ [ρ = 4-15(incr. 1) mm], and very similar noise levels, its value increases from 716 for $300MHz$, to 1010 at $1GHz$. This indicates that the diffusion approximation becomes less accurate as f increases.

Finally, cw ac reflectances and phase were simultaneously fit as absolute quantities at all three of the above modulation frequencies ($195MHz, 300MHz, 1GHz$). These frequencies span a fairly good range of those provided by a pulse of light, and thus gave an indication of whether a diffusion solution in the time domain would be more informative. Results from the Mrqrt-t and SA-f are shown in Table 10. They show that a combination of a few modulation frequencies has no advantage over a single frequency in improving the accuracy of the fitted optical properties. The uncertainties

Table 10. Continuous-Wave as Well as FD MC Data at Three Different Modulation Frequencies ($195MHz, 300MHz, 1GHz$) Simulateneously Fitted as Absolute cw, ac Reflectance, and Phase Measurements ($q_r = 1.0$, $q_{ph} = 0.0$)[a]

Parameters	Mrqrt-t	Error (%)	SA-f	Error (%)
μ_{a1} / mm^{-1}	6.767 $\times 10^{-2}$	14.78	6.853 $\times 10^{-2}$	11.57
μ_{s1}' / mm^{-1}	1.680	-12.77	1.686	-13.15
μ_{a2} / mm^{-1}	7.301 $\times 10^{-3}$	-4.29	7.344 $\times 10^{-3}$	-4.92
μ_{s2}' / mm^{-1}	1.002	-0.23	1.004	0.37
ℓ / mm	1.444	3.72	1.432	4.56
χ^2_{min}	54.6		42.5	
Evaluations	1320		242,001	

[a]The true parameters gave $\chi^2(t) = 1200$.

in the fitted parameters were smaller than in the single-frequency case, with the exception of μ_{a1}. The above does not imply that a combined MC data set of three modulation frequencies is no more informative than a data set at a single frequency. What it does imply is that the diffusion approximation cannot exploit that additional information.

4. Conclusions

The aim of our work was to find if, and how accurately, the diffusion approximation

could determine the true optical properties of a two-layer medium from low-noise MC data. This was done in order to find whether at least in principle it is possible for all five two-layer medium optical properties (μ_{a1}, μ_{s1}', μ_{a2}, μ_{s2}', ℓ) to be determined to an accuracy better than 10% under ideal conditions. This was investigated in detail for a particular set of optical properties corresponding to skin and underlying fat in the presence of an exogenous chromophore. The accuracy of the diffusion approximation in determining other sets of optical properties requires further investigation.

It was shown that the cw diffusion solution could never estimate all optical properties reliably, regardless of whether the data fitted were relative or absolute. The combined cw and FD diffusion could estimate μ_{a2}, μ_{s2}' and ℓ to an accuracy better than 10%, but the errors in μ_{a1} and μ_{s1}' were slightly more than that. This was only true if all of the fitting data, or at least the cw reflectance, were absolute. The inclusion of ac reflectance at a single modulation frequency did not improve the accuracy of the estimated parameters, nor did the simultaneous fitting of absolute cw and ac reflectance and phase at three different modulation frequencies. It is thought that there exists useful information in the MC data that the diffusion approximation cannot exploit because of the following:

(a) The useful information lies within reflectance measurements at smaller source-detector distances where the agreement between diffusion and MC data is not good.

(b) As the modulation frequency increases the diffusion approximation becomes less

accurate.

It was found that including data at small source-detector distances, and/or high modulation frequencies, reduced the quality of the fit and the accuracy of estimated optical properties (Table 7). For source-detector distances $\rho < 3$ mm, the difference between diffusion and MC results (Fig. 1) was ~8.5% at $\rho = 0.5$ mm, peaking to ~17% at $\rho = 1$ mm, and becoming progressively smaller thereon, reaching ~2% at $\rho = 6$ mm. Figure 1 also illustrates the interesting point that the two-layer diffusion approximation was no less accurate at small ρ compared with the semi-infinite medium solution. This last point leads to the conclusion that the discrepancy between the two-layer diffusion solution and corresponding MC results at small ρ does not stem from the more complicated geometry of the two-layer medium relative to the semi-infinite one. Rather, the discrepancy comes from the breakdown of the diffusion solution at small ρ and hence is a fundamental limitation of the model. For larger source-detector distances, though the MC data agreement with diffusion is good, the fraction of total pathlength that any photon spends in the top layer is small. Hence it is not surprising that μ_{a1} and μ_{s1}' and sometimes ℓ, are determined less accurately, regardless of efforts to increase the amount of information fed into the fitting procedures. Fitting relative data increased the uncertainty in estimates of the properties of the top layer.

We have also shown that the widely used Marquardt-Levenberg fitting algorithm was inadequate for determining the two-layer medium optical properties by fitting the

diffusion solution to the MC data, because the algorithm consistently was trapped in local minima close to the initial parameter guesses. Simulated annealing, on the other hand, proved to be a robust way of obtaining an approximate global χ^2_{min} most of the time. However, its vastly increased number of function evaluations compared to Marquardt made it a computationally expensive method. Hence it would be of interest to seek a global optimization algorithm that is at least as robust as SA but which requires many fewer function evaluations than SA to converge to a global minimum.

The trend of SA to converge to an approximate global minimum was found to be almost independent of initial parameter guess if an adequate number of function evaluations were allowed (results not shown). Therefore the fitting results produced from the false set of parameter guesses (Table 1, False column) can be generalized to any set of initial guesses, within reasonable physiological limits, for all optical properties. However, it should be realized that our conclusions concerning the accuracy to which the two-layer medium optical properties can be determined by fitting MC data to the diffusion approximation cannot be generalized to other sets of optical properties. That generalization would require the repetition of the above work for a large number of parameter sets. Our primary interest in this work was the accuracy of determination of the optical properties of skin and underlying fat in the presence of an exogenous chromophore. The top layer (skin) was very thin (1.5 mm), and hence it was not surprising that its optical properties could not be determined as accurately

as those of the bottom layer. The two-layer diffusion model may prove to be more successful in situations were the top layer is thicker, for example, in determining the optical properties of the neonatal brain through the overlaying scalp/skull.

Given the aim of our study, it is our intention to develop a more accurate radiation transport model for a two-layer medium at small source-detector distances. A hybrid model[15,16] that utilizes diffusion at larger distances has the potential for making the two-layer problem more well posed.

This research was supported by the National Institutes of Health grant P01-CA43892.

References

1. B. Chance, Q. Luo, S. Nioka, D. C. Alsop, and J.A. Detre, "Optical investigation of physiology: A study of biomedical contrast: Intrinsic and extrinsic," Philos. Trans. R. Soc. London B **352,** 707-716 (1997).

2. R. A. Weersink, J. E. Hayward, K. R. Diamond, and M. S. Patterson, "Accuracy of non-invasive *in vivo* measurements of photosensitizer uptake based on a diffusion model of reflectance spectroscopy," Photochem. Photobiol. **66,** 326-335 (1997).

3. J. R. Mourant., T. M. Johnson, G. Los, and I. Bigio, "Non- invasive measurements of chemotherapy drug concentrations in tissue: preliminary demonstra-

tions of *in vivo* measurements," Phys. Med. Biol. **44,** 1397-1417 (1999).

4. J. T. Bruulsema, J. E. Hayward, T. J. Farrell, M. S. Patterson, M. Essenpreis, G. Schmelzeiser-Redeker, D. Bocker, L. Heinemann, M. Berger, T. Koschinsky, J. Sandahl-Christiansen, and H. Orskov, "Correlation between blood glucose concentration in diabetics and non-invasively measured tissue optical scattering coefficient," Opt. Lett. **22,** 190-192 (1997).

5. T. J. Farrell, M. S. Patterson, and M. Essenpreis, "Influence of layered tissue architecture on estimates of tissue optical properties obtained from spatially resolved diffuse reflectometry," Appl. Opt. **37,** 1958-1972 (1998).

6. P. L. Williams, and R. Warwick, "The integument," in *Gray's Anatomy,* 36th ed. (Churchill Livingstone, Edindburgh,UK,1986), pp.1216-1222.

7. A. Kienle, M. S. Patterson, N. Utke, R. Bays, G. Wagnières, and H. van den Bergh, "Determination of the optical properties of two-layer turbid media," Appl. Opt. **37,** 779-791 (1998).

8. I. Dyan, S. Havlin, and G. H. Weiss, "Photon migration in a two-layer turbid medium. A diffusion analysis," J. Mod. Opt. **39,** 1567-1582 (1992).

9. A. Kienle, L. Lilge. M. S. Patterson, R. Hibst, R. Steiner, and B. C. Wilson, "Spatially resolved absolute diffuse reflectance measurements for noninvasive determination of the optical scattering and absorption coefficients of biological

tissue," Appl. Opt. **35,** 2304-2314 (1996).

10. B. W. Pogue, and M. S. Patterson, "Error assessment of a wavelength tunable frequency domain system for noninvasive tissue spectroscopy," J. Biomed. Opt. **1,** 311-323 (1996).

11. T. J. Farrell, and M. S. Patterson, "A diffusion theory model of spatially resolved, steady-state diffuse reflectance for the non-invasive determination of tissue optical properties *in vivo*," Med. Phys. **19,** 879-888 (1992).

12. R. C. Haskell, L. O. Svaasand, T.-T. Tsay, T.-C. Feng, M. S. McAdams, and B. J. Tromberg, "Boundary conditions for the diffusion equation in radiative transfer," J. Opt. Soc. Am. A **11,** 2727-2741 (1994).

13. W. H. Press, S. A. Teukolsky, W. T. Vetterling, and B. P. Flannery,*Numerical Recipes—The Art of Scientific Computing,* 2nd edition, (Cambridge U. Press, NY, 1996).

14. W. C. Goffe, G. D. Ferrier, and J. Rodgers, "Global optimization with statistical functions using simulated annealing," J. Econom. **60,** 65-100 (1994).

15. L. Wang, and S. L. Jacques, "Hybrid model of Monte Carlo simulation and diffusion theory for light reflectance by turbid media," J. Opt. Soc. Am. A **10,** 1746-1752 (1993).

16. S. T. Flock, B. C. Wilson, and M. S. Patterson, "Hybrid Monte Carlo-diffusion

theory modelling of light distributions in tissue," in *Laser Interaction with Tissue*, Proc. SPIE **908**, 20-28 (1988).

Chapter 3

Paper *II*

3.0.3 Introduction to Paper *II*

In Paper *I* it was shown that there exists a limit in the amount of information that can be extracted from a FD diffusive photon transport model for the two-layer geometry. In particular, the optical properties of a thin top layer were not well determined. It was concluded that this was because of the inadequacy of the diffusion approximation in describing photon transport at small source-detector distances. There, photons exit the medium only after a few scattering events and carry primarily information about the top layer. However, the transport of these photons is not well described by the diffusion approximation which is the forward model that was used in Paper *I* to infer the medium's optical properties. It was hoped that a more accurate photon transport model would improve the optical property estimates for the top layer. This was the motivation for the work presented in Paper *II*, where a

hybrid Monte Carlo (MC) - diffusion model for FD photon transport in a two-layer medium is presented. The MC component of the model takes into account the few-scatter events. The hybrid model is an extension of an idea first proposed by Wang and Jacques [J. Opt. Soc. Am. A **10,** 1746 (1993)] for a semi-infinite medium and steady-state illumination.

The work in this paper was performed by me under the supervision of Dr. Patterson. The MC component of the calculations was based on a MC code for photon transport in layered media previously developed by Dr. Farrell. The manuscript for Paper *II* was written by me and was edited by Drs. Patterson and Farrell.

3.0.4 Contents of Paper *II*

Monte Carlo diffusion hybrid model for photon migration in a two-layer turbid medium in the frequency domain.

George Alexandrakis, Thomas J. Farrell, and Michael S. Patterson

Department of Medical Physics, Hamilton Regional Cancer Centre

and McMaster University,

699 Concession Street, Hamilton, Ontario, Canada, L8V 5C2.

Applied Optics, Vol. 39, No. 13, 1 May 2000

Abstract

We propose a hybrid Monte Carlo (MC) diffusion model for calculating the spatially resolved reflectance amplitude and phase delay resulting from an intensity modulated pencil beam vertically incident on a two-layer turbid medium. The model combines the accuracy of MC at radial distances near the incident beam with the computational efficiency afforded by a diffusion calculation at further distances. This results in a single forward calculation several hundred times faster than pure MC, depending primarily on model parameters. Model predictions are compared with MC data for two cases that span the extremes of physiologically relevant optical properties: skin overlying fat and skin overlying muscle, both in the presence of an exogenous absorber. It is shown that good agreement can be achieved for radial distances from 0.5 to 20 mm in both cases. However, in the skin-on-muscle case the choice of model parameters and the definition of the diffusion coefficient can lead to some interesting discrepancies.

OCIS codes: 170.5280, 290.1990.

1. Introduction

Much effort has been devoted in recent years to quantify the optical properties of superficial biological tissue from spatially resolved reflectance measurements, as they can be used to infer important physiological information. Some examples include the non-invasive measurement of the concentration of chemotherapy drugs[1] or exogenous chromophores used for photodynamic cancer treatment[2,3] and the assesment of hemoglobin oxygenation in tissue.[4] The diffusion approximation to the Boltzmann equation has become the current standard for making theoretical predictions of spatially resolved reflectance because of its higher mathematical tractability compared to the general transport equation. In this regime, the parameters of interest are the absorption (μ_a) and scattering (μ_s) coefficients as well as an effective isotropic transport scattering coefficient $\mu_s{}' = \mu_s(1-g)$ where g is the average cosine of the deflection angle for a single scatter. To a first crude approximation, superficial tissue can be considered as a semi-infinite turbid medium. Diffuse reflectance models have been developed for that geometry in the steady state,[5,6] frequency,[7–9] and time-domains[8,10] corresponding to cw, intensity modulated, and pulsed sources respectively.

Naturally, the assumptions that are inherent in each model will be reflected in the accuracy of its predictions and, consequently, the accuracy of the optical properties that can be inferred from it. In reality, superficial tissue is a multi-layered structure[11] with each component having a different$\mu_s{}'$ and μ_a,[2,12] and potentially different pharmacokinetics of exogenous absorbers.[3] Recovery of the complete spatial distribution

of μ_a and μ_s' is the goal of optical tomography and it is an open question as to whether this can be accomplished with sufficient accuracy.[13]

In an attempt to mimic tissue structure more realisticaly than the semi-infinite medium model, an improved, yet still crude, two-layer turbid medium model of tissue structure may be utilized. In this model, a top layer thickness of $1 - 4$ mm that includes the epidermis and the dermis lies on top of a semi-infinite homogeneous medium that could be fat or muscle. Use of a semi-infinite medium photon migration model to interpret two-layer reflectance data has been demonstrated to be inadequate.[14,15] Hence an accurate model for photon migration in a two-layer turbid medium is required. Early research on this problem focused on modelling diffuse photon transport for steady-state illumination based on the Green's function[16,17] and random walk[18,19] approaches. Kienle *et al.*[20] have proposed a more accurate solution for the steady-state, frequency and time-domains. The accuracy and limitations of this model have been assessed with both simulated[21,22] and experimental[21] data. More recently, the validity of the two-layer model in analyzing time-resolved three-layer medium data has been explored,[23] and an ultra-fast solution for the time-domain has been developed.[24] Also, the feasibility of deducing the two-layer medium optical properties from amplitude-modulated plane wave reflectance data is being investigated.[25]

All of the above models are particular solutions of the diffusion equation. It is well known that diffusion is not an accurate description of the propagation of photons that

have undergone only a few scatters.[26] In the case of spatially resolved reflectance for a two-layer medium, such photons will have travelled primarily in the top layer and have exited the medium at radial distances close to the point of incidence of the pencil beam. The use of a diffusion model for source-detector separations less than 5 mm leads to erroneous results for the optical properties of both layers.[22] Thus an accurate model of photon migration at these distances should improve the quantification of the optical properties of the top layer.

One approach to overcome the limitations of diffusion is to develop a Monte Carlo (MC) diffusion hybrid model that combines the accuracy of MC at short distances with the computational efficiency of diffusion at larger ones. Wang and Jacques[27] were the first to propose such a model for the time-independent, spatially resolved reflectance from a semi-infinite medium. Wang[28] later extended that work to a slab geometry. In this work, we propose a MC-diffusion hybrid model for the spatially resolved reflectance from a two-layer turbid medium in the frequency-domain. The details of the model are explained in Section 2. In Section 2.A a simple-minded hybrid model is presented where the reflectance at short distances is computed by a mini-MC simulation and at larger ones by the known single point-source diffusion solution for a two-layer medium.[20] The shortcomings of this approach lead to the development of a distributed-source hybrid model which is explained in Section 2.B. The predictions of this hybrid model are compared to MC and pure diffusion data for two test cases of physiological relevance: skin on top of fat and skin on top of muscle, both in

the presence of an exogenous absorber. In both cases, significant improvements are observed over the pure diffusion predictions while the computation time is hundreds of times less than for pure MC.

2. Theory

A. Single-Source Hybrid Model

A MC simulation can provide an accurate prediction of the spatially resolved reflectance at short radial distances (ρ) from the point of incidence of a pencil beam, without having to track a huge number of photon histories. On the other hand, it has been shown that the point-source two-layer diffusion model is accurate for $\rho \gtrsim 5$ mm[20,22] for optical properties in the typical physiological range. Hence, a simple-minded strategy to combine the advantages of the two models would be the following:

Step 1: Make the *ad hoc* assumption that diffusion is accurate beyond a critical radial distance $\rho_c = 5$ mm.

Step 2: Track enough photon histories to obtain reliable reflectance estimates for distances up to ρ_c.

Step 3: Use the solution of the point-source two-layer diffusion equation as the reflectance prediction for all $\rho > \rho_c$. The point source solution is based on the assumption that the incident pencil beam results in an isotropic point source at a depth of one transport mean free path.

The MC component of the calculation is implemented using well-known methods[14] which will be discussed only briefly.

A photon is launched vertically into the medium and its history is tracked. A random number (RN , $0 < RN \leq 1$) is generated for each move, so that a photon path length (PL) is statistically determined by

$$PL = \frac{-ln(RN)}{(\mu_{a_i} + \mu_{s_i})} \quad , \quad i = 1, 2, \tag{1}$$

where μ_{a_i} and μ_{s_i} are the absorption and scattering coefficients of the top layer of thickness ℓ, and the bottom layer respectively. The photon then scatters into a new direction that is sampled from the Henyey-Greenstein phase function with an anisotropy factor $g = 0.8$.

The above process is repeated until the photon either exits the medium, or undergoes a Russian roulette if its history exceeds 500 scatters. This is done because photons that have undergone a large number of scatters have travelled deep into the medium and are unlikely to escape at radial distances of interest. Thus, it is computationally expedient to terminate their history and count their survival weight towards a different photon history. If a layer boundary is crossed, the fraction of the photon pathlength crossing that boundary is appropriately rescaled. A record of the number of scatters in the top ($NSCAT1$) and bottom ($NSCAT2$) layers is kept so that when a photon is scored on the exit surface, its final weight (W) is calculated as

$$W = a_1^{NSCAT1} \times a_2^{NSCAT2}, \tag{2}$$

where $a_i = \mu_{s_i}/(\mu_{a_i} + \mu_{s_i})$, $i = 1, 2$, is the albedo of each layer.

We implemented the two-layer diffusion component of the calculation using the previously reported solution of Kienle *et al.*[20]. It is assumed that all photons undergo their first scatter at a depth z_o of one transport mean free path

$$z_o = \frac{1}{(\mu_{a_1} + \mu_{s_1}')} = \frac{1}{mfp_1'}, \tag{3}$$

into the top layer and an isotropic photon source is established at that point. Continuity of fluence and flux are forced at the boundary between the two layers. The diffusion coefficients are defined as $D_i = 1/3(\mu_{a_i} + \mu_{s_i})$, $i = 1, 2$, for the top and bottom layers, respectively. The fluence is forced to zero at an extrapolated boundary $z_b = 2AD_1$, where $A = 1$ for refractive index-matched boundary conditions.[8] In this paper we present results for only such matched conditions. However, in the case of refractive index mismatched boundary at the tissue's top surface, the Fresnel boundary condition could be applied.[8] The photon weight is split into two fractions. The transmitted fraction is scored and the reflected fraction continues to be tracked as described above. The cylindrical symmetry of the problem is exploited to reduce its dimensionality by Fourier transforming its x and y components to a single spatial frequency variable s. An analytical solution can then be obtained for the Fourier transformed fluence $\phi_1(s, z, \omega)$:

$$\phi_1(s,z,\omega) = \frac{\sinh[\alpha_1(z_b+z_o)]}{D_1\alpha_1}\frac{D_1\alpha_1\cosh[\alpha_1(\ell-z)]+D_2\alpha_2\sinh[\alpha_1(\ell-z)]}{D_1\alpha_1\cosh[\alpha_1(\ell+z_b)]+D_2\alpha_2\sinh[\alpha_1(\ell+z_b)]} - \frac{\sinh[\alpha_1(z_o-z)]}{D_1\alpha_1}, \tag{4}$$

where $\alpha_i = (D_i s^2 + \mu_{a_i} + j\frac{\omega}{c_m})/D_i$, $i = 1,2$, c_m is the speed of light in both layers of the medium, ω is the circular amplitude modulation frequency of the incident light, and $j = \sqrt{-1}$.

The fluence in real space $\Phi_1(\rho,z,\omega)$ is then obtained by Fourier inversion of Eq. (4):

$$\Phi_1(\rho,z,\omega) = \frac{1}{2\pi}\int_0^\infty \phi_1(s,z,\omega)sJ_o(s\rho)\,ds, \tag{5}$$

where $J_o(s\rho)$ is the zeroth order Bessel function and $\rho = \sqrt{x^2+y^2}$.

Finally, the spatially resolved reflectance $R(\rho,\omega)$ for a refractive index matched boundary is given by[20]

$$R(\rho,\omega) = \frac{1}{4}\Phi_1(\rho,z=0,\omega) + \frac{1}{2}D_1\left.\frac{\partial\Phi_1(\rho,z,\omega)}{\partial z}\right|_{z=0}. \tag{6}$$

Because the incident beam is amplitude modulated, $R(\rho,\omega)$ is a complex quantity with an amplitude $ACR(\rho,\omega)$:

$$ACR(\rho,\omega) = \{(Im[R(\rho,\omega)])^2 + (Re[R(\rho,\omega)])^2\}^{1/2}, \tag{7}$$

and phase lag $\theta(\rho,\omega)$ relative to the source:

$$\theta(\rho,\omega) = \tan^{-1}\frac{Im[R(\rho,\omega)]}{Re[R(\rho,\omega)]}. \tag{8}$$

A schematic of this single-source hybrid model is shown in Fig. 1(a).

B. Distributed-Source Hybrid Model

The single-source hybrid model seems to be a rational first approach to a hybrid model, but three of its shortcomings are immediately apparent:

(*i*) A large number of MC histories are tracked without eventually being scored if photons exit the medium at $\rho > \rho_c$.

(*ii*) An *ad hoc* assumption is made about the range of validity of diffusion.

(*iii*) The assumption of a single isotropic photon source at one mfp' for all diffuse photons is not an accurate representation of the true photon distribution near the incident beam.

Wang and Jacques[27] have proposed a MC-diffusion hybrid model that avoids the shortcomings listed above. In this work, their strategy is followed closely, but it is adapted and modified for the case of a two-layer medium with amplitude modulated illumination. The steps of the calculation are as follows:

(*i*) Define a plane at a critical depth z_c inside the medium. This critical depth could be above or below the top layer boundary.

(*ii*) Track and score MC histories as described in Section 2.A. However, if a photon crosses the critical plane and its new statistically determined scatter direction is in the downward hemisphere, it is projected by one mfp' along that direction

and its history is terminated. At this point, the photon is considered to have established an isotropic point source. A schematic of steps (*i*) and (*ii*) is shown in Fig. 1(b).

(*iii*) Taking advantage of the cylindrical symmetry of the problem, the photon source locations are scored on a predetermined two-dimensional $\rho - z$ grid. The grid extends from $\rho_{min} = 0$ mm to $\rho_{max} = 10$ mm in the radial direction, and from $z_{min} = z_c$ to $z_{max} = z_c + 10$ mm in the $z-$direction. The resulting 10×10 mm square is divided in $N_\rho \times N_z$ equal parts ($N_\rho = N_z = 100$) such that the coordinates (ρ_i, z_i) of the center of each grid element are given by

$$\rho_i = (i - 0.5)\,\Delta\rho \qquad , \quad i = 1, N_\rho, \tag{9}$$

$$z_j = (j - 0.5)\,\Delta z \qquad , \quad j = 1, N_z, \tag{10}$$

where $\Delta\rho = \Delta z = \rho_{max}/N_\rho = z_{max}/N_z = 0.1$ mm. The dimensions of the grid were chosen to be large enough to collect virtually all photons that do not exit the medium.

(*iv*) A predetermined number of photon histories N_{ph} is tracked while the steps (*i*)-(*iii*) are followed. When the processes is complete, a fraction of the photons has exited the medium and has been scored as a direct MC contribution to the reflectance ($R_{MC}(\rho)$). The remaining photon histories have defined a spatially distributed photon source over which the two-layer point-source diffusion solution can be convolved, thus producing the diffusion contribution to the

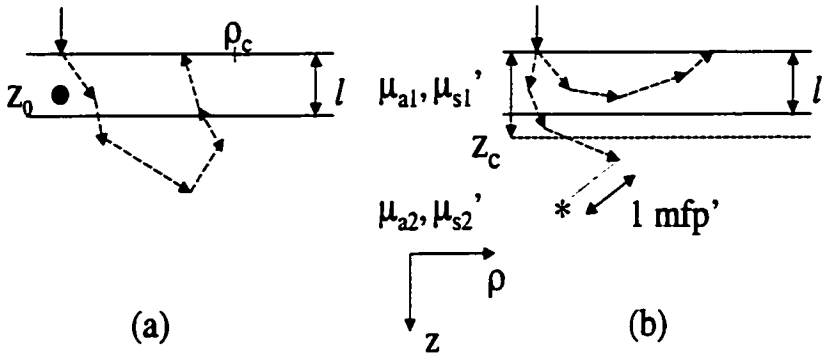

Fig. 1. (a) In the single-source hybrid model, photon histories are scored only if photons exit the medium at $\rho \leq \rho_c$. The reflectance calculation for $\rho > \rho_c$ is given by two-layer diffusion theory which assumes that all incident photons scatter at a depth $z_o = 1/(\mu_{a1} + \mu_{s1}')$. (b) The distributed-source hybrid model requires that if a photon migrates below a critical depth z_c ($\geq \ell$ or $< \ell$) and continues to move in the downward direction, its history is terminated. The photon's final location is defined to be one transport mean free path (mfp') along the direction of its last scatter. It is then assumed to have become an isotropic photon source (asterisk). All other photons are scored in a normal MC fashion.

reflectance ($R_{DIF}(\rho)$).

The details of calculating the $R_{MC}(\rho)$ and $R_{DIF}(\rho)$ reflectance components are as follows:

For the MC component, reflectance is scored in annuli of width $\Delta\rho_{MC} = 0.05$ mm. Hence, the total distributed photon weight $W_{MC}(\rho)$ in any radial bin of interest is

normalized to obtain

$$R_{MC}(\rho) = \frac{W_{MC}(\rho)}{2\pi\rho\Delta\rho_{MC}N_{ph}}. \tag{11}$$

The diffusion component of the calculation is somewhat more involved. Equation (4) is the Fourier space solution for each point source in the distributed- source grid at depth $z_o = z_{o_j}$, $j = 1, N_z$, where $z_{o_j} < \ell$. A corresponding solution for a point source in the bottom layer has not yet been reported because optical properties in the typical range will almost always define a point-source z_o [Eq. (3)] in the top layer. However, for the distributed source case, a large fraction of the scored photons define point sources at $z_{o_j} \geq \ell$ for which the corresponding Fourier space solution is required. The latter was obtained in a manner similar to that described in detail by Kienle *et al.*[20] for a point-source in the top layer. This was found to be:

$$\phi_2(s, z, \omega) = Y_2[Y_1 \cosh(\alpha_1(\ell - z)) + \sinh(\alpha_1(\ell - z))], \tag{12}$$

where

$$Y_1 = -\tanh(\alpha_1(\ell + z_b)), \tag{13}$$

and

$$Y_2 = \frac{1}{Y_1}\left\{\frac{1}{\left[\frac{1}{Y_1} - \frac{D_2\alpha_2}{D_1\alpha_1}\right]}\left[\frac{1}{Y_1\alpha_2 D_2}\sinh(\alpha_2(z_{o_j} - \ell)) - \frac{1}{\alpha_1 D_1}\cosh(\alpha_2(z_{o_j} - \ell))\right]\right.$$
$$\left. - \frac{1}{\alpha_2 D_2}\sinh(\alpha_2(z_{o_j} - \ell))\right\}, \tag{14}$$

and all other symbols are as defined for Eq. (4). Equations (4) and (12) collapse to the same limiting expression for $z_{o_j} = \ell$ which is as Eq. (12) but with a different

multiplicative factor Y_2':

$$Y_2' = \frac{1}{(Y_1\alpha_2 D_2 - \alpha_1 D_1)}. \tag{15}$$

The distributed photon source $[SRC(\rho_i, z_j), i = 1, N_\rho, j = 1, N_z]$ needs to be treated so that it can be incorporated naturally in a Fourier inversion procedure as was previously done for a single point-source of unit weight [Eq. (4)]. The first step is to normalize $SRC(\rho_i, z_j)$ so that the center of each grid element is considered to be a source of weight $W_{DIF}(\rho_i, z_j)$:

$$W_{DIF}(\rho_i, z_j) = \frac{SRC(\rho_i, z_j)}{2\pi\rho_i\Delta\rho\Delta z N_{ph}} \quad , \; i = 1, N_\rho, \;\; j = 1, N_z. \tag{16}$$

A Fourier transformed source term $W_{DIF}(s, z_{o_j})$ can now be defined:

$$W_{DIF}(s, z_{o_j}) = \int_0^\infty W_{DIF}(\rho, z_j)\rho J_o(s\rho)\, d\rho \quad , \; j = 1, N_z \tag{17}$$

The integral is performed using a 120-point Gaussian quadrature.[29] $W_{DIF}(\rho, z_j)$ is precomputed by a natural spline interpolation[29] of $W_{DIF}(\rho_j, z_j)$ [Eq. (16)] at all discrete ρ values required by the quadrature scheme.

Equation (17) defines a planar source in Fourier space for each depth z_{o_j}. A Fourier inversion scheme in the spirit of Eq. (4) can now be applied to calculate the contribution to the diffuse reflectance from each such source. The results can then be summed for all depths z_{o_j} to produce the total diffuse reflectance contribution $R_{DIF}(\rho)$:

$$R_{DIF}(\rho) = \sum_{j=1}^{N_z} \int_0^\infty W_{DIF}(s, z_{o_j})\phi_i(s, z_{o_j}, \omega) s J_o(s\rho)\, ds, \tag{18}$$

where $i = 1$ [Eq. (4)] if $z_{o_j} > \ell$, or 2 [Eq. (12)] if $z_{o_j} \leq \ell$. A 120-point Gaussian quadrature was used once more for the numerical integration. The oscillatory nature of the Bessel function $[J_o(s\rho)]$ calls for such a high order of quadrature. A factor of 2π coming from the volume element $2\pi s\, ds$ is cancelled by a factor $1/2\pi$ accompanying the Fourier inversion integral in Eq. (18).

Finally, once the MC [Eq. (11)] and diffuse [Eq. (18)] contributions to the reflectance have been calculated, they can be added to yield the total reflectance $R(\rho)$:

$$R(\rho) = R_{MC}(\rho) + R_{DIF}(\rho). \tag{19}$$

3. Results and Discussion

The predictions of the single and distributed-source models are compared to MC results for two sets of optical properties that span the extremes of the physiological range for superficial tissue at around 700 nm. These optical properties correspond to skin on top of fat and skin on top of muscle, both in the presence of an exogenous absorber (Table 1). The $\mu_s{}'$ values for skin and fat, as well as the skin thickness ℓ, used in this work are the average baseline values proposed by Farrell *et al.*[14] from a collection of human *in vivo* measurements. However, the μ_a's proposed[14] have been increased by a factor of ~ 2 to allow for the presence of an exogenous absorber (Table 1, skin-on-fat column). Pogue and Patterson[30] have reported optical properties deduced from *in vivo* measurements on rabbit muscle in the presence of an injected chromophore ($NiPcS_4$). They deduced $\mu_s{}'$ values in the $0.1-0.5$ mm^{-1} range

Table 1. The Two Sets of Tissue Optical Properties[a]

Tissue Optical Properties	Skin-on-Fat	Skin-on-Muscle
μ_{a1} / mm^{-1}	0.0775	0.0775
μ_{s1}' / mm^{-1}	1.49	1.49
μ_{a2} / mm^{-1}	0.007	0.0775
μ_{s2}' / mm^{-1}	1.0	0.4
ℓ / mm	1.5	1.5

[a]These two sets were used to generate MC data and compare them to model predictions correspond to skin on top of fat and skin on top of muscle, both in the presence of an exogenous absorber.

and μ_a values up to 0.055 mm^{-1}. For this work, a muscle μ_s' of 0.4 mm^{-1} and a μ_a equal to that of skin in the presence of absorber were chosen (Table 1, skin-on-muscle column). For all calculations performed, it may be assumed that the refractive index of tissues is 1.4, the tissue-surface boundary is refractive index-matched and the modulation frequency is $f = 100$ MHz, unless otherwise stated. In all pertinent figures, the reflectance amplitude $ACR(\rho, \omega)$ is plotted as $\ln[\rho^2 ACR(\rho)]$ for a given circular modulation frequency $\omega = f/2\pi$.

The performance of the single-source hybrid model (Section 2.A) for the above optical properties was investigated first. The mini-MC component of the simulations was run for 200,000 histories, and the diffusion contribution commenced at $\rho_c > 5$ mm . In Fig. 2 the reflectance amplitude is shown to be in good agreement with MC data for all radial distances in the skin-on-fat case. On the contrary, in the skin-on-

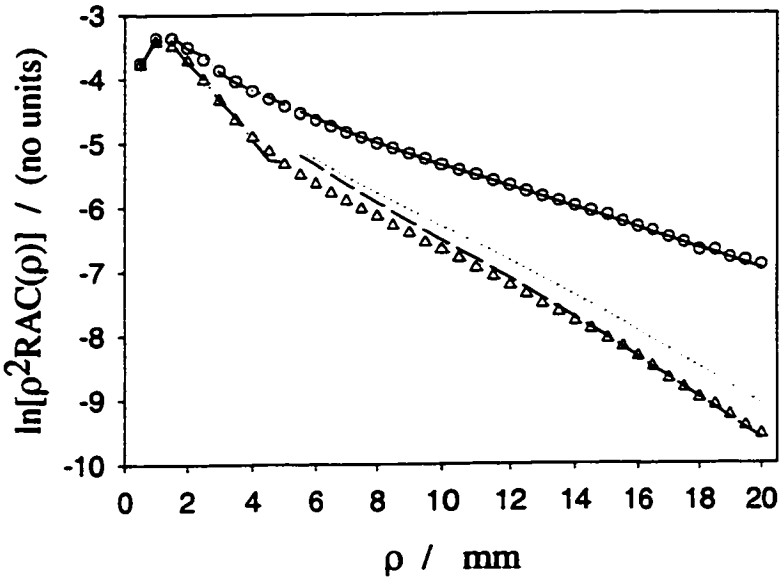

Fig. 2. The predicted frequency-domain reflectance amplitude from the single-source hybrid model (curves) are compared with the corresponding MC data (symbols) for the optical property sets shown in Table 1. Good agreement is observed with the skin-on-fat MC data (circles) where the mini-MC contribution (dash-dot-dot curve) connects seamlessly with the diffusion contribution (solid curve). On the contrary, the agreement is not good with skin-on-muscle MC data (triangles) where there is an abrupt gap between the mini-MC (dash-dot curve) and the diffusion contributions ($D_{w\mu_a}$, dashed curve, $D_{w/o\mu_a}$, dotted curve).

muscle case, a prominent break is observed in the predicted reflectance curve at $\rho = 5$ mm where the model switches from MC to diffusion. In this case, μ_{a2} is a sizable fraction of μ_{s2}' and, as a result, the definition of the diffusion coefficient affects the diffusion component of the calculation significantly. It can be seen that a diffusion

coefficient that includes absorption ($D_{w\mu_a} = 1/(\mu_s' + \mu_a)$) gives results that are closer to MC than the one without absorption ($D_{w/o\mu_a} = 1/\mu_s'$) although calculations based on the latter appear to have a slope that matches more closely that of MC data.

A similar break is observed in the phase delay *vs.* ρ data for the skin-on-muscle case, though it is not as pronounced as the one seen for the reflectance amplitude (results not shown). In the skin-on-fat case, $\mu_{s2}' \gg \mu_{a2}$, and no appreciable difference was observed if $D_{w\mu_a}$ or $D_{w/o\mu_a}$ were used.

It is clear that the single-source hybrid model is inadequate for modeling frequency-domain data over the full range of optical properties encountered physiologically. We believe that it is an instructive example of why a simple-minded hybrid model where the MC and diffusion components are completely independent will not work.

The distributed-source model was then investigated in the hope that the coupling between MC and diffusion would improve results. This is expected because a MC-defined distributed source at a depth greater than one mfp' is to replace a single point as the approximate photon source resulting from the incident pencil beam. However, it should be acknowledged that the fact that μ_{a2} is sizable compared to μ_{s2}' remains a fundumental limitation of diffusion and, consequently, of the hybrid model. Initially, a critical depth $z_c = 1$ mm and 100,000 photon histories were utilized, as was proposed for the semi-infinite medium hybrid model by Wang and Jacques.[27] Figure 3 shows the reflectance amplitude results for the skin-on-fat case. Good agreement between MC (circles) and the hybrid model (solid curve) is observed for all ρ. Pure diffusion

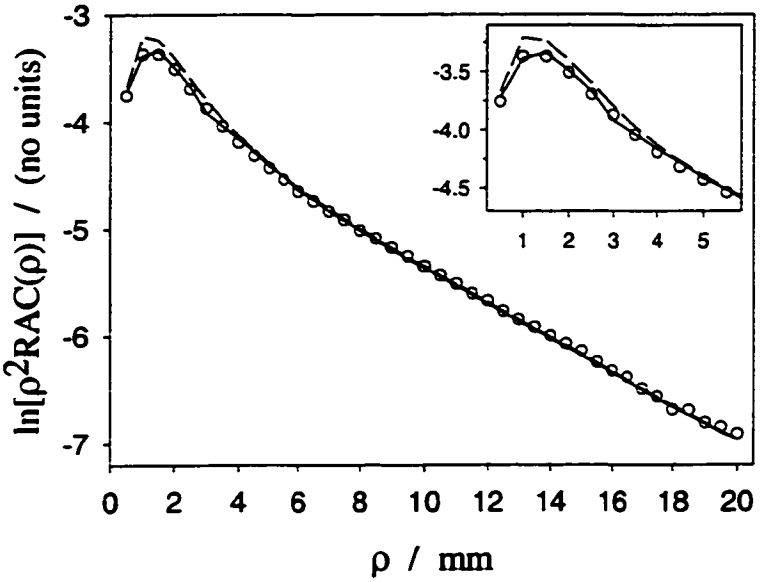

Fig. 3. Good agreement is observed between MC data (circles) and the distributed source hybrid model (solid curve) in the skin-on-fat case. Pure diffusion (dashed curve) also performs well except for $\rho < 5$ mm (inset). Simulation parameters: $f = 100$ MHz, $z_c = 1$ mm, 100,000 photon histories.

(dashed curve) also performs well except for $\rho < 5$ mm, as shown in the inset. As before, the choice of $D_{w\mu_a}$ or $D_{w/o\mu_a}$ for the skin-on-fat case is immaterial.

The predictions of the distributed-source hybrid model for the same simulation settings in the skin-on-muscle reflectance amplitude case are shown in Fig. 4. Some discrepancies are seen with respect to MC data (triangles) both at small and large ρ. In the $D_{w\mu_a}$ case (solid curve), fairly good agreement is achieved for $\rho < 5$ mm, but the model then obtains the wrong slope and predictions end up underestimating the true values for $\rho > 10$ mm. In contrast to that, for a $D_{w/o\mu_a}$ choice (dash-dot-dot

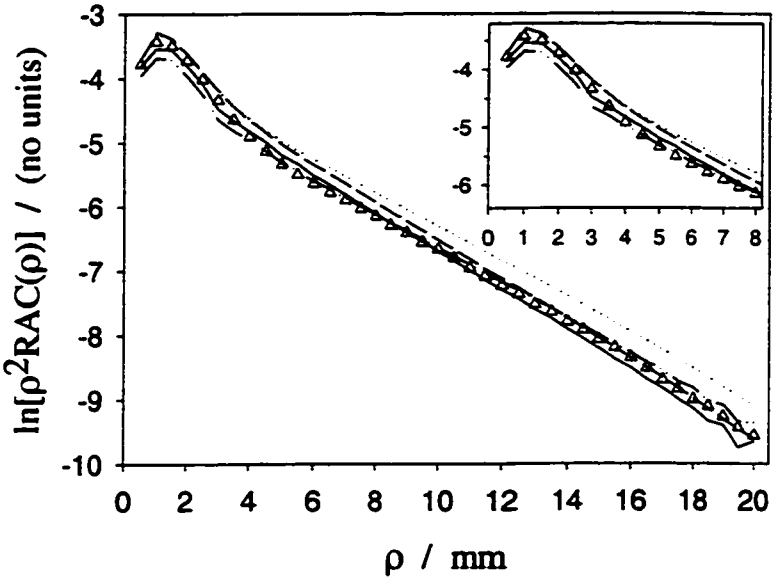

Fig. 4. Distributed source hybrid model appears to be less sensitive to the definition of the diffusion coefficient ($D_{w\mu_a}$, solid curve; $D_{w/o\mu_a}$, dash-dot-dot curve) relative to pure diffusion ($D_{w\mu_a}$, dashed curve; $D_{w/o\mu_a}$, dotted curve) in the skin-on-muscle case. Simulation parameters $f = 100$ MHz, $z_c = 1$ mm, 100,000 photon histories.

curve) the amplitude for $\rho < 4$ mm is underestimated, but in the $4 \leq \rho \leq 7$ mm range it performs better than $D_{w/o\mu_a}$. At large ρ the slightly erroneous slope leads to an overestimation of the MC data. The discrepancies between pure diffusion and MC data for $\rho > 5$ mm have been previously described in Fig. 2 as part of the diffusion component of the single-source hybrid model. Surprisingly, diffusion predictions are close to MC for both the $D_{w\mu_a}$ (dashed curve) and $D_{w/o\mu_a}$ cases for $\rho < 3$ mm. Both curves then proceed to considerably overestimate MC data, $D_{w\mu_a}$ in the $3 \leq \rho \leq 12$ mm range, and $D_{w/o\mu_a}$ for all $\rho > 3$ mm. Although the hybrid model predictions

seem to be less sensitive to the definition of the diffusion coefficient relative to pure diffusion, the latter seems to be performing somewhat better using $D_{w\mu_a}$ at large ρ. It is also interesting to note that the hybrid model predictions become noisy at large ρ. This is presumed to be because of the increased reflectance contribution from photon sources at large ρ and z, deep in the medium, due to their increased proximity to the point of interest on the surface. Inevitably, those sources are created by accumulation of only a small fraction of the injected photons, and are consequently noisy.

Similar trends are observed for the phase delay predictions, yet with differences that are less pronounced between the different simulation conditions described above. Good agreement is observed with predictions in the skin-on-fat case (Fig. 5). However, no significant difference is observed between $D_{w\mu_a}$ and $D_{w/o\mu_a}$ for the skin-on-muscle case (Fig. 6), in contrast to what was found for the reflectance amplitude. The hybrid model data appear to have a slightiy different slope and a small offset relative to the MC data. This leads to an overestimation of the true values for $\rho \leq 5$ mm and a small underestimation at large ρ. Interestingly, the diffusion data have a similar slope relative to the hybrid model, but no offset. This leads to them being more accurate than the hybrid model for $\rho \leq 4$ mm (inset), but to also consistently underestimate MC data at large ρ.

The distributed-source hybrid model clearly performs better than diffusion. However, for the skin-on-muscle case, where μ_{a2} is not negligible compared to μ_{s2}', some

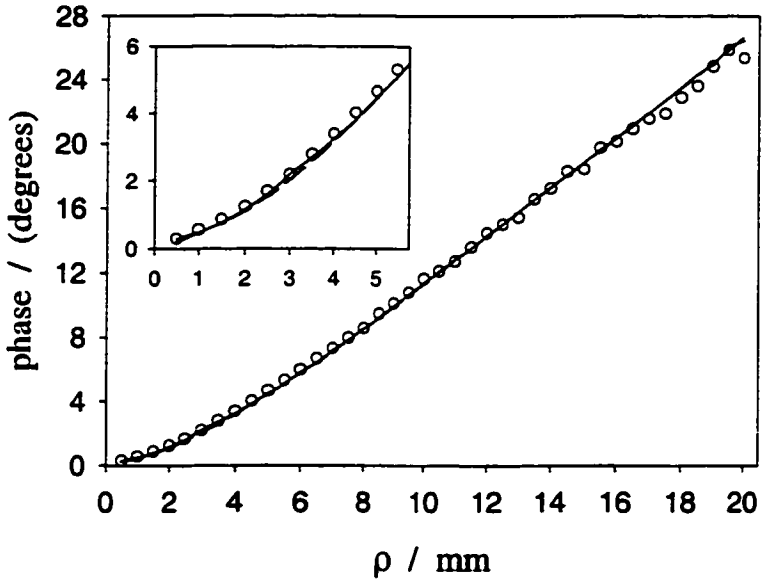

Fig. 5. Model predictions of phase delay for the skin-on-fat case. Symbol representation follows that of Fig. 3.

discrepancies with MC data are still seen at small ρ (Figs. 5 and 6). This is presumed to be because the small value of z_c (= 1 mm) allows for a sizable contribution from the diffusion component of the calculation even at small ρ. In an attempt to improve the model's performance z_c was increased to 4 mm. Unfortunately, increasing the critical depth decreases the fraction of the photons scored, and hence the noise, in the distributed-source term. It was found that the number of photon histories that needs to be tracked should be increased at least fourfold, as z_c was, in order to calculate the reflectance to acceptable precision. It was decided that 800,000 photon histories would be tracked per simulation to largely eliminate any such noise considerations. This increased the computation time, as performed on an Ultra-1 Sparc workstation,

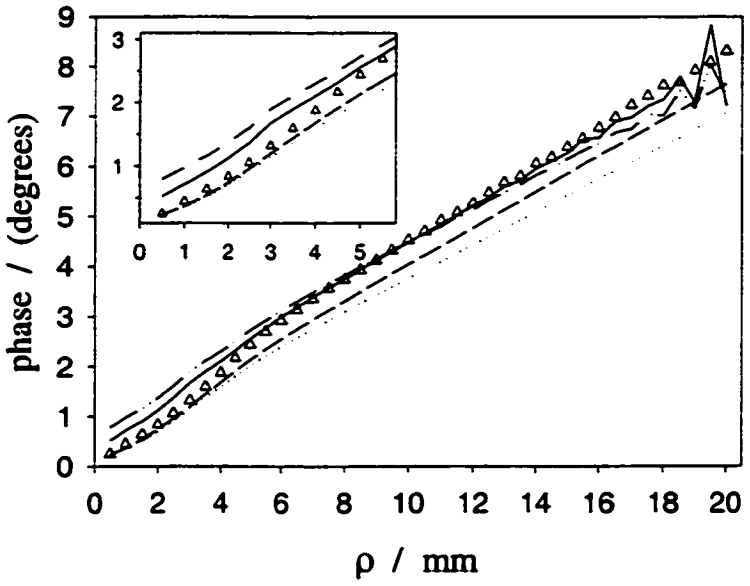

Fig. 6. Model predictions for phase delay for the skin-on-muscle case. Symbol representation follows that of Fig. 4.

from 12 seconds for $z_c = 1$ mm to 90 seconds for $z_c = 4$ mm. This is to be compared with the several hours required for a pure MC simulation. Figure 7 shows the reflectance amplitude calculated under these more computationally demanding simulation conditions. As before, the skin-on-fat calculation (dashed curve) agrees nicely with MC data (circles). For the skin-on-muscle case (triangles), the predictions for $D_{w\mu_a}$ (solid curve) and $D_{w/o\mu_a}$ (dash-dot curve) differ very little and are significantly improved relative to the $z_c = 1$ mm case. The inclusion of μ_a in $D_{w\mu_a}$ leads to an underestimation of the MC data at large ρ and also makes distributed-source noise effects more conspicuous. The change of z_c also appears to affect the slope of the reflectance data at large ρ. In contrast to the $z_c = 1$ mm case, $D_{w/o\mu_a}$ gives accurate

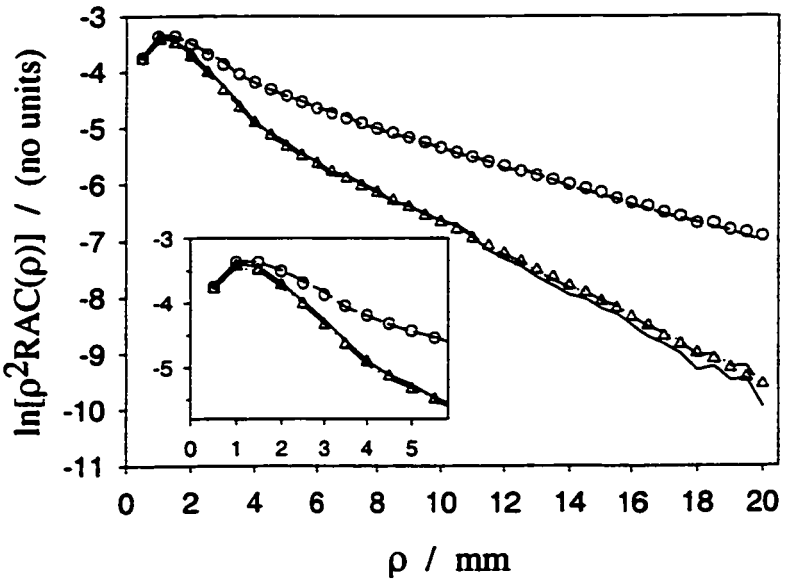

Fig. 7. When z_c is increased to 4 mm agreement with MC data (fat, circles; muscle, triangles) improves relative to the $z_c = 1$ mm case. Good agreement is observed for the skin-on-fat predictions of the hybrid model (solid curve). Differences between $D_{w\mu_a}$ (solid curve) and $D_{w/o\mu_a}$ (dash-dot-dot curve) diminish relative to Fig. 4 and are now closer to MC data (inset). Simulation parameters $f = 100$ MHz, 800,000 photon histories.

results at large ρ whereas $D_{w\mu_a}$ results in a slope that leads to an underestimation of the MC data. A slight improvement in the predicted phase delay [Fig. (8)] is also seen both at small ρ (inset) and at large ρ relative to the $z_c = 1$ mm case.

Similar patterns in model predictions were observed for modulation frequencies other than $f = 100$ MHz, with $D_{w/o\mu_a}$ performing better than $D_{w\mu_a}$ at large ρ. As an example, in Fig. 9 the predicted reflectance amplitude for $D_{w/o\mu_a}$ at $f = 1$ GHz

is shown to compare well with MC data (symbols) for both the skin-on-fat (circles, dashed curve) and skin-on-muscle (triangles, dash-dot-dot curve) combinations. Similar agreement was observed for the phase delay (results not shown).

The frequency-domain reflectance from a semi-infinite medium was also calculated using the two-layer distributed source model by setting the μ_{a1}, μ_{s1}' of the top layer equal to those of fat or muscle [μ_{a2}, μ_{s2}' (Table 1)]. The top layer thickness ℓ can take any value. In the case of fat as a bottom layer, a $z_c = 1$ mm and 100,000 photon histories were adequate to accurately model MC data, which is consistent with Wang and Jacques.[27] However, in the case of muscle as the bottom layer, discrepancies at small ρ similar to those seen in Fig. 4 were observed. As in the two-layer case (Figs. 7 and 8), a $z_c = 4$ mm gave improved model predictions and diminished differences between $D_{w\mu_a}$ and $D_{w/o\mu_a}$.

Recently, evidence for a diffusion coefficient independent of absorption has been proposed.[31,32] In contrast to that, Durian[33] has proposed that a $D_{1/3} = 1/3(\mu_s' + \mu_a/3)$ gives better agreement with MC data. Aronson and Corngold[34] propose a $D_\alpha = 1/3(\mu_s' + \alpha\mu_a)$ with $\alpha = 1 - (4/5)(1 - f_1)/(1 - f_2)$ for small absorption, where $f_\ell = g^\ell$ are the partial wave expansion coefficients for a Henyey-Greenstein phase function of anisotropy g. For $g = 0.8$ this expression gives $\alpha = 0.56$. Throughout the above test cases of the distributed-source hybrid model the $D_{w\mu_a}$ and $D_{w/o\mu_a}$ definitions of the diffusion coefficient were explored for the skin-on-muscle case. The above two alternative definitions[33,34] were also investigated. Since only a fraction of

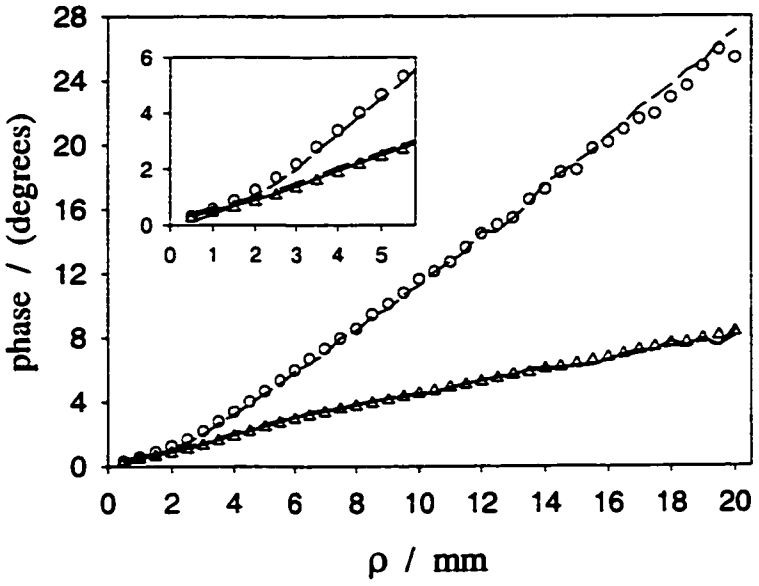

Fig. 8. Phase delay model predictions for $z_c = 4$ mm. The symbol representation follows that of Fig. 7.

the full μ_a is added to μ_s', it was not surprising to find that the reflectance results they produced fell between those of $D_{w\mu_a}$ and $D_{w/o\mu_a}$. Thus, for $z_c = 1$ mm (Fig. 4), $D_{1/3}$ and D_α both gave improved results at large ρ, as $D_{w/o\mu_a}$ overestimated and $D_{w\mu_a}$ underestimated the MC data. On the other hand, it was found that $D_{w\mu_a}$ performed better in the pure diffusion calculations (Fig. 4, dashed curve). Finally, in the hybrid model calculations with $z_c = 4$ mm it was $D_{w/o\mu_a}$ that gave a slope which best matched the MC data at large ρ (Fig. 7, dash-dot-dot curve). It thus appears that a choice of $D_{w/o\mu_a}$ and $z_c = 4$ mm is the only one that performs well for all ρ, from 0.5 mm to 20 mm, for both sets of optical properties explored in this work (Table 1) that span the physiological range for superficial tissue. The dependence of model

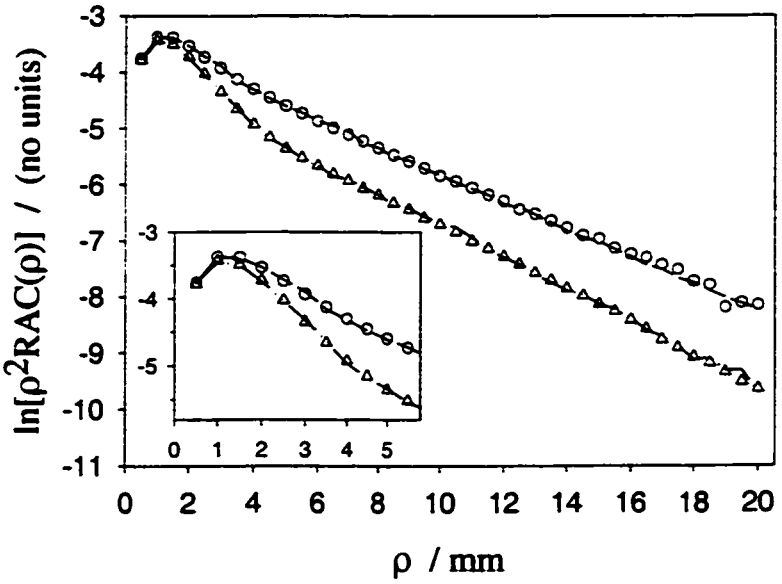

Fig. 9. The reflectance amplitude predicted by the hybrid model (curves) at $f = 1\ GHz$ ($D_{w/o\mu_a}$, $z_c = 4$ mm) agree well with the corresponding MC data (symbols) for both skin-on-fat (circles, solid curves) and skin-on-muscle (triangles, dotted curve). The agreement appears to be good both at small ρ (inset) and at large ρ.

predictions on the definition of the diffusion coefficient is a feature of the model and cannot be used to make general conclusions about the correct definition for other applications.

4. Conclusions

A spatially resolved reflectance hybrid model in the frequency domain was developed for photon migration in a two-layer turbid medium. It combines the accuracy of MC at short distances with the computational expediency and accuracy of diffusion

further from the source. Model predictions were tested against MC data for two cases that span the extremes of physiologically relevant optical properties: skin-on-fat and skin-on-muscle, both in the presence of an exogenous absorber (Table 1).

First, a simple-minded model was presented where MC is the only contribution to reflectance within a predefined radial distance ($\rho_c \leq 5$ mm) and the single point-source two-layer diffusion solution takes over at larger ρ. It was shown that this model is inadequate for the case where μ_a was sizable compared to μ_s' for the bottom layer.

A hybrid model was then presented in which MC-generated photons that travel close to and exit the surface are scored, but others traveling downward deeper than a critical depth z_c in the medium define a distributed photon source to be convolved with the two-layer diffusion solution. This model follows the principles first proposed by Wang and Jacques[27] for a semi-infinite medium and steady-state illumination. The frequency-space solution of the diffusion equation for a source in the bottom layer had to be found in order to implement the model [Eq. (12)]. The MC-defined distributed source term was also converted to frequency-space [Eq. (17)] so that it naturally blended into the Fourier inversion procedure that yielded the real-space reflectance [Eq. (18)]. The distributed-source hybrid model always yielded improved results relative to a pure diffusion calculation in the skin-on-fat case where $\mu_{s2}' \gg \mu_{a2}$. However, in the skin-on-muscle case and $z_c = 1$ mm, where μ_{a2} is comparable to μ_{s2}' and the diffusion contribution is a sizable fraction of the total, the model did not perform as well at small ρ (Figs. 4 and 6). It appeared though, that model predictions

were less sensitive than pure diffusion with respect to the definition of the diffusion coefficient ($D_{w\mu_a}$, $D_{w/o\mu_a}$). When the MC contribution at small ρ was increased by setting z_c to 4 mm, and a concomitant increase in photon histories was tracked, good agreement with MC data was observed (Figs. 7 and 8). Similar trends were observed at modulation frequencies higher than $f = 100$ MHz (eg. Fig. 9, $f = 1$ GHz).

The differences observed between the $D_{w\mu_a}$ and $D_{w/o\mu_a}$ in the skin-on-muscle case raised the question of what is the optimal choice for the diffusion coefficient. Alternative definitions were explored [33,34] in addition to the above two. It was found that the diffusion coefficient that best matched MC data was a function of the model's parameters which effectively shows the limitation of diffusion when μ_{a2} is sizable compared to μ_{s2}'. A choice of $z_c = 4$ mm and $D_{w/o\mu_a}$ was the only one that resulted in accurate model predictions for both sets of optical properties explored in this work (Table 1) for all radial distances ρ up to 20 mm.

Future research will focus on incorporating the above model as part of an iterative fitting algorithm with the goal of obtaining improved optical property estimates, especially for the top layer, relative to pure diffusion[22]. Any such possible improvements for frequency-domain measurements on two-layer phantoms[35] will also be explored along with *in vivo* applications.

We are thankful to Dr. William Prestwich and Dr. Alwin Kienle for their helpful suggestions. This research was supported by the National Institutes of Health grant

P01—CA43892.

References

1. J. R. Mourant., T. M. Johnson, G. Los, and I. Bigio, "Non- invasive measurements of chemotherapy drug concentrations in tissue: preliminary demonstrations of *in vivo* measurements," Phys. Med. Biol. **44,** 1397-1417 (1999).

2. M. S. Patterson, B. C. Wilson, J. W. Feather, D. M. Burns, and W. Pushka, "The measurement of dihematoporphyrin ether concentration in tissue by reflectance spectrophotometry," Photochem. Photobiol. **46,** 337-343 (1987).

3. R. A. Weersink, J. E. Hayward, K. R. Diamond, and M. S. Patterson, "Accuracy of non-invasive *in vivo* measurements of photosensitizer uptake based on a diffusion model of reflectance spectroscopy," Photochem. Photobiol. **66,** 326-335 (1997).

4. S. Fantini, M. A. Franceschini-Fantini, J. S. Maier, S. A. Walker, B. Barbieri, and E. Gratton, "Frequency-domain multichannel optical detector for noninvasive tissue spectroscopy and oximetry," Opt. Eng. **34,** 32-42 (1995).

5. T. J. Farrell, and M. S. Patterson, "A diffusion theory model of spatially resolved, steady-state diffuse reflectance for the non-invasive determination of tissue optical properties *in vivo*," Med. Phys. **19,** 879-888 (1992).

6. A. Kienle, L. Lilge. M. S. Patterson, R. Hibst, R. Steiner, and B. C. Wilson, "Spatially resolved absolute diffuse reflectance measurements for noninvasive determination of the optical scattering and absorption coefficients of biological tissue," Appl. Opt. **35,** 2304-2314 (1996).

7. M. S. Patterson, J. D. Moulton, B. C. Wilson, K. W. Berndt, and J. R. Lakowicz, "Frequency-domain reflectance for the determination of the scattering and absorption properties of tissue," Appl. Opt. **30,** 4474-4476 (1991).

8. R. C. Haskell, L. O. Svaasand, T.-T. Tsay, T.-C. Feng, M. S. McAdams, and B. J. Tromberg, "Boundary conditions for the diffusion equation in radiative transfer," J. Opt. Soc. Am. A **11,** 2727-2741 (1994).

9. S. Fantini, M. A. Franceschini, and E. Gratton, "Semi-infinite-geometry boundary problem for light migration in highly scattering media: a frequency-domain study in the diffusion approximation," J. Opt. Soc. Am. B **11,** 2128-2138 (1994).

10. A. Kienle, and M. S. Patterson, "Improved solutions for the steady-state and the time-resolved diffusion equations for reflectance from a semi-infinite turbid medium," J. Opt. Soc. Am. A **14,** 246-254 (1997).

11. P. L. Williams, and R. Warwick, "The integument," in *Gray's Anatomy,* 36th ed. (Churchill Livingstone, Edindburgh,UK,1986), pp.1216-1222.

12. R. Marchesini, A. Bertoni, S. Andreola, E. Melloni, and A. E. Sichirollo, "Extinction and absorption coefficients and scattering phase functions of human tissues *in vitro*," Appl. Opt. **28,** 2318-2324 (1989).

13. S. R. Arridge, "Why optical tomography is hard," in *Biomedical Optics: New Concepts in Therapeutic Laser Applications, Novel Biomedical Optical Spectroscopy, Imaging, and Diagnostics, Advances in Optical Imaging, Photon Migration, and Tissue Optics,* OSA Technical Digest Series (Optical Society of America, Washington, D.C., 1999), paper AMB1-1.

14. T. J. Farrell, M. S. Patterson, and M. Essenpreis, "Influence of layered tissue architecture on estimates of tissue optical properties obtained from spatially resolved diffuse reflectometry," Appl. Opt. **37,** 1958-72 (1998).

15. M. A. Franceschini, S. Fantini, L. A. Paunescu, J. S. Maier, and E. Gratton, "Influence of a superficial layer in the quantitative spectroscopic study of strongly scattering media," Appl. Opt. **37,** 7447-7458 (1998).

16. S. Takatani, and M. D. Graham, "Theoretical analysis of diffuse reflectance from a two-layer tissue model," IEEE Trans. Biomed. Eng. **BME-26,** 656-664 (1979).

17. J. M. Schmitt, G. X. Zhou, E. C. Walker, and R. T. Wall, "Multilayer model of photon diffusion in the skin," J. Opt. Soc. Am. A **7,** 2141-2153 (1990).

18. H. Taitelbaum, S. Havlin, and G. Weiss, "Approximate theory of photon migration in a two-layer medium," Appl. Opt. **28** 2245-2249 (1989).

19. I. Dyan, S. Havlin, and G. H. Weiss, "Photon migration in a two-layer turbid medium. A diffusion analysis," J. Mod. Opt. **39,** 1567-1582 (1992).

20. A. Kienle, M. S. Patterson, N. Utke, R. Bays, G. Wagnières, and H. van den Bergh, "Determination of the optical properties of two-layer turbid media," Appl. Opt. **37,** 779-791 (1998).

21. A. Kienle, T. Glanzmann, G. Wagnières, and H. van den Bergh, "Investigation of two-layered turbid media with time-resolved reflectance," Appl. Opt. **37,** 6852-6862 (1998).

22. G. Alexandrakis, T. J. Farrell, and M. S. Patterson, "Accuracy of the diffusion approximation in determining the optical properties of a two-layer turbid medium," Appl. Opt. **37,** 7401-7410 (1998).

23. A. Kienle, and T. Glanzmann, "*In vivo* determination of the optical properties of muscle with time-resolved reflectance using a layered model," Phys. Med. Biol. submitted (1999).

24. J.-M. Tualle, E. Tinet, J. Prat, B. Gelebart, and S. Avrillier, "Light propagation in layered turbid media: A new analytical model for ultrafast calculation of the direct problem," in *Biomedical Optics: New Concepts in Therapeutic*

Laser Applications, Novel Biomedical Optical Spectroscopy, Imaging, and Diagnostics, Advances in Optical Imaging, Photon Migration, and Tissue Optics, OSA Technical Digest Series (Optical Society of America, Washington, D.C., 1999), paper AMA3-1.

25. L. O. Svaasand, T. Spott, J. B. Fishkin, T. Pham, B. J. Tromberg, and M. W. Berns, "Reflectance measurements of layered media with diffuse photon-density waves: a potential tool for evaluating deep burns and subcutaneous lesions," Phys. Med. Biol. **44,** 801-813 (1999).

26. A. Ya Polishchuk, and R. R. Alfano, "Photon diffusion in the velocity sphere," Opt. Lett. **21,** 916-918 (1996).

27. L. Wang, and S. L. Jacques, "Hybrid model of Monte Carlo simulation and diffusion theory for light reflectance by turbid media," J. Opt. Soc. Am. A **10,** 1746-1752 (1993).

28. L. Wang, "Rapid modeling of diffuse reflectance of light in turbid slabs," J. Opt. Soc. Am. A **15,** 936-944 (1998).

29. W. H. Press, S. A. Teukolsky, W. T. Vetterling, and B. P. Flannery, *Numerical Recipes—The Art of Scientific Computing,* 2nd edition, (Cambridge U. Press, NY, 1996).

30. B. W. Pogue, and M. S. Patterson, "Error assessment of a wavelength tunable

frequency domain system for noninvasive tissue spectroscopy," J. Biomed. Opt. **1,** 311-323 (1996).

31. M. Bassani, F. Martelli, G. Zaccanti, and D. Contini, "Independence of the diffusion coefficient from absorption: experimental and numerical evidence," Opt. Lett. **22,** 853-855 (1997).

32. T. Durduran, A. G. Yodh, B. Chance, and D. A. Boas, "Does the photon-diffusion coefficient depend on absorption?," J. Opt. Soc. Am. A **14,** 3358-3365 (1997).

33. D. J. Durian, "The diffusion coefficient depends on absorption," Opt. Lett. **23,** 1502-1504 (1998).

34. R. Aronson, and N. Corngold, "Photon diffusion coefficient in an absorbing medium," J. Opt. Soc. Am. A **16,** 1066-1071 (1999).

35. G. Alexandrakis, R. A. Weersink, J. T. Bruulsema, and M. S. Patterson, "Estimation of optical properties of two-layer tissue simulating phantoms from spatially resolved frequency-domain reflectance," in *Optical Tomography and Spectroscopy of Tissue III,* B. Chance, R. R. Alfano, and B. J. Tromberg, eds., Proc. SPIE **3597,** 155-163 (1999).

Chapter 4

Paper *III*

4.0.5 Introduction to Paper *III*

Once the hybrid two-layer MC-diffusion FD model was developed it was time to find out if it can indeed provide improved optical property estimates relative to the corresponding pure diffusion model presented in Paper *I*. Because of the increased computational burden of the hybrid model relative to pure diffusion a new efficient global optimization method had to be introduced, which made iterative fitting of the hybrid model possible. The capacity of the hybrid model to determine all of the optical properties of a two-layer medium was explored with both MC-simulated and experimental measurements. Two-layer tissue simulating phantoms were utilized for the latter. The optical property sets explored correspond to skin on top of fat or muscle in the presence of an exogenous chromophore.

The theoretical calculations were performed by me under the supervision of Dr.

Patterson. The experimental set-up and data acquisition procedure for the two-layer phantom experiments was developed by Dr. Faris of SRI International and myself. The two-layer phantom experiments were performed by Mr. Busch who was a year 2000 summer student for SRI International, working under the supervision of Dr. Faris. The probe design was a suggestion of Dr. Patterson. The low noise FD system that was used for the experimental measurements had been previously built and characterized by Dr. Faris and collaborators.

4.0.6 Contents of Paper *III*

Determination of the optical properties of two-layer turbid media using a frequency domain hybrid Monte Carlo diffusion model

George Alexandrakis, David R. Busch, Gregory W. Faris, and Michael S. Patterson

G. Alexandrakis and M. S. Patterson are with the Department of Medical Physics, Hamilton Regional Cancer Centre and McMaster University, 699 Concession Street, Hamilton, Ontario, Canada, L8V 5C2.

D. R. Busch and G. W. Faris are with SRI International, Molecular Physics Laboratory, 333 Ravenswood Avenue, Menlo Park, CA 94025.

Submitted electronically to *Applied Optics* on 17 November 2000

(Manuscript No. OT 17583)

Abstract

The general two-layer inverse problem in biomedical photon migration is to estimate the absorption and scattering coefficients of each layer as well as the top layer thickness. We attempted to solve this problem using experimental and simulated spatially resolved frequency domain (FD) reflectance for optical properties typical of skin-on-muscle or skin-on-fat in the near infrared. Two forward models of light propagation were used: a two-layer diffusion solution [Appl. Opt. **37,** 779 (1998)] and a hybrid Monte Carlo (MC) diffusion model [Appl. Opt. **37,** 7401 (1998)]. MC simulated FD reflectance data were fitted as relative measurements to the hybrid and pure diffusion models. It was found that the hybrid model could determine all of the optical properties of a two-layer medium to ~5%. Also, the same accuracy could be achieved by fitting MC simulated CW reflectance data as absolute measurements, but fitting them as relative ones is an ill-posed problem. In contrast, two-layer diffusion could not retrieve the top layer optical properties as accurately for FD data and was ill-posed for both relative and absolute CW data. The hybrid and pure diffusion models were also fitted to experimental FD reflectance measurements from two-layer tissue simulating phantoms representative of skin-on-fat and skin-on-muscle baseline optical properties. Both the hybrid and diffusion models could determine the optical properties of the lower layer. The hybrid model demonstrated its potential to retrieve quantitatively the transport scattering coefficient of skin (the upper layer), which was not possible with the pure diffusion model. Systematic discrepancies be-

tween model and experiment may compromise the accuracy of the deduced top layer optical properties. Identifying and eliminating such discrepancies is critical to the practical applicability of the method.

Key words: Photon migration, frequency domain, two-layer turbid medium, tissue-simulating phantoms, diffusion equation, Monte Carlo, hybrid model, tissue optics.

1. Introduction

The optical absorption and scattering coefficients of tissue can provide useful information about its composition, physiological function and structure. For example, the absorption coefficient can be used to deduce the concentration of endogenous (e.g. hemoglobin[e.g.1,2]) or exogenous (e.g. photosensitizers for photodynamic therapy[3,4]) chromophores. Temporal changes in the absorption can be related to physiological functions, such as drug uptake and clearance[4,5]. The scattering coefficient has been related to tissue glucose concentration,[6] structural,[7,8] and pathological changes in tissue.[9] Optical methods have been used *in vivo* to probe skin, muscle, liver, breast, and brain, as well as abnormalities in these tissues such as tumors. In an ideal situation the tissue of interest is accessible to direct measurement but this is not often the case in practice. Measurements may have to be performed through an intervening layer of skin, muscle, or bone. In some cases it may be desirable to measure the optical properties of two tissue layers simultaneously – for instance, the uptake of a photosensitizer in a tumor and the overlying normal skin. Thus, while early progress in noninvasive optical measurements was made by considering tissue to be a uniform, semi-infinite medium, many applications require a more realistic physical model.

A simple two-layer model may be adequate for many situations. The problem of particular interest in this paper is that in which a layer of skin 1-4mm thick covers a much thicker (essentially semi-infinite) layer of fat or muscle. Of course, skin itself

is a layered structure, but the dermis is much thicker than the other two layers and useful information may be gained despite this simplification. In this case, the goal is to estimate five quantities: μ_{a1}, the absorption coefficient of the skin; μ_{s1}', the reduced scattering coefficient of the skin; ℓ, the skin thickness; and μ_{a2} and μ_{s2}', the corresponding properties of the fat or muscle. This problem has been addressed by a number of researchers.[10-12] Estimates of the five optical properties (or a subset of these) are obtained by minimizing the difference between optical measurements and corresponding predictions of a forward model of light propagation in the two-layer structure. The measurements consist of some characterization of incident light which is scattered out of tissue, i.e. the diffuse reflectance. The incident light may be continuous wave (CW), pulsed, or intensity modulated and the reflectance measurements may correspondingly be CW, time-resolved, or frequency domain (FD). Measurements may also be performed at multiple locations on the surface, so that the reflectance at a range of source-detector distances is used to solve the inverse problem. In this paper, spatially resolved FD reflectance is the quantity used.

Despite considerable activity in this area, the general skin-on-fat or skin-on-muscle problem has not been solved. Useful results have been obtained when one or more or the five parameters is known[10,12] or when attempts have been made to recover the optical properties of only the bottom layer.[13,14] In earlier work[11] it was shown that the general problem could not be solved when a two-layer diffusion model was used as the forward model of reflectance. This is because the diffusion model is

inaccurate at small source-detector distances but it is these distances that provide information about the skin layer. To overcome this limitation, a hybrid Monte Carlo (MC) diffusion model was recently developed.[15] This model maintains the accuracy of MC at short distances but provides the computational efficiency of diffusion farther from the source. It also offers improved performance when the absorption coefficient is a significant fraction of the reduced scattering coefficient - a condition under which pure diffusion is known to fail.[16] In this paper we return to the general skin-on-muscle and skin-on-fat problems and attempt to solve them using the hybrid model.

The Theory section begins with a brief summary of the FD hybrid MC-diffusion model for photon migration in a two-layer medium, which has been previously reported in detail.[15] An efficient global optimization algorithm (Section 2.B.) was employed to determine the two-layer medium optical properties, using the hybrid model as the forward estimator. Spatially resolved reflectance FD data were simulated by MC and were utilized as ideal measurements, free of additional experimental complications. Such data helped explore the intrinsic limits in the ability of the hybrid model to determine all optical properties of a two-layer medium.

In addition, experimental FD measurements were performed on liquid two-layer tissue simulating phantoms. A previously described low noise FD system was utilized for these measurements.[17] The potential sources of systematic errors in the experimental measurements and their effect on the recovered optical properties were examined in detail. Eliminating these biases is shown to be critical if the theoretical limits

in the accuracy of determining the two-layer medium optical properties are to be approached.

2. Theory

A. The forward calculation: Monte Carlo diffusion hybrid model

The MC-diffusion hybrid model combines the accuracy of MC at short source-detector distances with the efficiency of diffusion at larger ones, resulting in a reflectance calculation as accurate as pure MC but hundreds of times faster.[15] The hybrid model idea was initially proposed by Wang and Jacques[18] for a semi-infinite geometry and CW illumination. The extension of that model to FD photon migration for a two-layer turbid medium has been previously described in detail.[15] A brief description will be repeated here to set the context for this work.

A two-layer turbid medium is characterized by the absorption and scattering coefficients of each layer (μ_{a_i}, μ_{s_i}; $i = 1, 2$ where 1 and 2 refer to the upper and lower layers respectively), as well as the top layer thickness ℓ. The transport scattering coefficient in each layer is defined as $\mu_{s_i}{}' = \mu_{s_i}(1 - \mathrm{g})$, where g is the mean cosine of the scattering angle. A transport mean free path ($mfp' = 1/(\mu_{a_i} + \mu_{s_i}{}')$; $i = 1, 2$) is also defined for each layer.

The pure diffusion solution for a two-layer medium needs to be considered first.[10] For this case, the approximation is made that all the photons from a vertically incident beam, intensity modulated at a circular frequency ω, scatter for the first time at a

distance $z_0 = 1\ mfp'$ into the first layer and thus create an isotropic photon source. The problem then reduces to finding the Green's function solution to the diffusion equation for the two-layer geometry. The problem's cylindrical symmetry is exploited by reducing the fluence solution of the diffusion equation $\Phi(\rho, z, \omega)$ to one dimension by Fourier transforming it to frequency space coordinates $\phi(s, z, \omega)$. The analytical solution for the latter can then be obtained, and its subsequent Fourier inversion gives the real space fluence solution:

$$\Phi(\rho, z, \omega) = \frac{1}{2\pi} \int_0^\infty \phi(s, z, \omega) s J_o(s\rho)\, ds \tag{1}$$

where $J_o(s\rho)$ is the zeroth order Bessel function and $\rho = \sqrt{x^2 + y^2}$. The diffuse reflectance for a refractive index matched boundary can then be obtained:[10]

$$R(\rho, \omega) = \frac{1}{4}\Phi(\rho, z = 0, \omega) + \frac{1}{2} D_1 \left. \frac{\partial \Phi(\rho, z, \omega)}{\partial z} \right|_{z=0} \tag{2}$$

In this work, the definition of the diffusion coefficient was $D_i = 1/3(\mu_{s_i}')$, $i = 1, 2$, because in the context of the hybrid model it was shown to produce improved agreement with MC data when compared to a $D_i = 1/3(\mu_{a_i} + \mu_{s_i}')$ definition that includes the absorption coefficient.[15]

In FD photon migration, reflectance is a sinusoidaly varying function of time with a circular frequency ω. Using a complex number representation, the FD reflectance can be expressed in terms of an amplitude $ACR(\rho, \omega)$:

$$ACR(\rho, \omega) = \sqrt{(Im[R(\rho, \omega)])^2 + (Re[R(\rho, \omega)])^2} \tag{3}$$

and a phase lag $\theta(\rho,\omega)$ relative to the incident beam:

$$\theta(\rho,\omega) = \tan^{-1}\frac{Im[R(\rho,\omega)]}{Re[R(\rho,\omega)]} \tag{4}$$

In the hybrid model, photons of the incident beam are initially tracked by MC. Those traveling superficially through tissue exit primarily at small ρ and are scored in radial bins of 0.05mm width to produce the direct MC contribution to the reflectance $R_{MC}(\rho)$. However, the photons that travel deeper in tissue and cross a predetermined critical depth z_c are treated differently. A new scatter direction is sampled and if it points downwards, then the photon path is extrapolated by 1 mfp' in the current layer along the direction of last scatter. At that point the photon is considered to have become an isotropic photon source and its weight is scored on a predefined $\rho - z$ grid. When a large number of photon histories has been tracked, the photons traveling deep in tissue have defined a spatially distributed photon source $W(\rho,z)$. If the radial dimension of the latter is Fourier transformed to spatial frequencies, the resulting photon source $W(s,z)$ can be naturally incorporated into a Fourier inversion procedure of the same general form as eq. 1. To that end, the frequency space diffusion solution for a point source in the bottom layer had to be computed.[15] The sum of the Fourier inversions over all z then computes the diffuse reflectance $R_{DIF}(\rho)$ resulting from the distributed photon source. The latter can be added to the direct MC contribution $R_{MC}(\rho)$ to give the total reflectance $R(\rho)$.

In accordance with previous experience[15], a critical depth z_c = 4mm and 10^6 photon histories were used to produce accurate reflectance predictions for all sets

of two-layer medium optical properties within the physiological range for superficial tissue. For all calculations, the stochastic noise resulting from the MC component of the hybrid model was suppressed by applying a median filter[19] to the distributed source term $W(\rho, z)$ before Fourier transforming it to frequency space. Also, when fitting experimental FD measurements the known finite size and numerical aperture of the source and detector fibers were incorporated in the hybrid model calculation.

B. The Inverse problem: Hybrid simplex-simulated annealing parameter search

The simplex is a polygon with N+1 vertices, where N is the number of optical properties of a two-layer medium that are being fitted as free parameters. Each polygon vertex represents the χ^2 value corresponding to a particular set of two-layer medium optical properties. The simplex search algorithm samples parameter space with a well-defined strategy whose net result is a pure downhill motion until the simplex vertices engulf the nearest minimum χ^2 value found (χ^2_{min}) to a predetermined tolerance.[19]

Clearly this could lead to a local minimum that is not necessarily the global one. The simulated annealing (SA) algorithm has been shown to be a robust optimizer for the two-layer inverse problem.[11] However, a large number of function evaluations is necessary because of the purely stochastic nature of the method's parameter search strategy. A hybrid simplex-SA algorithm has been recently proposed.[19] The principle of the method is that it can get to the nearest χ^2 minimum with few function eval-

uations using the simplex strategy, but uses its SA component to escape from that minimum if it is only local. Stochastic perturbations to the value of χ^2, controlled by a fictitious temperature parameter T, are applied at each vertex of the simplex, one at a time. The value of T is such that if a random number generator produces a number $\in [0, 1)$ greater than a Boltzmann-like factor $\exp(-E/T)$, where E is the stochastically perturbed value of χ^2 for the current vertex, an uphill move is accepted. Thus the hybrid search algorithm tends to move downhill, but can also accept uphill moves that help it escape from local minima. As with pure SA, T is gradually reduced at a user-defined rate with lower rates resulting in a more comprehensive parameter search at the expense of an increased number of function evaluations. When T is so small that the resulting stochastic perturbations on χ^2 values are negligible, the method reduces to pure simplex and finally converges to the nearest χ^2_{min}. For a given set of measurements the hybrid simplex-SA algorithm converged to the same global minimum as pure SA, but with less function evaluations by more than an order of magnitude. This economy was critical to the current work as a single hybrid MC-diffusion model calculation takes $\sim$ 5min on an Ultra-1 Sparc workstation and pure SA requires several tens of thousands of function evaluations (model calculations) for a single run. Thus the hybrid parameter search technique made the the inverse problem computationally feasible. A Marquardt-Levenberg code[19] was used to estimate the uncertainties in the fitted parameters.

In all fitting procedures involving relative FD data, rf amplitude and phase delay

model predictions were matched to the corresponding measurements by computed scaling factors that gave the minimum value of χ^2 at each iteration.[11]

3. Experimental Methods

A. Tissue-simulating phantoms

All phantoms were liquid and the solvent was water. The scattering agent was a suspension of polydisperse acrylic-styrene hollow spheres (Ropaque, OP-62, Rohm and Hass Company, PA). The absorbing agent was non-waterproof ink (Higgins Black India, Eberhard Faber Inc., Lewisburg, TN). The ink's absorbance was characterized by spectrophotometer measurements for a wide range of dilutions of the stock solution.

For the infinite phantom measurements, a 3.5l container was found to be sufficiently large to eliminate any effects from the phantom boundaries. A transparent acrylic cubic container on a 15cm side was used for the semi-infinite medium measurements. In addition, for the two-layer measurements a second acrylic box (10×10×5cm) without a bottom was placed on legs made of the same material inside the larger container [Fig. 1(a)]. A thin transparent membrane (Saran Wrap, Dow Chemical Company, Ontario, Canada) served as the separation between the liquid held in the inner box, defining the top phantom layer, and the bottom one. The membrane was streched as taught as possible and fixed onto the outer wall of the inner box by double-sided tape. Where necessary, the membrane was tightened further with

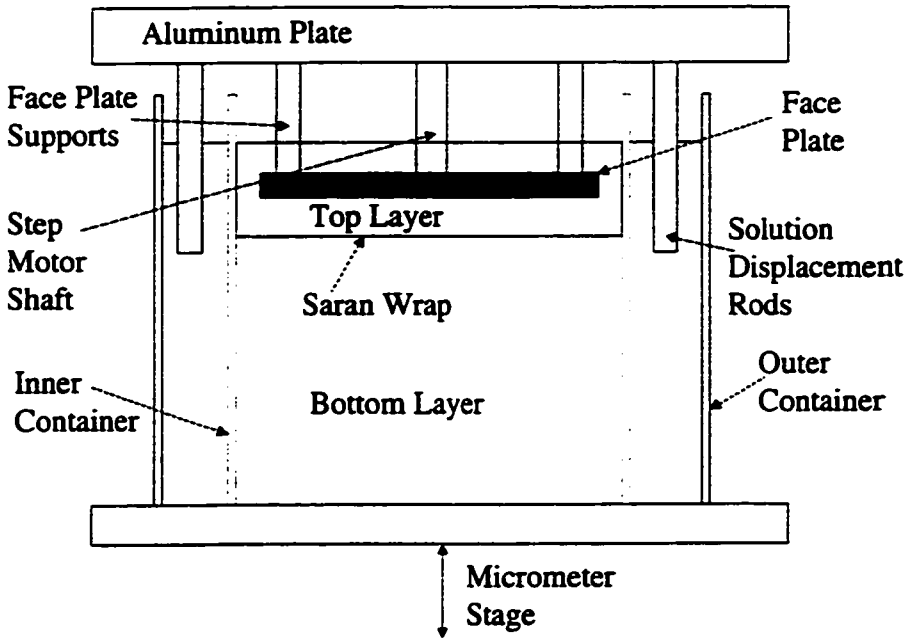

Fig. 1. (a) The two-layer phantom and FD system probe design. The source and detector fibers have been left out for clarity.

the aid of a heat gun. When the phantom liquid for the bottom layer was placed into the larger container great care was taken to avoid air bubbles being trapped under the membrane. This was achieved by tilting the inner box when immersing it in the lower layer liquid. The phantoms were prepared a day or more prior to their use and bubble formation from dissolved gas[21] was found not to be a problem. Experiments showed that the presence of the membrane has no effect on the measurements.[20] For the two-layer phantom measurements, the top layer thickness was defined as the distance between the bottom of the FD system probe's face plate (Section 3.B.) and

the surface of the membrane. The top layer thickness was adjusted by a micrometer stage which moved the entire two-layer phantom vertically. The face plate was kept fixed in space by aluminum rods [Fig. 1(a)] and was always fully submerged in the liquid of the top layer. As the micrometer stage moved the phantom in the upward or downward directions, different portions of the face plate support rods and motor shaft were submerged and thus displaced a corresponding amount of liquid in the inner box. This resulted in different liquid levels in the inner and outer containers which could cause deflection of the membrane. To avoid this effect, rods of the appropriate diameter were used to displace an equal volume of liquid in the outer container [Fig. 1(a)].

B. Reflectance detection and data acquisition

Homodyne FD measurements on tissue-simulating phantoms were performed for infinite, semi-infinite and two-layer geometries. The FD system components and the methods for high accuracy measurements in the infinite geometry have been previously reported.[17,22,23] The optical properties of phantoms obtained in the infinite geometry were used as the gold standard values that were to be recovered from measurements in the semi-infinite and two-layer geometries using the same FD system. However, for the latter geometries a new probe was introduced and some modifications in the data acquisition procedure were necessary. These new elements are described below.

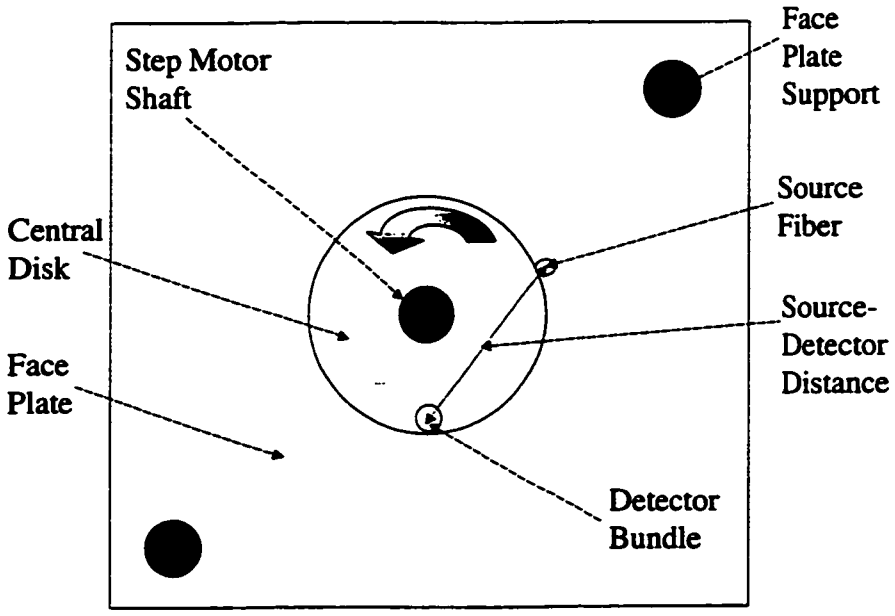

Fig. 1. (b) Bottom view of the probe face plate.

The design of the probe used for the semi-infinite and two-layer phantoms is shown in Fig. 1(b). It consists of a 3cm diameter central disk that can rotate freely about its central axis within an outer 9×9cm square. Both components are made of the same, 0.5cm thickness, black acrylic and together make a face plate that defines the top surface of the phantom and a nearly matched refractive index boundary condition. Light from a 677nm laser diode (TOLD9211F, Toshiba Corp., Tokyo, Japan) was intensity modulated at $100MHz$ and was delivered to the phantom with a 200μm core multimode optical fiber (Oz Optics Inc., Ontario, Canada). The fiber was fixed with epoxy resin into a 500μm diameter hole at the inner circular edge of the square

piece, and was polished flush with the face plate's lower surface. A 4.7mm hole bordering the outer edge of the circular disk was drilled to accommodate the 2mm diameter light collection fiber bundle and its metal casing. The part of the fiber bundle casing in the plane of the face plate was painted black. The square piece of the face plate was fixed by aluminum rods while a stepper motor rotated the inner disk [Fig. 1(b)]. The rotation varied the distance between source and detector fibers. In practice, the range of center-to-center source-detector radial distances that could be obtained was between 3.03 and 27.97mm.

For all measurements the collected light was detected by a photomultiplier tube (PMT; Hamamatsu R928, Tokyo, Japan) and the resulting electronic signal was processed by low noise digitizing electronics.[17] Data acquisition was controlled by a program written in LABVIEW (National Instruments Inc., Austin, TX). For each set of measurements at least 10 runs were averaged to reduce noise. To avoid signal contamination from extraneous light sources, all measurements were performed with the room lights off. To minimize rf signal cable pick-up from the system's rf oscillator, the latter was sealed in an aluminum box.

Because of the steep fall-off of reflectance intensity with source-detector distance ρ (typically four orders of magnitude), low noise measurements for all ρ in a single run were not possible. Instead data were acquired in a piecewise manner, each with its optimal PMT gain setting, with partially overlapping ranges in ρ. The pieces were then assembled into a single data set by a program written in a macro language (Igor

Pro, Wavemetrics Inc., Lake Oswego, OR) that smoothly matched the end values and gradients of each section of data. For the data section which included the smallest possible value for ρ (at which point the source fiber and detector bundle are adjacent), data were acquired from both sides of that point. The resulting minimum value found in the measured rf amplitude and phase delay provided data for the position at the minimum value of ρ.

C. Experimental Modifications

The frequency domain instrumentation has been shown to operate very accurately in the infinite medium geometry when the source-detector separations are at least several centimeters.[22] As for those measurements, the anode current from the photomultiplier was maintained below 1 μA to maintain linearity. However, for the short source detector separations for this work, two new effects related to the photomultiplier were encountered, both related to the large gradients in amplitude at small values of ρ. These effects are due to photomultiplier hysteresis, which influences the phase at high light intensities, and the phase bias on the photocathode (photocathode transit time difference).

Hysteresis refers to the transient change in photomultiplier response over a period of seconds after a rapid change in light intensity. The standard explanation of such behavior is a build-up of electrostatic charge on the insulating dynode supports when photocurrent increases.[24,25] Although hysteresis usually refers to a variation in the

intensity response, it is clear that any such charge buildup will influence the electron paths through the photomultiplier as well, thus changing the electron transit times and rf phase. Hysteresis has proven not to be a problem when the photocathode current is kept low. However, at small values of ρ the photocathode current was high enough to produce very large phase hysteresis. We have observed changes of up to one degree within a minute of increasing the illumination of the photocathode.

The phase hysteresis can be eliminated by reducing the light intensity for small ρ. For a given anode current, this means the photocathode current is lower, producing less charge, and the photomultiplier voltage is higher, leading to a smaller electron transit time. Initially we used a pair of polarizers between the fiber collection bundle and the photomultiplier to attenuate the light at small ρ values. By rotating one of the polarizers the intensity could be easily varied over approximately four orders of magnitude. This approach was rejected, however, as the source light was not completely depolarized at small ρ, and the use of polarizers would cause new systematic effects. As a second approach, we used an iris to adjust the light intensity. However, we found that reducing the light intensity with an iris did not actually prevent the hysteresis. While closing the iris did reduce the total power incident the photocathode, the peak light intensity was not reduced. Thus the hysteresis is related to the photoelectron current density at the photocathode, not just the total photocathode current. The method we used successfully to eliminate the phase hysteresis was to place different neutral density filters before the photomultiplier. As a practical mat-

ter, the phase hysteresis was kept at negligible levels when the photocathode was uniformly illuminated, the photomultiplier voltage was kept above 800 V, and the anode current was kept below 1 μA.

It is well known that the electron transit time in a photomultiplier varies across the photocathode, particularly in a side-illuminated photomultiplier.[24,25] This spatially varying transit time, called photocathode transit time difference, is equivalent to a spatially-varying phase bias, particularly since a frequency domain instrument can detect changes in electron path of as little as a few hundred μm. Although the collection fiber bundle was not an imaging fiber bundle, there is still very strong spatial correlation across the face of the fiber bundle. At small ρ, the change in light intensity across the fiber bundle area (light gradient) can be significant. Because there is some imaging character in the fiber bundle, this light intensity gradient is transferred to a gradient across the photocathode, leading to a potential phase bias at small ρ. In principle, this phase bias could be reduced by focusing the light from the collection fiber bundle onto a small region of the photocathode. However, this would increase the potential for phase hysteresis. Instead, we eliminated the phase bias by placing a diffuser in front of the photocathode. We used thin paper cardstock as diffusers for this purpose.

We used a filter wheel (Spex Industries, Edison, NJ) placed between the collection fiber bundle and the photomultiplier to hold the neutral density filters and diffusers. A diffuser and one or more neutral density filters were used to allow simple adjustment

of the light intensity. At the largest values of ρ, we used neither a neutral density filter nor a diffuser. A diffuser is not necessary for large ρ as the reflectance gradients are quite small, and furthermore, it is desired to collect as much light as possible to maintain a good signal-to-noise ratio.

Even after taking these steps we found some residual bias effects evident as a small asymmetry in measurements taken across the minimum ρ value. We found that we were able to further reduce these systematic effects by measuring over smaller ranges of ρ. There was a compromise between the reduced range of light intensities sampled per measurement and the maximum number of data segments acquired without introducing perturbations in the continuity of the overall data set. It was decided that four segments (approximately 3-5mm, 5-10mm, 10-17mm, and 17-28mm) was a near-optimal choice, though the length of each segment was somewhat dependent on the phantom optical properties.

After the implementation of the above measures, the detected phase equilibrated within noise level in about 1s. A time delay of 2s was introduced between successive measurements at different ρ for all runs. Although the strongest instrumental biases were eliminated, it is possible that all systematic effects were not removed.

4. Results and Discussion

A. Fitting to MC simulated measurements

Low noise MC simulated FD reflectance data (5×10^7 photon histories) provide ideal 'measurements' free of additional experimental uncertainties. At source-detector separations of 1mm, the standard deviations of the MC data were typically 0.2% in amplitude and 0.002° in phase. These degraded to about 5% and 0.1° at 18mm. Such data allow assessment of the intrinsic capacity of the hybrid model to quantify all of the optical properties of a two-layer turbid medium. FD data for the two-layer geometry were generated using a MC code for photon migration in layered media[13]. The optical properties chosen for the layers are shown in Table 1 and correspond to skin-on-fat (Column 1) and skin-on-muscle (Column 2) in the presence of an exogenous chromophore such as PDT photosensitizer.[11] In the figures to follow, the difference between the model based fitting estimate for each optical property (μ_{fit}) and the corresponding MC value (μ_{MC}) used to generate the FD reflectance data is expressed as a percentage error (%err):

$$\%err = (\mu_{fit} - \mu_{MC})/\mu_{MC} \times 100 \tag{5}$$

A Marquardt-Levenberg algorithm was used to compute the covariance matrix for the fitted optical properties. In all figures error bars, representing 95% confidence limits, are also shown for each %err value as deduced from the corresponding diagonal elements of the covariance matrix. Note that due to the stochastic component of the

hybrid model calculations, the resulting 95% confidence limits are always larger than the corresponding pure diffusion ones.

As the hybrid model has been shown to be more accurate than pure diffusion at small source-detector distances,[15] it is worth investigating the effect of gradual exclusion of reflectance data from these distances on two-layer optical property estimates. Photons exiting at short distances have traveled primarily in the top layer. Thus their exclusion from the fitting procedure should degrade the optical property estimates for that layer. An interesting %err pattern for μ_{a1} develops in Fig. 2 where skin-on-fat reflectance data for 1mm$\leq \rho \leq$20mm (1-6mm, increment 1mm; 8-20mm, increment 2mm) were fitted to the hybrid model. In Fig. 2 the abscissa labels 1, 2,... signify that the hybrid fit included a source-detector separation range 1mm$\leq \rho \leq$20mm, 2mm$\leq \rho \leq$20mm,... etc. It appears that the hybrid model can determine μ_{a1} to $\sim$5% even though ρ values up to 4mm are excluded from the fit. Beyond that distance, the hybrid model can no longer deduce enough information about μ_{a1} and the %err increases significantly. Except for this last case, the fitted %err values are not statistically different from zero as demonstrated by the corresponding 95% confidence limits. On the other hand, inclusion of small ρ in the two-layer pure diffusion fit induces biased μ_{a1} estimates as this model is not accurate at these distances.[11] This apparent bias is supported by the fact that the 95% confidence limits deduced from difusion theory are always smaller than the corresponding %err values. Hence, in this case, exclusion of the first few ρ appears to benefit the accuracy of μ_{a1} estimates though it

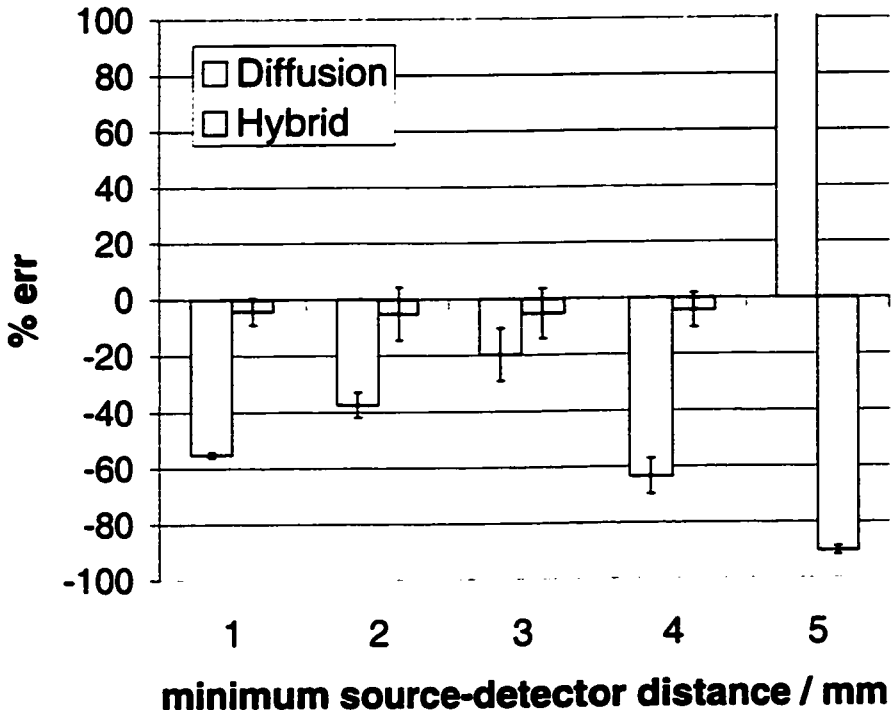

Fig. 2. Percentage errors (%err) for the retrieved value of μ_{a1} in the MC simulated skin-on-fat case when using two-layer diffusion (white bars) and the hybrid model (gray bars). The abscissa values indicate the smallest source-detector distance included in the fits (see text). Error bars indicate the 95% confidence intervals on each fitted optical property %err value.

never gets better than ~20%. Excluding reflectance data for ρ <3mm deprives the diffusion model fit of enough information about the top layer and degrades the μ_{a1} estimate, as was the case for the hybrid model.

The μ_{s1}' estimates for the same optical properties follows a similar %err pattern as shown in Fig. 3. In this case though, pure diffusion can determine μ_{s1}' to no

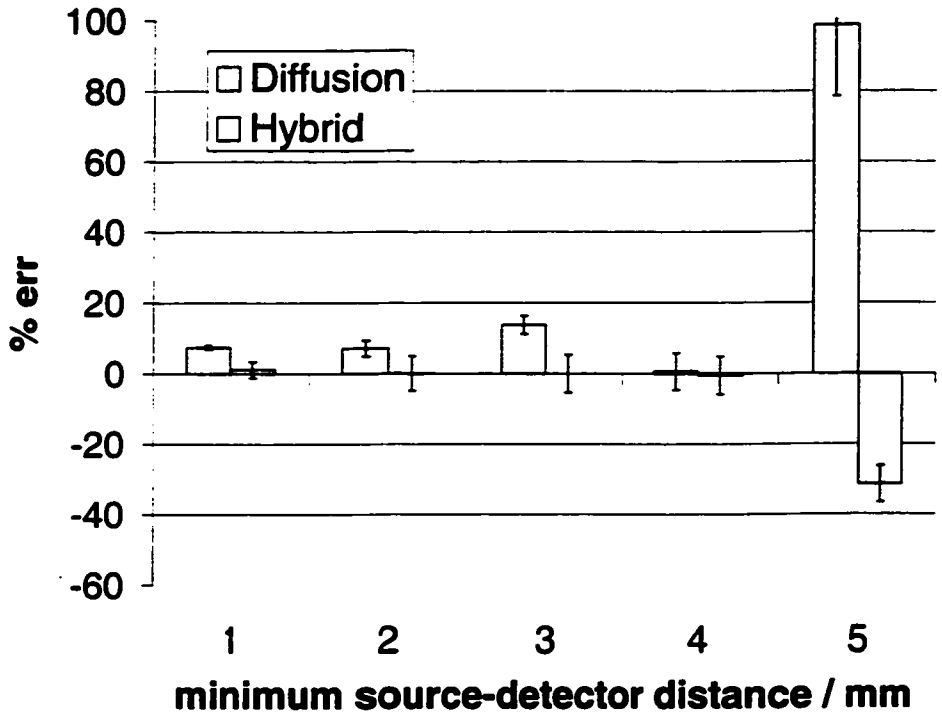

Fig. 3. As in Fig. 2 but for μ_{s1}' in the skin-on-fat case.

worse than ~14% if results for ρ <5mm are included in the fit. The hybrid model accuracy is ~1% or less for the same distances. It was somewhat surprising to find that the pure diffusion %err values for top layer thickness ℓ, though they followed the same pattern as μ_{a1} and μ_{s1}' were always no worse than ~15% compared to ~5% for the hybrid model (results not shown). Photon migration in the bottom layer is well described by diffusion. It was therefore not surprising to find that μ_{a2} and μ_{s2}' were equally well determined by both models to within ~5% for all fitting ranges in ρ (results not shown).

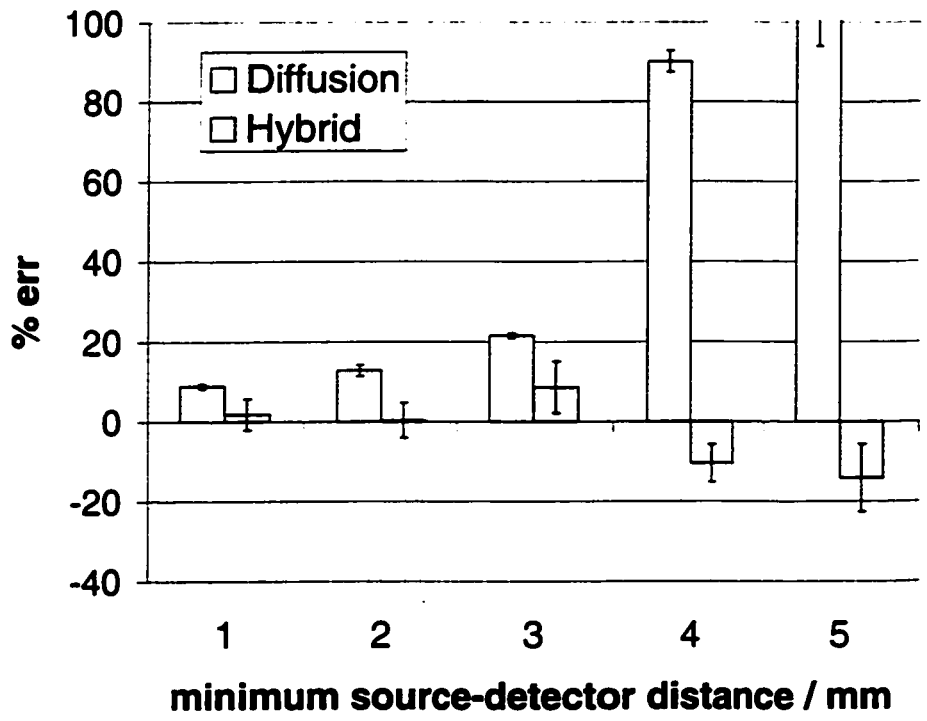

Fig. 4. As in Fig. 2 but for μ_{s1}' in the skin-on-muscle case.

For the skin-on-muscle case (Table 1, Column 2) it has been shown that the hybrid model can predict reflectance data more accurately than pure diffusion for *all* ρ when μ_{a2} is significant compared to μ_{s2}'.[15] The corresponding hybrid model fitting %err results for μ_{a1}, μ_{a2}, and ℓ showed quantitatively similar patterns in %err to those described above for the skin-on-fat case (results not shown). An unexpected pattern appeared for both μ_{s1}' and μ_{s2}' though. Fig. 4 shows the variation of %err versus the fitting range in ρ for μ_{s1}'. It appears that inclusion of the small ρ in the fit improves the pure diffusion predictions even though the quality of fit for those distances, evidenced by an large increase in χ^2, is not good. This fortuitous result

may be attributed to the large difference in value between μ_{s1}' and μ_{s2}' that helps discriminate the contribution of these two transport scattering coefficients to the measured reflectance. The fact that MC data are fitted as relative measurements, and therefore scaled to fit model predictions at each iteration, also helps improve the match with diffusion as the latter produces systematic discrepancies for all ρ.[15] The corresponding %err values for μ_{s2}' show a similar pattern with diffusion performing its best for 1mm$\leq \rho \leq$ 20mm giving an ~8% error compared with ~3% error for the hybrid model (data not shown).

The importance of the correct *a priori* choice of phase function was also investigated. It is known that tissue is highly forward scattering,[26] but the choice of phase function is most often dictated by computational convenience. In this work, a Henyey-Greenstein (HG) phase function with g= 0.8 was used to generate all MC data. To test the robustness of this assumption, a Mie theory phase function[27] with g= 0.9 was used to generate MC data for the skin-on-fat optical properties (Table 1, Column 1). A hybrid model assuming a HG phase function and g= 0.8 was then used to fit the MC data generated using Mie theory. Fig. 5 shows that the overall fitted optical property errors were no better or worse compared to those observed when the correct phase function is used. The 95% confidence limits show the equivalence of the two fits, though there is a small bias of a few percent in the %err value for μ_{s1}' when fitting to the Mie theory MC data. On the other hand, increased discrepancies appeared, primarily for μ_{a1} which could not be recovered at all, when the same hybrid

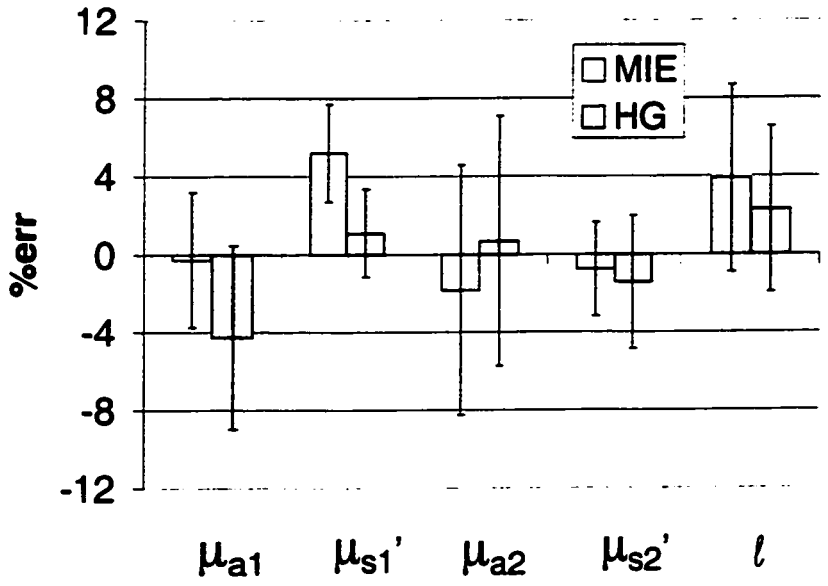

Fig. 5. Percentage errors (%err) for the retrieved skin-on-fat optical properties (Table 1, Column 1) when MC data generated with a Mie theory phase function (g= 0.9, white bars), or a HG phase function (g= 0.8, gray bars) are fitted as relative measurements to the hybrid model with HG (g= 0.8).

model was fitted to HG, g= 0 MC data (results not shown). These results indicate that accurate *a priori* knowledge of the phase function is not essential as long as highly forward scattering is assumed.

Though not the focus of this work, it is important to consider whether CW reflectance data can also be used in conjunction with the hybrid model to determine the optical properties of a two-layer medium. CW reflectance data for 1mm$\leq \rho \leq$20mm and skin-on-fat optical properties (Table 1, Column 1) were fitted to the hybrid model

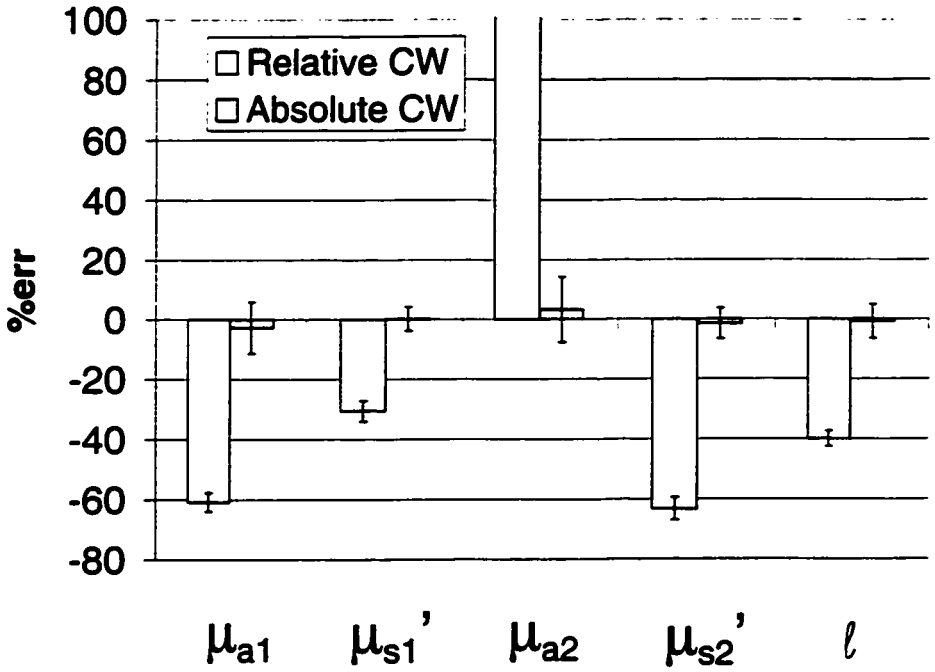

Fig. 6. Percentage errors (%err) for the retrieved skin-on-fat optical properties from fitting skin-on-fat (Table 1, Column 1) CW MC data to the hybrid model as relative (white bars), or absolute (gray bars) measurements.

both as relative and absolute measurements. The model can produce CW reflectance calculations by simply setting the source intensity modulation frequency f to zero. In Fig. 6 it can be seen that fitting for relative data is an ill-posed problem as has also been shown for a pure diffusion model in the two-layer geometry.[11] However, fitting for absolute CW reflectance measurements yields excellent recovery of all optical properties of a two-layer medium. This is an important result since CW measurements are easier to perform. On the other hand, performing absolute light intensity measure-

ments relies heavily on an accurate calibration measurement which is difficult. The latter would likely involve the simultaneous use of a phantom of precisely known optical properties, a standard which is hard to produce and maintain. It is also possible that CW reflectance measurements would suffer from intensity dependent systematic measurement errors at short source-detector distances.

B. Fitting to experimental FD measurements on two-layer phantoms

The practical utility of the hybrid model was assessed by fitting FD reflectance measurements from skin-on-fat and skin-on-muscle two-layer tissue simulating liquid phantoms with different top layer thicknesses. The optical properties for the phantom solutions composing each layer were determined by high accuarcy FD measurements in the infinite geometry,[17,22] and are shown in Table 2 (skin, Column 1; fat, Column 2; muscle, Column 3). These are representative of baseline values previously estimated from *in vivo* measurements,[13] and were the target optical properties we attempted to recover using two-layer measurements and the hybrid model. The difference between the optical properties obtained from the hybrid model and the corresponding infinite medium measurements was expressed as a percentage error (%err), as for the fitting results to MC simulated measurements (Eq. 5). Some representative results from these experiments are presented in this Section. Estimated measurement uncertainties are typically 3% in rf amplitude and 0.3° in phase.

Figures 7(a) and (b) show the measured relative rf reflectance amplitude RAC(ρ),

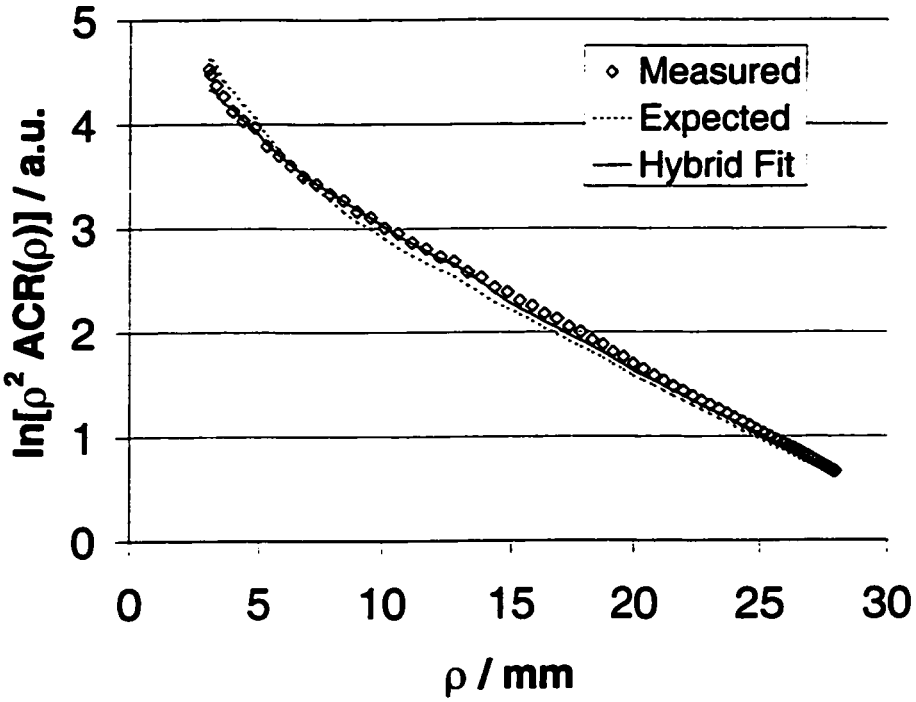

Fig. 7. (a) Rf amplitude reflectance [ACR(ρ)] measurements, plotted as ln[ρ^2ACR(ρ)], for a skin-on-fat phantom (open diamonds), ℓ = 3mm, versus the hybrid model predictions for the best fit optical properties (solid curve) and those based on the infinite medium measurements (dashed curve).

plotted as ln[ρ^2RAC(ρ)] and phase delay respectively, as a function of source-detector separation ρ, for a skin-on-fat phantom with a top layer thickness ℓ = 3mm. The hybrid fit (solid curves) is a closer match to the experimental data (open diamonds) than the hybrid model predictions based on optical properties determined from the infinite medium measurements of the two phantom components (dashed curves). The discrepancies between the two curves were not very large though, with maximum

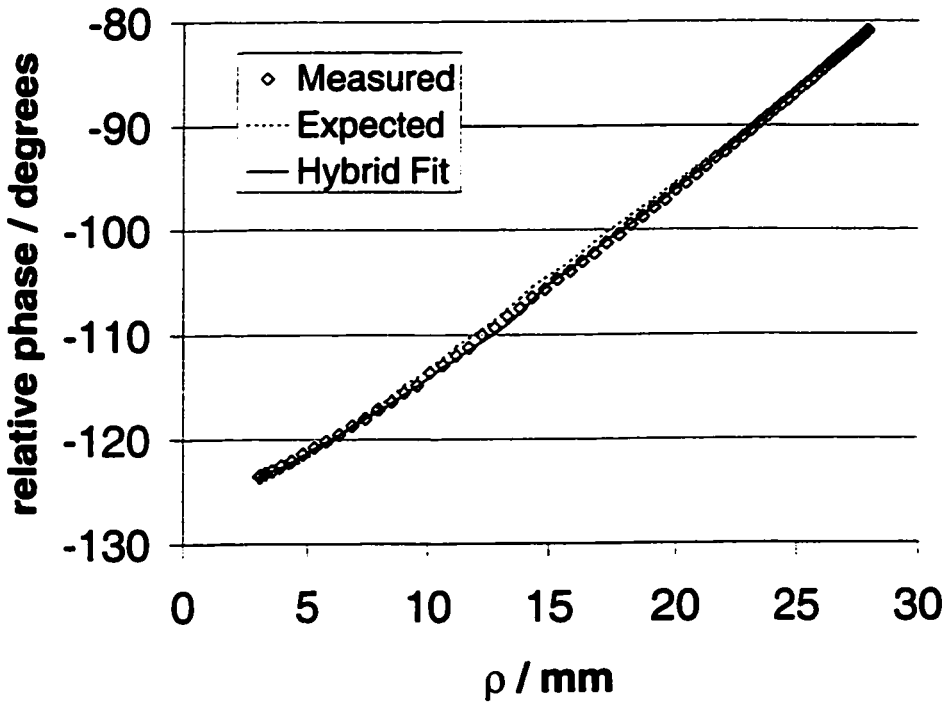

Fig. 7. (b) Phase delay measurements and corresponding hybrid model predictions [symbol and curve styles as in Fig. 7(a)]. The experimental measurement error estimates are comparable to the size of the symbols and have been left out for clarity.

differences reaching ~17% in rf amplitude and ~0.8° in phase. In Fig. 8 the %err values for the optical properties deduced from the hybrid model (gray bars) are compared to those from two-layer diffusion (white bars). Both models can retrieve the optical properties of the bottom layer with comparable accuracy, and no worse than ~10%. The hybrid model performs somewhat better than the diffusion model in determining μ_{s1}' and ℓ but the errors are still fairly large, ~27% and ~45% respectively. Finally, μ_{a1} eludes recovery for both models.

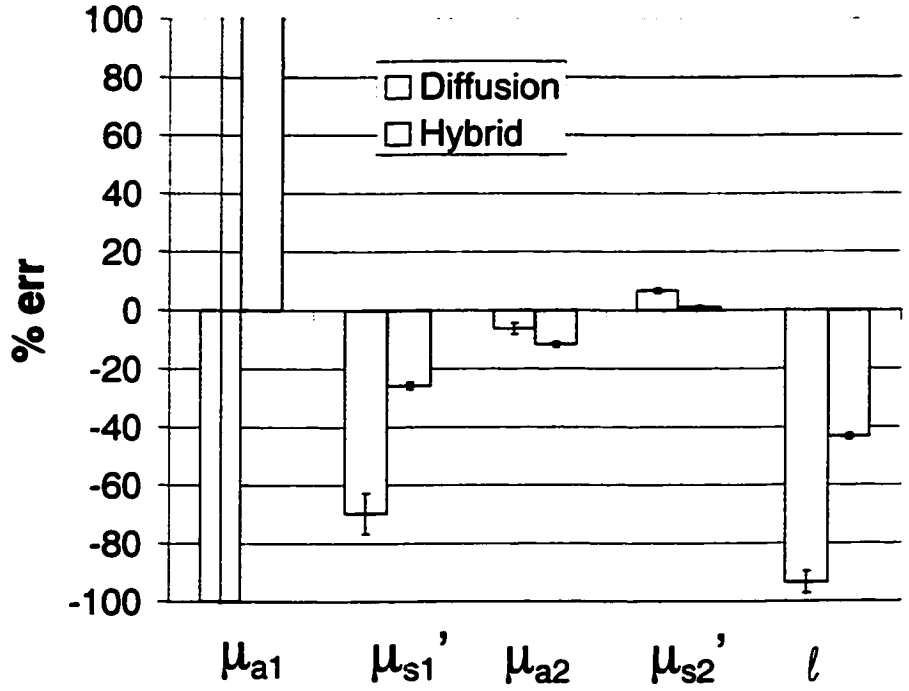

Fig. 8. Percentage errors (%err) for the retrieved skin-on-fat, ℓ = 3mm, optical properties as determined by the hybrid model (gray bars) and pure two-layer diffusion (white bars).

FD measurements were also performed on skin-on-muscle phantoms. Figures 9(a) and (b) show typical results for the measured rf amplitude and phase, with ℓ = 3mm. Once again, the hybrid model fit (solid curve) matches well the rf amplitude experimental data (open diamonds) whereas discrepancies up to ~30% in amplitude are seen when the expected optical properties are used in the forward calculation. The hybrid model also produced a good fit for the phase data [Fig. 9(b)].

Figure 10 shows the %err values for the hybrid model fit (gray bars), and the

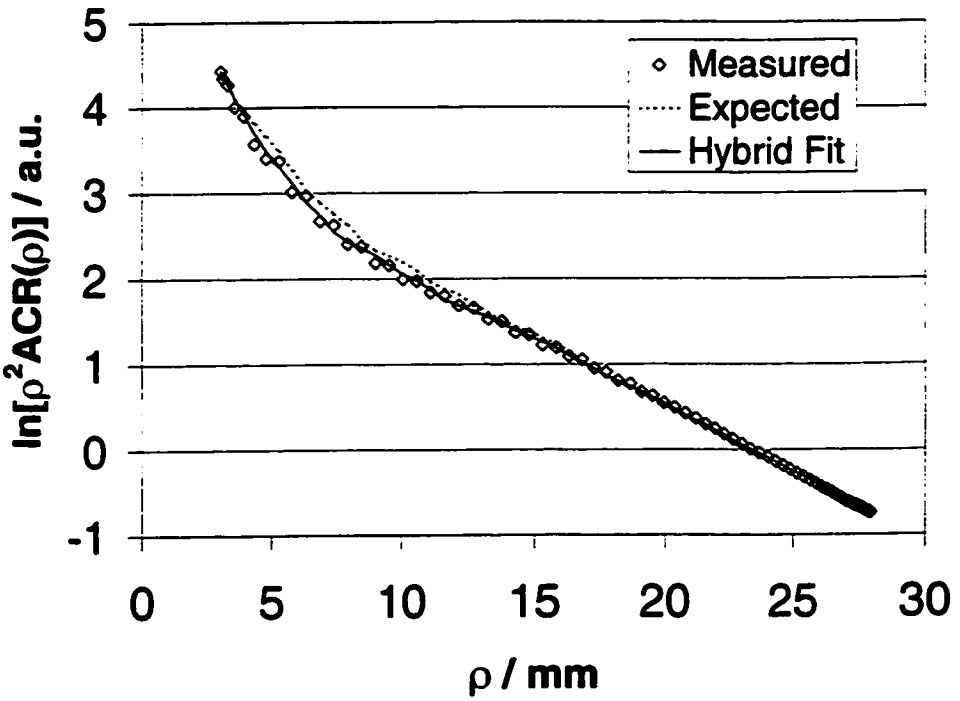

Fig. 9. (a) As in Fig. 7(a), but for a skin-on-muscle, $\ell = 3$mm, phantom.

corresponding two-layer diffusion results (white bars). As in the skin-on-fat case, the hybrid model retrieved the bottom layer optical properties with an accuracy similar to that of diffusion. On the other hand, the hybrid model could determine μ_{s1}' and ℓ more accurately.

The above fitting results indicate that the hybrid model can perform better in determining the optical properties of a two-layer medium than diffusion in a real experiment. However, the hybrid model's performance was not as good as fitting to MC simulated measurements would predict. The existence of systematic discrepancies between model and experiment is supported by the fact that the 95% confidence limits

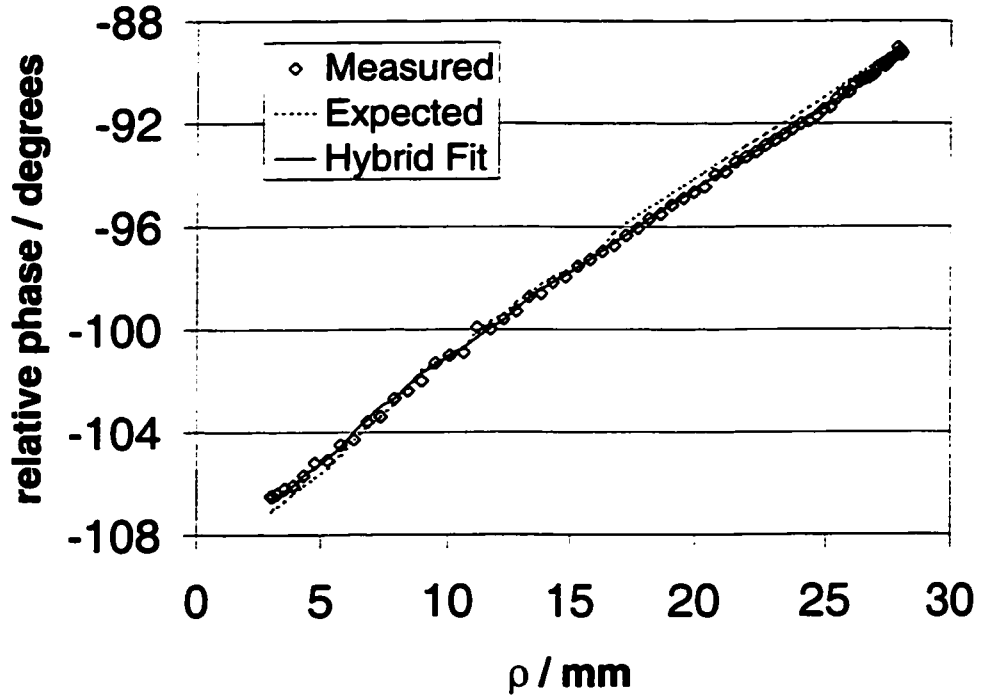

Fig. 9. (b) As in Fig. 9(a), but for the phase delay data.

deduced from fitting the experimental data to the hybrid model were much smaller than the corresponding %err values (Figs. 8 and 10). The possibility that errors in the estimated top layer optical properties were due only to noise in the experimental measurements was examined. To that end, the experimental conditions producing the reflectance data shown in Figs. 7(a),(b) and 9(a),(b) were simulated as accurately as possible by MC. The optical properties shown in Table 2, and ℓ = 3mm, were used to produce FD reflectance data (5×10^7 photon histories) at the ρ values corresponding to those used in the experimental measurements. Gaussian noise was then added to the rf amplitude and phase delay MC simulated data, using noise

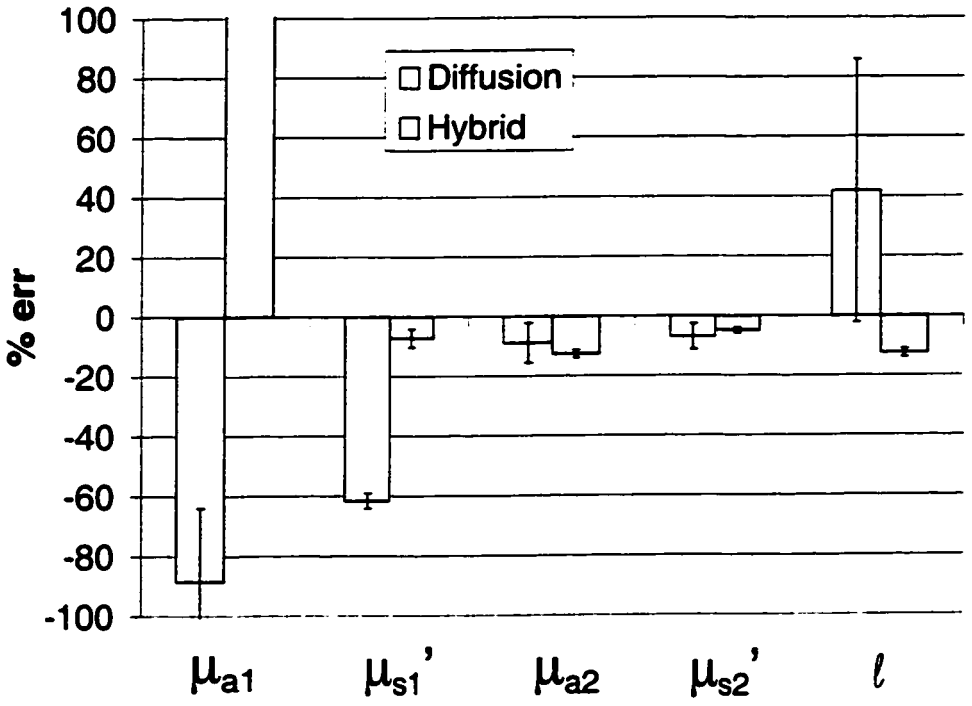

Fig. 10. As in Fig. 8, but for a skin-on-muscle, $\ell = 3$mm, phantom.

levels which matched the experimentally observed rf amplitude and phase uncertainty estimates at each ρ. The resulting data set was then fitted to the hybrid model. It was found that the hybrid model could still obtain the top layer optical properties to better than 10%. These results demonstrated that experimental measurement noise is not responsible for any discrepancies $\gtrsim$10% in the estimated μ_{s1}' and ℓ values and is not thereason for the failure to recover μ_{a1} in any experiment.

Attention was then focussed on the possibility of systematic discrepancies between model and experiment and their variation with ρ. FD measurements were performed on semi-infinite phantoms whose optical properties could be determined accurately

with a diffusion model[28] using only large source-detector separations (i.e. greater than 10mm). The deduced optical properties were in agreement with the corresponding infinite geometry results to within 5%. Hybrid model fits to the semi-infinite geometry data obtained optical properties that were also within 5% of the diffusion results. However, the fitted values produced rf amplitude and phase delay predictions which were systematically less than the corresponding experimental data at small ρ. This underestimate was a function of the phantom's optical properties and was highest at the shortest possible source-detector separation of ρ = 3mm, where it could be as large as ~30% in rf amplitude and ~0.5° in phase, but steeply decreased and reached noise level by ρ = 7mm (results not shown). These apparent systematic discrepancies might be related to intensity-dependent measurement biases due to the higher intensity gradient at small ρ, or to inadequate modelling of the actual light source and detection bundle details, but we have not been able to identify the cause conclusively.

The hybrid model could retrieve μ_{s1}' to ~7.5% for the skin-on-muscle phantom, but errors for skin-on-fat increased to ~27%. There is a larger difference in μ_s' values between the two-layers in the skin-on-muscle case. This difference results in a clear slope break in the reflectance data [Figs. 9(a) and (b)] making the inverse problem better posed. On the other hand μ_{a1} could never be recovered. This is a problem inherent to the measurements, as the effect of absorption from a thin top layer is a substantial contribution to the overall reflectance signal only at small ρ.

Discrepancies between experiment and model at those distances could overwhelm the μ_{a1} contribution to the reflectance signal. The MC simulations demonstrated that elimination of the discrepancies should improve the top layer optical property estimates.

5. Conclusions

The feasibility of determining the optical properties of a two-layer medium from spatially resolved FD relative reflectance measurements was examined. First, MC simulated measurements were used to assess the capability of the hybrid model to determine the optical properties of a two-layer medium, without any additional experimental uncertainties. It was found that the hybrid model could determine all optical properties of such a medium to ~5%. Inclusion of reflectance data for $\rho < 5$mm was critical to improved optical property estimates, particularly for the top layer. In contrast, inclusion of reflectance data from these distances for a pure diffusion model fit did not improve the quality of retrieved optical properties, with the exception of μ_{s1}' and μ_{s2}' in the skin-on-muscle case. In most cases, the inability of diffusion to describe accurately photon transport at small ρ led to biased optical property estimates. On the other hand, not including FD reflectance data for $\rho < 5$mm in the fitting procedures led to poor top layer optical property estimates for both the hybrid model and pure diffusion. Most photons exiting the two-layer medium at small ρ have travelled primarily in the top layer and thus, exclusion of reflectance data from these

distances deprives the fitting models of enough information about the top layer. It was also found that exact knowledge of the scattering phase function was not critical to deducing the medium's optical properties, as long as a highly forward scattering phase function is assumed.

Experimental FD measurements from two-layer tissue simulating phantoms representative of skin-on-fat and skin-on-muscle baseline optical properties were also fitted to pure two-layer diffusion and the hybrid model. In the case of pure diffusion it was found that only the bottom layer optical properties could be determined to better than 10%. The hybrid model performed better than pure diffusion, but not as well as predicted by the preceding theoretical results. It was encouraging to see that the hybrid model could retrieve μ_{s1}' quantitatively for the skin-on-muscle case. A somewhat larger error in determining μ_{s1}' was found for the skin-on-fat case. The increased similarity of the μ_s' values of the two layers makes the inverse problem less well-posed and thus more susceptible to discrepancies between model and experiment. Such discrepancies are expected to be largest at small source-detector separations where the rf reflectance amplitude gradient is large and the specific model details of light delivery and collection from the phantom become important. It is clear that such systematic discrepancies need to be eliminated if the hybrid model is to reach its full capacity in determining the top layer optical properties.

The above two-layer diffusion results are not inconsistent with those recently reported[12] for FD measurements on liquid two-layer phantoms. In contrast to this

work, plane wave illumination was employed and data were acquired at many modulation frequencies in the 10-1500MHz range. It was found that three optical properties could be retrieved, at best, if the values of the other two were known. Accuracy of $\pm 9\%$ and $\pm 5\%$ could be achieved for μ_a and μ_s' when the other three optical properties were known.

As an aside, it was shown that absolute CW reflectance measurements, but not relative ones, can in principle also determine accurately all of the optical properties of a two-layer medium. An accurate calibration is critical to absolute reflectance measurements. The current lack of a gold standard optical phantom and any discreapancies between model and experiment, as those discussed in Section 4.B., pose serious difficulties for a successful experimental realization of the method. However, CW measurements are easier to perform which makes them appealing in clinical practice. The possibility of performing accurate CW reflectance measurements in the two-layer geometry, perhaps in combination with spectrally resolved reflectance information, will be the object of future work.

The authors wish to thank William Olson of SRI International and Alan Hazelhurst of the Hamilton Regional Cancer Center for their technical support in performing experimental measurements. This research was supported by the National Institutes of Health grant P01—CA43892. David R. Busch was supported by the Research Experiences for Undergraduates program of the National Science Foundation.

References

1. R. A. De Blasi, N. Almenräder, P. Aurisicchio, and M. Ferrari, "Comparison of two methods of measuring forearm oxygen consumption ($\dot{V}O_2$) by near infrared spectroscopy," J. Biomed. Opt. **2,** 171-175 (1997).

2. M. Nitzav, A. Babchencko, B. Khanokh, and H. Taitelbaum, "Measurement of oxygen saturation in venous blood by dynamic near infrared spectroscopy," J. Biomed. Opt. **5,** 155-162 (2000).

3. M. S. Patterson, B. C. Wilson, J. W. Feather, D. M. Burns, and W. Pushka, "The measurement of dihematoporphyrin ether concentration in tissue by reflectance spectrophotometry," Photochem. Photobiol. **46,** 337-343 (1987).

4. R. A. Weersink, J. E. Hayward, K. R. Diamond, and M. S. Patterson, "Accuracy of non-invasive *in vivo* measurements of photosensitizer uptake based on a diffusion model of reflectance spectroscopy," Photochem. Photobiol. **66,** 326-335 (1997).

5. J. R. Mourant, T. M. Johnson, G. Los, and I. J. Bigio, "Non-invasive measurement of chemotherapy drug concentrations in tissue: preliminary demonstrations of *in vivo* measurements," Phys. Med. Biol. **44,** 1397-1417 (1999).

6. J. T. Bruulsema, J. E. Hayward, T. J. Farrell, M. S. Patterson, M. Essenpreis,

G. Schmelzeisen-Redeker, D. Bocker, L. Heinemann, M. Berger, T. Koschinsky, J. Sandahl-Christiansen, and H. Orskov, "Correlation between blood glucose concentration in diabetics and non-invasively measured tissue optical scattering coefficient," Opt. Lett. **22,** 190-192 (1997).

7. I. S. Saidi, S. L. Jacques, and F. K. Tittel, "Mie and Rayleigh modeling of visible-light scattering in neonatal skin," Appl. Opt. **34,** 7410-7418 (1995).

8. J. M. Schmitt and G. Kumar, "Optical scattering properties of soft tissue: a discrete particle model," Appl. Opt. **37,** 2788-2797 (1988).

9. B. Beauvoit, and B. Chance, "Time-resolved spectroscopy of mitochondria, cells and tissues under normal and pathological conditions," Mol. Cell. Biochem. **184,** 445-455 (1998).

10. A. Kienle, L. Lilge. M. S. Patterson, R. Hibst, R. Steiner, and B. C. Wilson, "Spatially resolved absolute diffuse reflectance measurements for noninvasive determination of the optical scattering and absorption coefficients of biological tissue," Appl. Opt. **35,** 2304-2314 (1996).

11. G. Alexandrakis, T. J. Farrell, and M. S. Patterson, "Accuracy of the diffusion approximation in determining the optical properties of a two-layer turbid medium," Appl. Opt. **37,** 7401-7410 (1998).

12. T. H. Pham, T. Spott, L. O. Svaasand, and B. J. Tromberg, "Quantifying the

properties of two-layer turbid media with frequency-domain diffuse reflectance," Appl. Opt. **39,** 4733-4745 (2000).

13. T. J. Farrell, M. S. Patterson, and M. Essenpreis, "Influence of layered tissue architecture on estimates of tissue optical properties obtained from spatially resolved diffuse reflectometry," Appl. Opt. **37,** 1958-72 (1998).

14. M. A. Franceschini, S. Fantini, L. A. Paunescu, J. S. Maier, and E. Gratton, "Influence of a superficial layer in the quantitative spectroscopic study of strongly scattering media," Appl. Opt. **37,** 7447-7458 (1998).

15. G. Alexandrakis, T. J. Farrell, M. S. Patterson, "Monte Carlo diffusion hybrid model for photon migration in a two-layer turbid medium in the frequency domain," Appl. Opt. **39,** 2235-2244 (2000).

16. A. Ishimaru, *Wave Propagation in Scattering and Random Media* (Academic, New York, 1978), Chaps. 7 and 9.

17. M. Gerken and G. W. Faris, "High accuracy optical property measurements using a frequency domain technique," in *Optical Tomography and Spectroscopy of Tissue III,* B. Chance, R. R. Alfano, and B. J. Tromberg, eds., Proc. SPIE **3597,** 593-600 (1999).

18. L. Wang, and S. L. Jacques, "Hybrid model of Monte Carlo simulation and diffusion theory for light reflectance by turbid media," J. Opt. Soc. Am. A **10,**

1746-1752 (1993).

19. W. H. Press, S. A. Teukolsky, W. T. Vetterling, and B. P. Flannery, *Numerical Recipes—The Art of Scientific Computing,* 2nd edition, (Cambridge U. Press, NY, 1996), Chaps. 10 and 15.

20. D. E. Hyde, T. J. Farrell, and M. S. Patterson,"A diffusion theory model of spatially resolved fluorescence from depth dependent fluorophore concentrations," Submitted to Phys. Med. Biol. (August 2000).

21. "Appendix B, Degassing Procedures," in *IEEE Guide for Medical Ultrasound Field Parameter Measurements,* IEEE Std **790-1989,** F. W. Kremkau, W. T. Coakley, P. D. Edmonds et al., eds., (The Institute of Electrical and Electronics Engineers, Inc., New York) 91-94 (1990).

22. M. Gerken and G. W. Faris, "High precision frequency-domain measurements of the optical properties of turbid media," Opt. Lett. **24,** 930-932 (1999).

23. M. Gerken and G. W. Faris, "Frequency-domain immersion technique for accurate optical property measurements of turbid media," Opt. Lett. **24,** 1726-1728 (1999).

24. R. W. Engstrom, *Photomultiplier Handbook* (RCA, Lancaster, Pennsylvania) pp. 32, 47-52 (1980).

25. *Photomultiplier Tube: Principle to Application,* H. Kume, ed. (Hamamatsu Photonics K. K., Hamamatsu City, Japan), pp. 36, 47-49 (1994).

26. H. C. van de Hulst and R. Graaff, "Aspects of similarity in tissue optics with strong forward scattering," Phys. Med. Biol. **41,** 2519-2531 (1996).

27. C. F. Bohren and D. R. Huffman, *Absorption and Scattering of Light by Small Particles,* (Wiley, NY, 1983).

28. Haskell R. C. Haskell, L. O. Svaasand, T.-T. Tsay, T.-C. Feng, M. S. McAdams, and B. J. Tromberg, "Boundary conditions for the diffusion equation in radiative transfer," J. Opt. Soc. Am. A **11,** 2727-2741 (1994).

Chapter 5

Concluding Considerations

5.1 Thesis conclusions

Much work in the field of biomedical optics is devoted to developing non-invasive methods that provide quantitative diagnostic information about human superficial tissue. Within this context, one of the long term goals of research at the Hamilton Regional Cancer Center (HRCC) is the determination of tissue optical properties as a function of depth from the surface, as deduced from spatially resolved reflectance measurements. In this work a first step was taken towards the above goal by assuming superficial tissue to have an idealized two-layer structure corresponding to skin on top of fat or muscle. The FD method was employed to interrogate the two-layer turbid medium by generating spatially resolved DC and rf reflectance amplitude and phase delay data. Thus the question that this thesis work attempted to answer was:

Can one determine accurately all of the optical properties of a two-layer turbid medium from FD spatially resolved reflectance measurements?

The starting point was the solution to the FD diffusion equation for a two-layer turbid medium as reported by Kienle *et al.*[36]. From that work it was not clear what the limits were in the FD diffusion approximation to determine the optical properties of a two-layer medium. This question was answered in Chapter 1. A global optimization simulated annealing (SA) algorithm was applied to the two-layer FD diffusion solution. It was shown that CW diffuse reflectance alone was not sufficient to determine the optical properties of a two-layer medium. This was because there existed optical property sets far from the true one that produced reflectance predictions matching well the MC-simulated measurements. The importance of applying SA to the problem was demonstrated by comparing the deduced optical properties with those found by the pure downhill Marquardt-Levenberg method which was sensitive to the initial parameter guesses. Different combinations of DC, rf reflectance amplitude and phase delay diffusion predictions were also fitted to MC-simulated data for relative or absolute measurements. The general conclusion was that the diffusion model can determine accurately the bottom layer optical properties (μ_{s2}', μ_{a2}) and the top layer thickness (ℓ). Reasonable estimates of the top layer transport scattering coefficient (μ_{s1}') could also be made, but the top layer absorption (μ_{a1}) was not well determined. This was attributed to the inability of the diffusion approximation to

describe accurately the migration of few-scatter photons that escape at small source-detector distances ρ. These photons carry most of the information about the top layer. Inclusion of information from higher modulation frequencies did not improve optical property estimates, again because of diffusion approximation limitations. It was speculated that a photon transport model that would take into account the few-scatter events at small ρ would be needed to improve the optical property estimates of the top layer.

Chapter 3 describes the efforts to develop a model to achieve the above purpose. A hybrid MC-diffusion model for FD photon migration in a two-layer turbid medium was developed. It was based on an idea initially proposed by Wang and Jacques[28] for calculating the spatially resolved CW reflectance from a semi-infinite medium. The essence of the model is that it exploits the accuracy of MC at small ρ and the computational efficiency of diffusion which is an accurate description of photon migration at large ρ. Thus FD reflectance predictions as accurate as MC were achieved, but $\sim$100 times faster. The substantial improvement in computational efficiency allows the hybrid model to become part of an iterative fitting algorithm. Model parameters were fine-tuned so that its predictions were in good agreement with corresponding MC data for the entire physiological range of superficial tissue optical properties.

In Chapter 4 the question of whether a hybrid MC-diffusion model can give improved optical property estimates relative to pure diffusion was explored. A hybrid simplex-SA global optimization routine was introduced and was found to be as ro-

bust, but faster than pure SA by an order of magnitude. Due to the substantially increased computational burden of the hybrid MC-diffusion model relative to pure diffusion, the more efficient hybrid simplex-SA optimization algorithm was required to make iterative fitting of the former model computationally feasible. FD two-layer MC data were used as ideal experimental measurements. Thus the intrinsic capacity of the model to retrieve the two-layer medium optical properties, free of additional experimental complications, was investigated. It was found that the hybrid model always performed better than pure diffusion, and in contrast to the latter, was able to determine all of the optical properties of a two-layer medium within 5%. It was also shown that exact knowledge of the medium's phase function was not critical to the accuracy of the retrieved optical properties. Since CW measurements are easier to make than FD ones, the hybrid model CW reflectance predictions were also fitted to corresponding MC two-layer data. When the model predictions were fitted for relative MC-simulated measurements, it was found that the two-layer medium optical properties could not be determined accurately. On the other hand, absolute CW reflectance MC-simulated predictions could be used to determine the two-layer medium optical properties as accurately as relative FD ones.

In contrast to the theoretical FD results, the top layer optical properties could not be determined accurately from FD measurements on two-layer liquid phantoms. This was attributed to systematic measurement biases appearing at small ρ that could not be accounted for. Since most of the information about the top layer comes

from measurements at small ρ, it was the top layer optical properties that were affected by this measurement bias. It appears that the standard light collection and amplification technology used to detect FD spatially resolved reflectance is not yet free from systematic measurement errors that ultimately manifest themselves as amplitude-phase cross-talk, or false rf amplitude and phase gradients.

It is hoped that this thesis work has provided some of the necessary stepping stones towards the future *in vivo* implementation of the method. Some preliminary results are shown in the following section.

5.2 Some *in vivo* measurements and future work

5.2.1 Towards quantitative *in vivo* measurements

It is of interest to examine the capacity of a two-layer FD photon migration model to retrieve superficial tissue optical properties from FD *in vivo* measurements. In Chapter 4 it was shown that due to experimental biases, use of the hybrid MC-diffusion model did not render substantially improved optical property estimates relative to pure diffusion. As there are even more potential complications with *in vivo* measurements, to be discussed below, the pure two-layer diffusion model was primarily used to analyze these data.

Experiments were performed with the FD system available at HRCC. This system in somewhat different from the one used at SRI International for the two-layer liquid

phantom measurements described in Chapter 4. The main differences are that the HRCC system utilizes heterodyne, as opposed to homodyne, detection and its probe consists of a light collection bundle and several different source fibers at fixed separations. Overall, the HRCC system had a higher level of noise in its detected signal (2% in rf amplitude and 0.5° in phase) relative to the SRI system (1% in rf amplitude and 0.3° in phase) and appeared to suffer from similar amplitude-phase cross-talk biases. A more detailed description of the HRCC system is given in Appendix A.

In our *in vivo* model we attempted to quantify non-invasively the concentration in skin and underlying tissue of a non-fluorescent and photodynamically inactive chromophore (copper phtalocyanine-tetrasulfonate, $CuPcS_4$) that was injected intravenously in New Zealand White rabbits. The FD system probe was placed directly onto the rabbit dorsal skin. The dorsal area was chosen for these measurements because muscle is a tissue of interest for pharmacokinetic studies and there exists enough of it in that anatomical location to make a reasonable semi-infinite second layer. Blood samples were obtained before and after the systemic injection of $CuPcS_4$ in order to obtain information on the drug's clearance rate from the blood. A detailed description of the animal handling procedure is given in Appendix B.

FD reflectance measurements on four animals were performed in the vicinity of the $CuPcS_4$ absorption peak (675nm) and far from it (750nm) as controls. In all cases a substantial decrease in the measured rf reflectance amplitude and phase delay at 675nm was observed shortly after drug injection (2.5mg/kg), but there were no

observable changes at 750nm. Some representative results from measurements at both wavelengths are presented here.

All FD measurements obtained were fitted to the two-layer diffusion model[36]. The accumulation of $CuPcS_4$ in the rabbit skin, visible as a blue tint, was confirmed with the rapid increase of the deduced absorption coefficient for the top layer (μ_{a1}) from its baseline value, almost immediately after drug injection (Fig. 5.1). It appears that some of the drug was retained in the skin as μ_{a1} reached a plateau value during the course of the experiment. The pre-injection value for μ_{a1} was substantially higher than its excpected physiological value of $\sim 0.03 mm^{-1}$. Also, the deduced top layer transport scattering coefficient (μ_{s1}'), was much lower than its expected physiological value of $\sim 1.5 mm^{-1}$, though it remained relatively constant pre- and post-injection. As it has been shown in Chapter 2 that the two-layer diffusion model cannot recover quantitatively the optical properties of the top layer, the results shown in Fig. 5.1 should only be considered as qualitative trends. Some measurement perturbations whose nature is unknown seem to appear within the first hour post-injection. The equivalent μ_a value for the sampled blood plasma, as deduced from its measured extinction coefficient, implies a rapid $CuPcS_4$ plasma clearance. A few measurements were also performed 24hr post-injection in order to get an idea of the drug's long term retention. In Fig. 5.1 it appears that the amount of $CuPcS_4$ in skin is reduced as implied by a reduction in μ_{a1} which is consistent with the pre-injection values of the day before. However, the increase in μ_{s1}' towards its expected physiological value

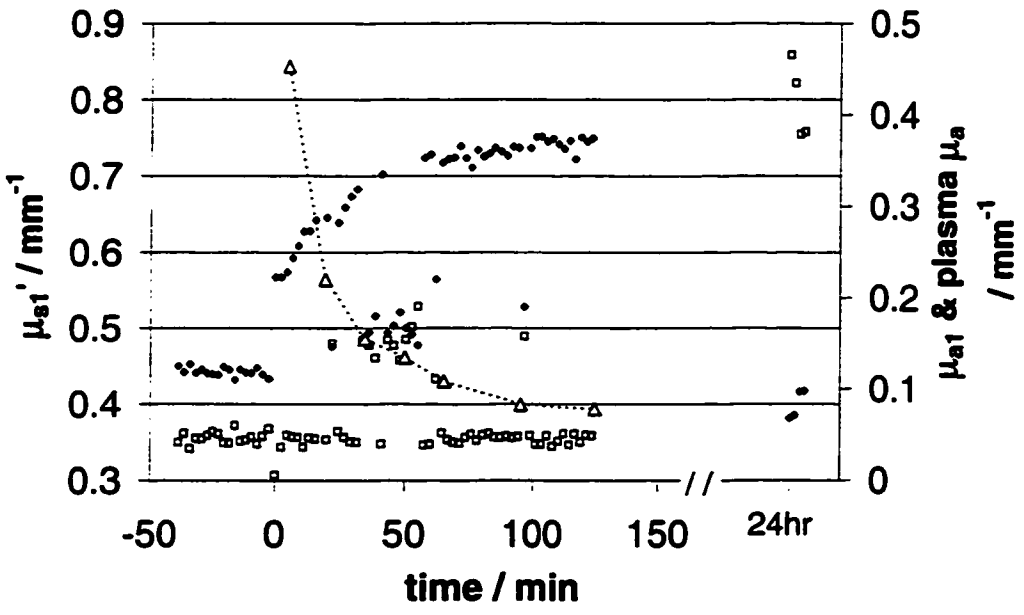

Figure 5.1: The top layer $\mu_{s1}{}'$ (open squares) and μ_{a1} (filled diamonds) optical properties pre- and post-injection. The μ_a plasma values (shaded triangles connected by dotted lines) indicate a rapid $CuPcS_4$ clearance rate. The 24hr time-point measurements are also illustrated by the corresponding symbols.

was not consistent with the low $\mu_{s1}{}'$ values obtained throughout the previous day's measurements. Therefore, the reduction in $CuPcS_4$ concentration would diminish such absorption-scattering cross-talk. One should also have in mind that two-layer diffusion cannot retrieve accurately the top layer optical properties (Chapter 2) and therefore the observed changes in μ_{a1} and $\mu_{s1}{}'$ are qualitative rather than quantitative.

Figure 5.2 shows the corresponding bottom layer optical property values, μ_{a2} and $\mu_{s2}{}'$, for the same animal. As was the case for μ_{a1}, there is a clear increase in

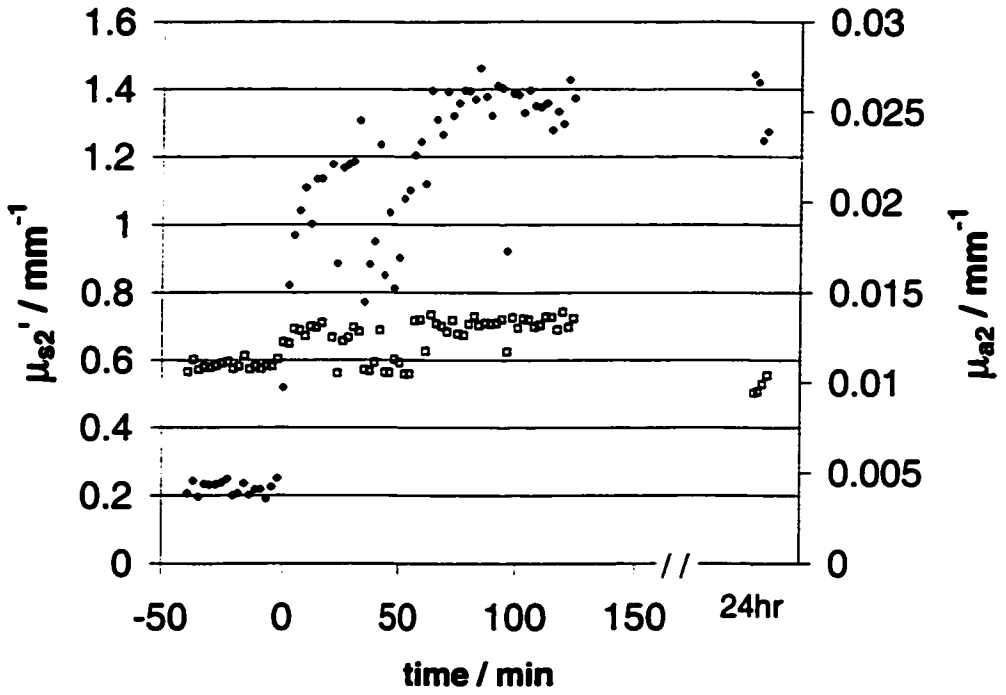

Figure 5.2: The bottom layer μ_{s2}' (open squares) and μ_{a2} (filled diamonds) optical properties follow the same pattern as those of the top layer. The lower μ_{a2} values imply a lower $CuPcS_4$ retention in the underlying tissue relative to skin. The 24hr time-point implies drug retention for this time interval.

μ_{a2} shortly after $CuPcS_4$ injection, some measurement perturbations are observed in the first hour post-injection, and a plateau value is established after that. In contrast to μ_{a1} though, the μ_{a2} values are more than an order of magnitude smaller which is consistent with the increased vascularization of skin and its higher retention of the drug[4]. Also, the value of μ_{a2} does not seem to have changed significantly 24hrs later which implies that the drug was retained in the underlying tissue. The

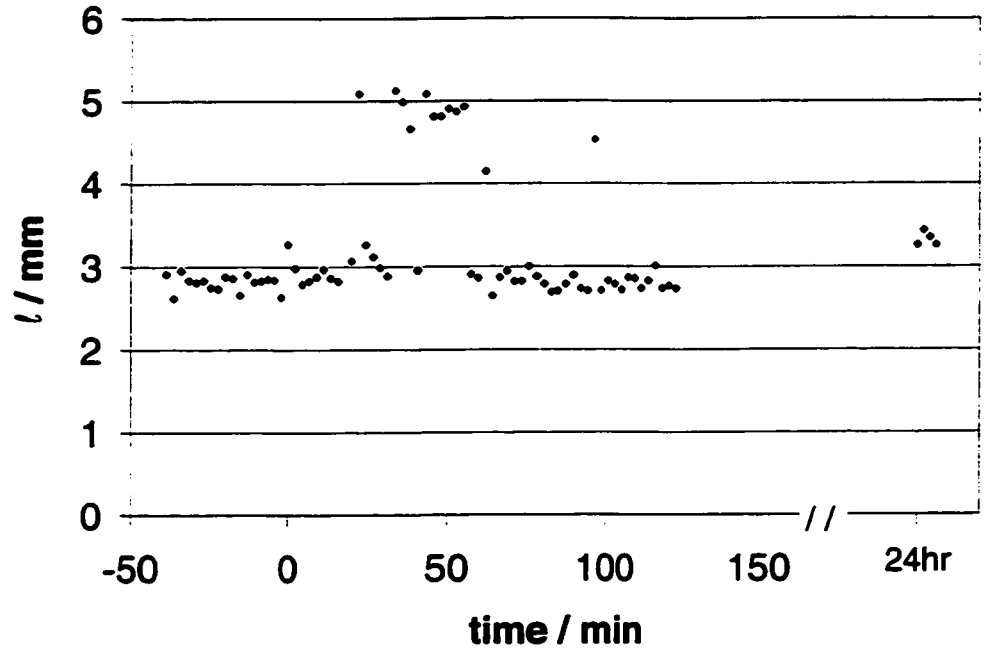

Figure 5.3: The fitted top layer thickness (ℓ) appears constant throughout the experiment except for certain perturbations also encountered in Figs. 5.1 and 5.2 for the same time-points. The 24hr measurements were reasonably consistent with those of the previous day.

deduced value of $\mu_{s2}{}'$ is not too different from that of the day before and closer to the expected physiological value for muscle. It is also encouraging to see in Fig. 5.3 that the deduced top layer thickness seems to be unaffected, other than the aforementioned perturbations, by injection and was unchanged at 24 hours.

Measurements were also performed at 750nm where $CuPcS_4$ absorption was negligible, as confirmed from solution measurements with a spectrophotometer. As

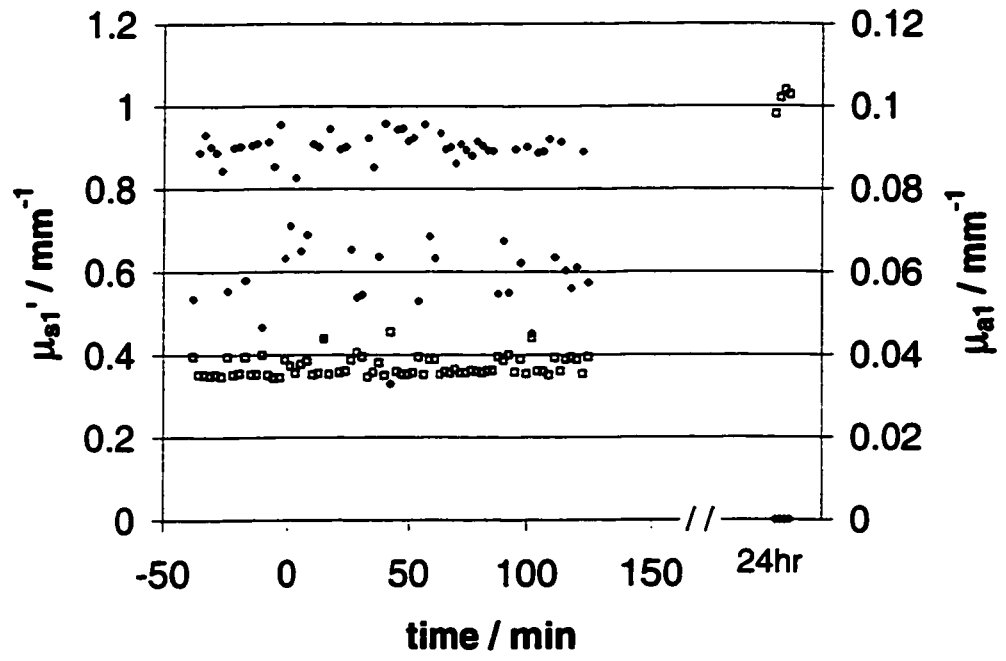

Figure 5.4: At 750nm both $\mu_{s1}{}'$ (open squares) and μ_{a1} (filled diamonds) appear to be relatively constant, unaffected by the $CuPcS_4$ injection at $t = 0$min.

expected, the deduced μ_a and $\mu_s{}'$ values for the top (Fig. 5.4) and bottom (Fig. 5.5) layers as a function of time seem to be unaffected by the $CuPcS_4$ injection. Curiously, the top layer thickness seems to oscillate between two possible solutions at $\ell \approx 1.5$mm and $\ell \approx 2.2$mm. In contrast to the 24hr time-point measurements made at 675nm, the 750nm data did not appear consistent with those of the previous day for any of the two-layer optical properties. At present no explanation can be offered for this discrepancy.

The animal was euthanized at the end of this experiment and the dorsal skin flap

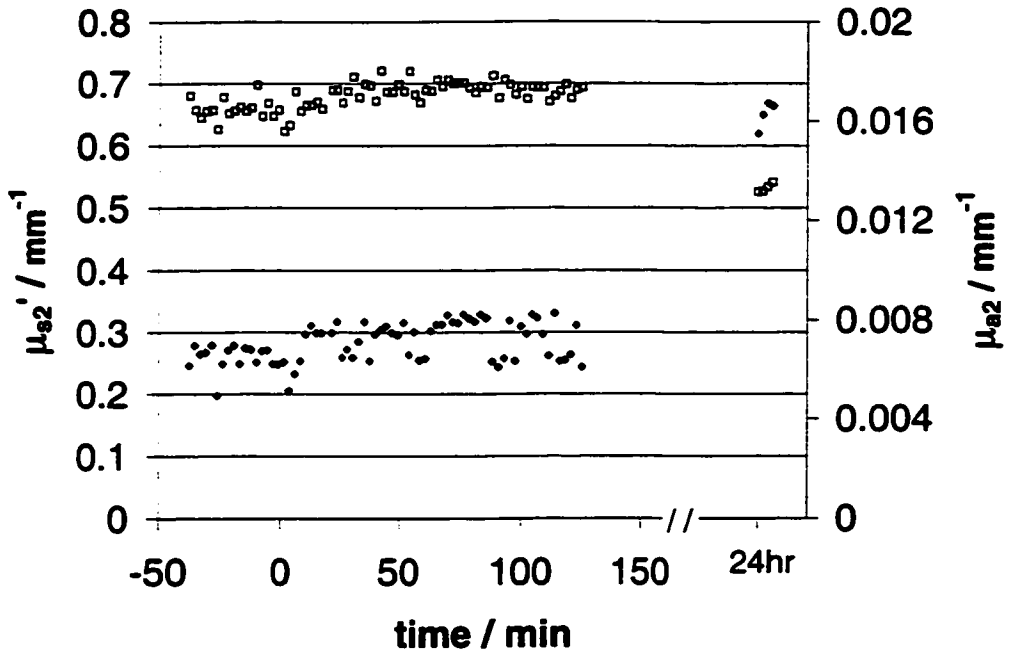

Figure 5.5: As in Fig. 5.4, μ_{s2}' (open squares) and μ_{a2} (filled diamonds) remain relatively constant throughout the experiment though μ_{s2}' showed a ~12% variation.

was removed in order to study the structure of the underlying tissue. As measured with calipers, the thickness of the skin flap was ~1.8mm. Below that was a very thin layer (~0.5mm) of connective tissue and fat under which there was muscle tissue. Interestingly, the deduced top layer thickness values at 750nm (Fig. 5.6) oscillate between the directly measured thickness of the skin flap and the sum of the latter with the connective tissue layer. On the other hand, the values deduced at 675nm appear to consistently overestimate the observed anatomical values.

The deduced two-layer optical properties as a function of pre- and post-injection

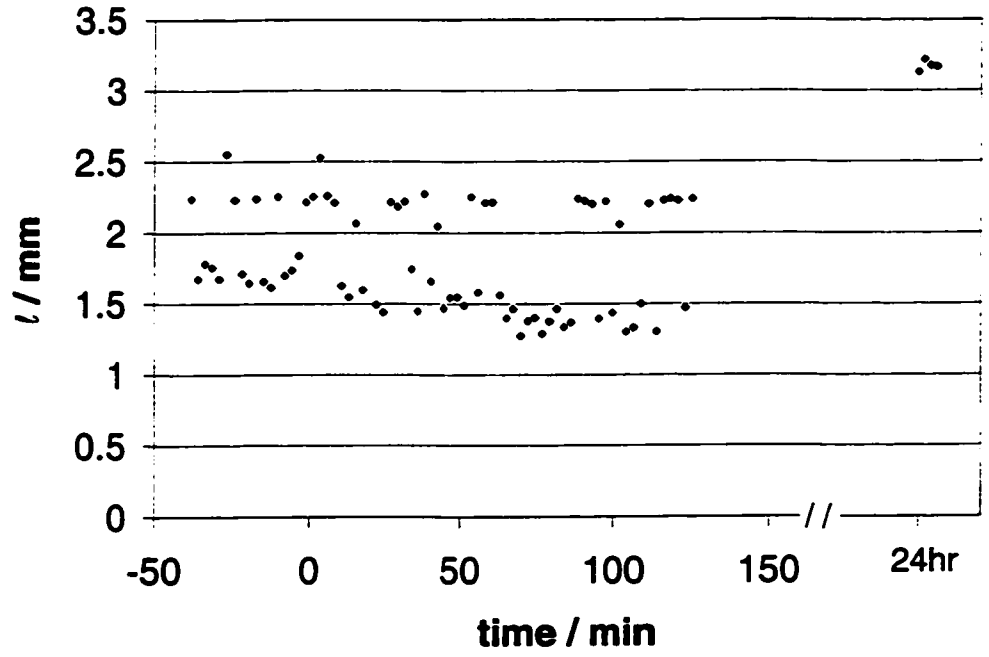

Figure 5.6: The fitted top layer thickness (ℓ, filled diamonds) obtained at 750nm seems to offer two possible solutions at ~1.5mm and ~2.2mm.

time followed very similar trends for all four of the rabbit experiments performed with one notable exception. For one of the animals, the post-injection variation of μ_{a2} values hinted an initial accumulation followed by rapid clearance of $CuPcS_4$ from the underlying tissue (Fig. 5.7) as opposed to tissue retention (Fig. 5.2).

Another point of interest is that the deduced values for μ_{s2}' in all rabbit experiments was on the high end of the expected physiological values ~0.2mm-0.6mm^{-1}. Part of the reason for the overestimate might have been that the rabbit superficial tissue is not an ideal two-layer medium. It was speculated that the thin layer of connective tissue and fat that exists under the skin may have contributed to some

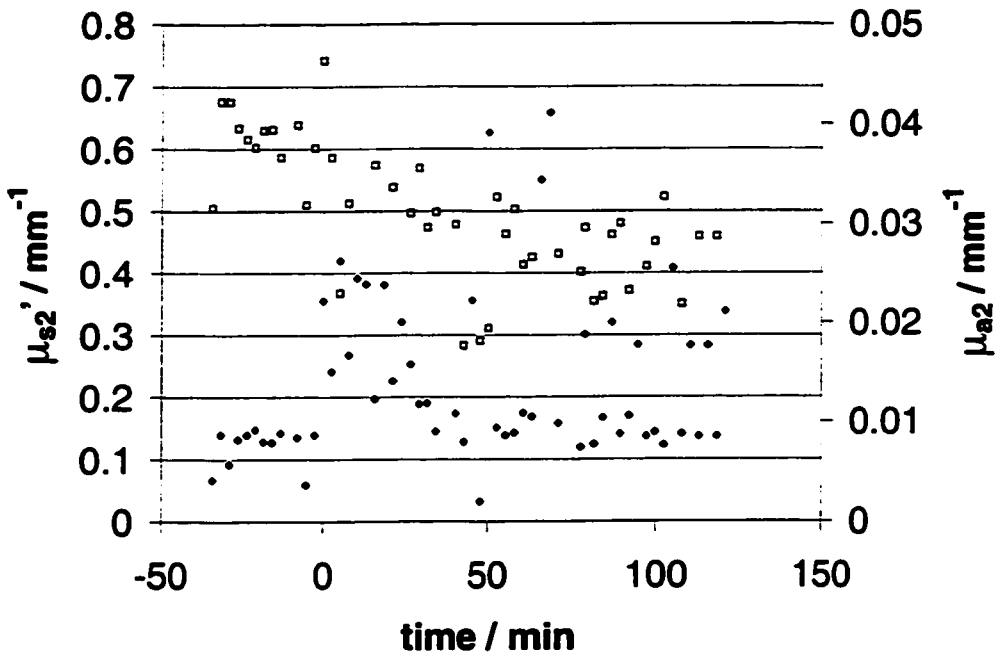

Figure 5.7: The variation of μ_{a2} (filled diamonds) with time implies a rapid clearance of $CuPcS_4$ within an hour post-injection. The deduced $\mu_{s2}{}'$ values (open squares) exhibit some variability but largely remain in the 0.4-0.7mm^{-1} range.

kind of average for a semi-infinite bottom layer that was higher than the pure muscle value. To test this hypothesis, three-layer MC data were generated with skin lying on top of a thin layer of fat followed by a semi-infinite muscle medium, all in the presence of an exogenous chromophore. The values for these optical properties can be found in Chapter 4 (Paper III, Table 1). Two MC simulations were run, with fat layer thicknesses ℓ_f =0.5mm, and 2.5mm that may well be encountered physiologically. The light modulation frequency was $100MHz$. Source detector distances of 1-18mm (1-7mm, increment 1mm; 8-18mm, increment 2mm) were included in the

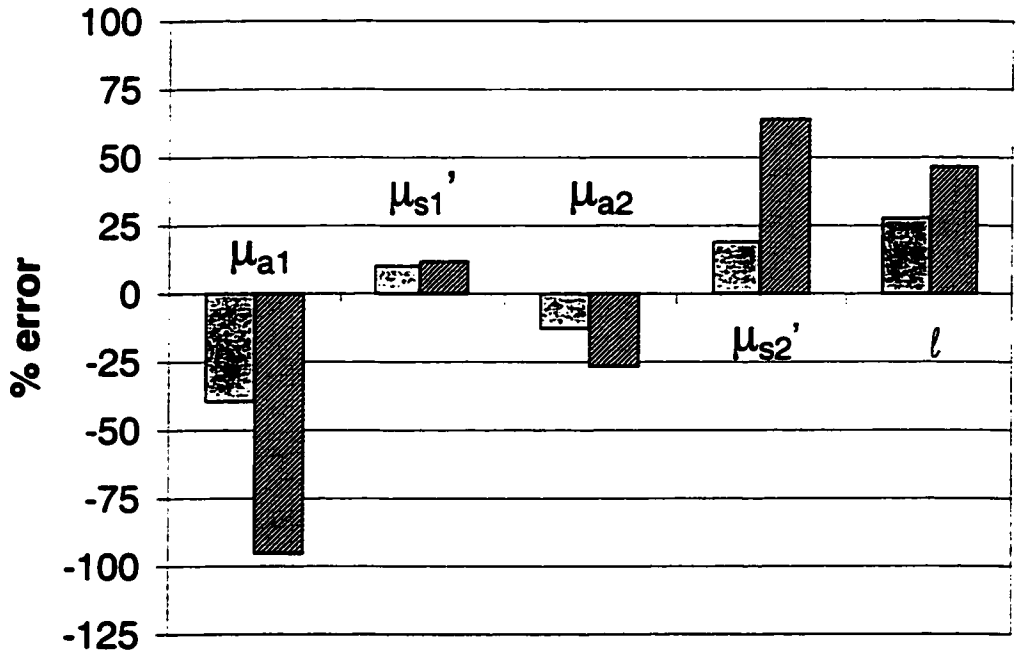

Figure 5.8: Two-layer FD diffusion fits to three-layer MC data corresponding to skin on top of a thin fat layer of thickness ℓ_f, followed by a semi-infinite muscle medium (see Chapter 4, Table 1 for optical property values). The columns indicate the % error of the retrieved two-layer parameters relative to those for skin and muscle with which the MC data were generated (gray columns, ℓ_f = 0.5mm; shaded columns, ℓ_f = 2.5mm).

two-layer diffusion fit. The MC data were fitted as relative FD measurements. Figure 5.8 shows the percentage errors of the deduced two-layer optical properties relative to the true values for skin and muscle. One can see that the errors in $\mu_{s2}{}'$ are always overestimates of the true value for muscle, being higher by ~20% even for a thin fat

layer thickness ℓ_f =0.5mm, and reaching ~75% for ℓ_f =2.5mm. Errors in the bottom layer parameters were not improved substantially even when the small source-detector distances were excluded from the fits. More generally, the results in Fig. 5.8 imply that for improved quantitative optical property estimates it may be necessary to develop a photon migration model that takes into account tissue inhomogeneity more accurately than the two-layer model can.

Tissue inhomogeneity is not the only difficulty with *in vivo* measurements. The quality of the skin-probe contact may well affect measurements also. This was evidenced by outlier points in the reflectance measurements when the skin-probe contact was poor. Also, the animal's physiological condition may alter during an experiment which in turn may change the baseline optical properties. Perspiration of the skin may also alter the skin-probe contact conditions. Potential long-term drifts of the HRCC FD system electronics did not appear to be a major contributor to systematic measurement errors, as was checked from continual reflectance measurements on solid tissue-simulating phantoms over a period of several hours.

A few selected data sets were also fitted with the hybrid model. In Chapter 4 it was shown that the hybrid model primarily improves the top layer optical property estimates relative to pure diffusion. The fact that we could not quantify the top layer optical properties of liquid two-layer phantoms using the SRI FD system, which had superior signal-to-noise characteristics relative to the HRCC one, together with the additional complication of *in vivo* measurements discussed above rendered the

hybrid model's utility for the rabbit measurements questionable. Indeed, for the few fits attempted no significant improvement relative to the pure diffusion results was observed (results not shown).

5.2.2 Future directions

5.2.2.1 Improved experimental methods

In this thesis work it was shown that one can in principle determine all of the optical properties of a two-layer turbid medium from FD spatially resolved reflectance measurements. In practice, the top layer optical properties were not well determined due to additional experimental biases discussed in Chapter 4. In particular, there was evidence for the existence of experimental biases at small source-detector separations even for CW reflectance measurements. It was speculated that the bias was related to the large reflectance gradient which affected the PMT response, and the details of light delivery and collection geometries that become important at these distances. Clearly, this is an issue that needs to be resolved if one is to perform accurate FD spatially resolved reflectance measurements at small source-detector distances.

An alternative method would be to perform absolute CW reflectance measurements that were shown in Chapter 4 to be able, in principle, to determine accurately the two-layer medium optical properties. It would be reasonable to explore that possibility experimentally as it is easier to make CW measurements relative to FD ones. An absolute reflectance measurement can be performed by calibrating the measuring

system with a homogeneous phantom of known optical properties e.g. a polystyrene sphere suspension[37]. An accurate calibration measurement would require a reproducible and stable coupling between the probe surface and the calibration phantom. It is also likely that CW reflectance measurements will suffer from a light intensity dependent PMT response at small source-detector distances, as was described above for the FD measurements. Such a dependence would clearly perturb calibration measurements and thus optical property estimates.

A CW reflectance measurement system has been previously used to to perform *in vivo* measurements in our lab[4]. The basic probe design for the system is shown in Fig. 5.9. Several different light collection fibers are arranged on the circumference of a circle and another fiber is located at the center. The latter is called the calibration fiber because if the probe is placed on a homogeneous phantom, the central fiber should deliver the same amount of light to all fibers on the circle's circumference and hence allow correction for their individual transmission. A source fiber is also found on the circumference of the circle and thus the different source-detector distances can be sampled. In-line attenuators are placed for the small source-detector distance fibers. The effect of the attenuators on the measured signal is accounted for by the calibration measurement. Their purpose is to increase the dynamic range of the instrument by avoiding CCD saturation and maintaining its linear response. To check for an intensity dependent CCD response, the attenuation for individual source-detector distances could be varied to study the effect of the collected light intensity

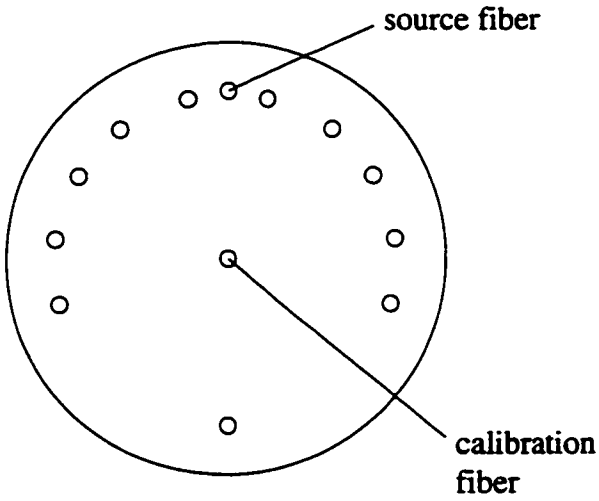

Figure 5.9: The CW reflectance measurement probe design.

on the deduced reflectance signal. The FD probe of the HRCC system described in Appendix A was used for the *in vivo* measurements but it is not self-calibrating. Therefore a new probe for that system with the design of the CW probe described above would be advantageous.

5.2.2.2 New photon migration models

In Section 5.2.1 of this chapter it was shown that even when ignoring other inhomogeneities rabbit superficial tissue is at least a three-layer medium with a layer of fat and connective tissue lying between skin and muscle. Fitting the two-layer model to three-layer MC-simulated FD data could result in substantial errors in optical property estimates (Fig. 5.8). It would thus be of interest to develop a three-layer model for photon migration, or a more general one allowing for the variation of opti-

cal properties as continuous functions of depth. The number of unknown parameters that such a model could determine and how that changes when using CW versus FD or TD data, relative or absolute, would be of great interest to explore.

5.2.2.3 Combining fluorescence with reflectance measurements

The top layer absorption coefficient of a two-layer medium is difficult to determine. This is because the few-scatter photons that carry most of the information about the top layer do not have long pathlengths and thus a correspondingly low probability of being absorbed. The bottom layer absorption coefficient may also be ill-determined if its value is very small ($\lesssim 0.001\text{mm}^{-1}$) as it can be swamped by experimental noise. A fluorescent absorber will have higher specificity of detection and may provide a solution to the absorption coefficient quantification problems. Pogue and Burke[38] designed a fiber optic bundle that can collect mostly unscattered fluorescence photons from a small volume close to the light collection aperture and thus obtained quantitative estimates of fluorophore concentration in tissue-simulating phantoms. Modeling the spatially resolved reflectance and fluorescence resulting from depth dependent fluorophore concentrations is the object of recent work in our lab[39]. Spatially resolved fluorescence measurements do not have good temporal resolution because of the lifetime of the excited state which adds a time delay, typically in the subnanosecond range, to the multiply scattered light[40]. Thus, combining the higher temporal resolution of FD reflectance, to resolve tissue inhomogeneities, with the increased

sensitivity of fluorescence could be advantageous. Most PDT photosensitizers used clinically to date are fluorescent[40] and perhaps amenable to this approach.

However, the long lifetime of the fluorescent state poses another problem. Even if we ignore the phase information from the fluorescence FD signal, a tail of the fluorescence peak may overlap with the wavelength range of its excitation peak that is measured as the reflectance signal[4]. Unless the fluorescence contribution is removed, e.g. by a cut-off filter, even a small contamination from the former peak will disturb the reflectance phase signal. The CW reflectance is susceptible to the same contamination problem but is less sensitive to it because it depends only on the time-independent intensity overlap, which is a small percentage of the measured signal. Hence for a combined reflectance-fluorescence FD measurement to be viable, the fluorophore's Stoke shift should be large enough that the contaminating fluorescence signal can be isolated. Another issue is that fluorescence introduces more unknown parameters into the inverse problem as the optical properties of tissue will be different at the excitation and emission wavelengths.

5.2.2.4 Spectral measurements

It is possible that the dependence of tissue optical properties on light wavelength can be used to advantage. Fitting for the concentrations of chromophores with known absorption spectra, rather than fitting independently at each wavelength makes the determination of *in vivo* optical properties, when assuming a homogeneous tissue ge-

ometry, more robust[41]. At the same time, the variation of the scattering coefficient can be assumed to be a slowly varying function of wavelength. Also, measurements can be made at a few specific wavelengths. For example one can measure at a wavelength where fat absorption is high and at others near the absorption peaks for oxy- and deoxy-hemoglobin found in the blood perfusing primarily skin and muscle tissue. Combining the information from these wavelengths may make the determination of the optical properties of layered superficial tissue a more well-posed problem[42].

The CW reflectance measurement system available at the HRCC is ideal for spectral measurements. It utilizes a broad-band source and the collected light from each source-detector distance is dispersed at a grating and imaged onto a CCD camera. Thus the reflectance as a function of distance and wavelength is simultaneously detected[4]. A corresponding FD system would be costly and harder to construct because of the technological challenges involved with a broad-band light source[45] and CCD camera[46] that can have their response modulated at high frequencies.

5.2.2.5 *In vivo* measurements on humans

The ultimate purpose of the two-layer model, as in fact of any biomedical photon migration model, is to prove its utility *in vivo*. To that end it would be interesting to perform some *in vivo* measurements on human volunteers, perhaps with the aid of ultrasound. The latter will provide information about tissue layer thicknesses and other underlying tissue inhomogeneities. Kienle and Glanzmann[43] have attempted

just that with TD reflectance data, but with limited success. They attributed the discrepancies found to the non-ideal, multilayered structure of superficial tissue. It is the aspiration of the current thesis work that it has identified some of the critical barriers to be overcome, and has inspired further thought, towards a successful *in vivo* implementation of the method.

Appendix A

The HRCC FD system

The apparatus (a schematic is shown in Fig. A1) includes a surface probe and software that have recently been developed in our lab[44]. A 750nm diode laser (Oriel) and a tunable diode laser (New Focus Inc., 662.8-667.7nm) had their outputs modulated by a frequency generator at $100MHz$. Light from these lasers was focused into separate optical fibers and directed into a 5×10 fiber optic switcher (Dicon GP700). The output from the tunable laser was set at 675nm because that wavelength was in the vicinity of $CuPcS_4$ absorption maximum. Also, at that wavelength the tunable laser could provide the maximum possible rf modulation depth and hence the best signal-to-noise ratio. The surface probe contains 17 possible source fibers (200μm core diameter) and a 2mm collection bundle.Ten of the probe's source fibers are connected to the output of the fiber switcher. At the probe face, the 17 source fibers are located at distances ranging from 2 to 30mm from the center of the collection bundle.

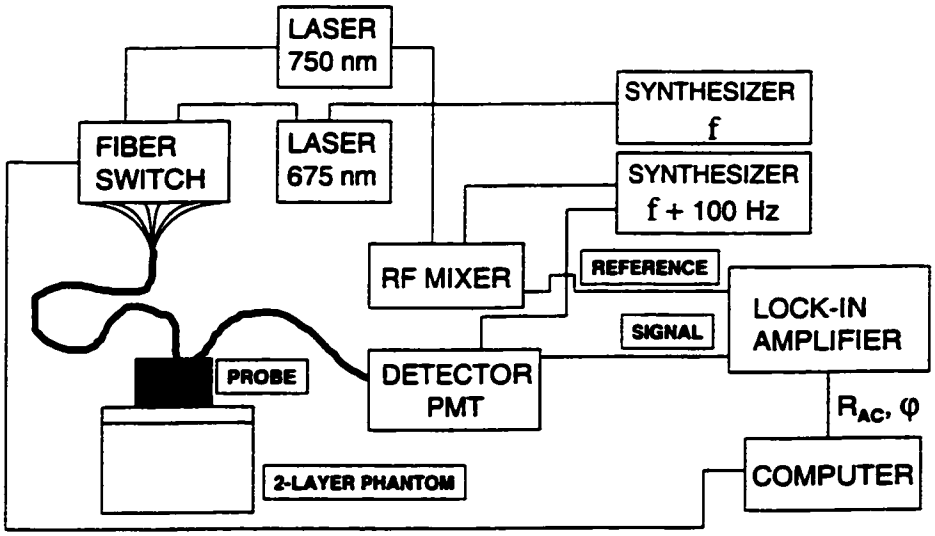

Figure A.1: Schematic diagram of the HRCC spatially resolved frequency-domain system.

Fibers are spaced 1mm apart close to the collection bundle and 2mm apart at further distances. For these measurements, reflectance was measured with source-detector separations of 3 to 18mm.

Source light is directed down one of the probe's source fibers, selected by the switcher. The reflected light is collected by the bundle, which is coupled to the photomultiplier tube (PMT; Model R928 Hamamatsu). The gain of the PMT is modulated by a second frequency generator at $100.0001MHz$. The heterodyne PMT signal at $100Hz$ is fed into a lock-in amplifier. A $100Hz$ reference signal for the

lock-in is the output of an RF mixer with inputs from both frequency generators. The lock-in detection provides the rf amplitude and phase delay of the detected light relative to the reference signal. Attenuators are placed along the paths of source fibers closest to the collection bundle. This ensures a linear PMT response over the light intensities sampled and increases the dynamic range of the instrument. Both the fiber optic switcher and the lock-in amplifier are controlled by a PC running Visual Basic software that has been developed in our lab.

Rf intensity calibration of the system was performed by inserting the probe into the port of an integrating sphere (10 in. diameter) and measuring the detector signal as each source fiber was used to sequentially illuminate the sphere. Phase calibration was performed by measuring the phase on the surface of a polystyrene sphere suspension of known optical properties. The measured phases were corrected to correspond with the calculated values based on Mie theory. Alternatively, the differences in the measured phase using a single optical fiber for all source-detector distances of interest, and the ones measured with the probe gave a quantitatively similar phase calibration. For the latter calibration method the phantom optical properties do not have to be known.

A single set of measurements including all ten source fiber - collection bundle separations lasted approximately one minute. The PC data acquisition software was designed such that alternate measurements were made at 675nm and 750nm. Thus there was a two minute interval between successive measurements at a given wavelength. From repeated measurements on homogeneous phantoms of different optical

properties the measurement uncertainties are estimated to be ~2% for the rf amplitude and ~0.5° for the phase.

Appendix B

Animal experiment protocol

Four New Zealand White rabbits were purchased from the McMaster University animal quarters and used when 3-6 months of age. At the time of the experiments the rabbits' weights were in the 2.7-3.9kg range. Copper phtalocyanine-tetrasulfonate ($CuPcS_4$; Porphyrin Products Inc., Logan, Utah) was diluted in phosphate buffer saline (PBS, 0.9% $NaCl$ to make a 4mg/ml stock solution. The extinction coefficient of the stock solution at 675nm, as determined from spectrophotometer measurements on diluted stock solution aliquots, was $0.0257 mm^{-1} \mu g^{-1} g$. The rabbit ear was chosen as the location of drug injection and blood sampling due to the easy access to its vasculature at that location. $CuPcS_4$ was injected intravenously at 2.5mg/kg. Blood was sampled one time before drug injection, every 15 minutes for the first hour post-injection, and every half hour for a further one and a half hours at which point the experiment ended. Prior to each experiment the animals had their dorsal area

shaved so that the FD probe could be placed directly onto the skin. The animals were then anesthetized with an intramuscular injection of lidocaine hydrochloride (xylazine, 5mg/kg) and 10 minutes later with a mixture of ketamine hydrochloride (50mg/kg) and acepromazine maleate (Apravet, 0.75mg/kg). During the course of the FD reflectance measurements the animals were kept under general anesthetic by injection of ketamine (25mg/kg) and xylazine (0.8mg/ml) mixture via an ear vain at a rate of 1.3mg/kg/hr. To avoid dehydration 0.6ml/kg of glycopyrolate was injected and maintenance fluids were provided at a rate of 3.5ml/kg/hr for the duration of the experiments. For two of the animals 24hr time-point measurements were performed. For those animals a mark was drawn onto the rabbit dorsal skin indicating the probe's position and orientation. Clearly, this was required for the accurate repositioning of the probe on the animal the next day. The animal's body temperature was kept constant by placing it on a heating pad. The cardiac rhythm was monitored with electrodes and blood oxygenation with an oxymeter that was fastened onto one of the rabbit's paws. To maintain good skin-probe contact the skin was held taught while the probe was placed on it and was taped down so that it wouldn't move during the course of the experiment. The blood samples (2ml each) obtained during the course of the experiments were spun at 2000rpm and the extinction coefficient of the recovered plasma fluid at 675nm was measured with a spectrophotometer. One of the animals was sacrificed with intravenous injection of Euthanol (sodium pentobarbital, 2ml). A section in the animal's dorsal tissue was made and the thickness of the skin flap

and other underlying anatomical layers discernible by the eye were measured with calipers.

Bibliography

[1] J. T. Bruulsema, J. E. Hayward, T. J. Farrell, M. S. Patterson, M. Essenpreis, G. Schmelzeiser-Redeker, D. Bocker, L. Heinemann, M. Berger, T. Koschinsky, J. Sandahl-Christiansen, and H. Orskov, 1997,"Correlation between blood glucose concentration in diabetics and non-invasively measured tissue optical scattering coefficient," Opt. Lett. **22**, 190-192.

[2] J. R. Mourant., T. M. Johnson, G. Los, and I. Bigio, 1999,"Non-invasive measurements of chemotherapy drug concentrations in tissue: Preliminary demonstrations of *in vivo* measurements," Phys. Med. Biol. **44**, 1397-1417.

[3] M. S. Patterson, B. C. Wilson, J. W. Feather, D. M. Burns, and W. Pushka, 1987,"The measurement of dihematoporphyrin ether concentration in tissue by reflectance spectrophotometry," Photochem. Photobiol. **46**, 337-343.

[4] R. A. Weersink, J. E. Hayward, K. R. Diamond, and M. S. Patterson, 1997,"Accuracy of non-invasive *in vivo* measurements of photosensitizer uptake based on a diffusion model of reflectance spectroscopy," Photochem. Photobiol. **66**, 326-335.

[5] R. A. De Blasi, N. Almenräder, P. Aurisicchio, and M. Ferrari, 1997"Comparison of two methods of measuring forearm oxygen consumption ($\dot{V}O_2$) by near infrared spectroscopy," J. Biomed. Opt. **2**, 171-175.

[6] M. Nitzav, A. Babchencko, B. Khanokh, and H. Taitelbaum, 2000,"Measurement of oxygen saturation in venous blood by dynamic near infrared spectroscopy," J. Biomed. Opt. **5**, 155-162.

[7] P. L. Williams and R. Warwick, "The integument," in *Gray's Anatomy*, 36th edition (Churchill Livingstone, Edinburgh, UK, 1986, 1216-1222.

[8] A. Ishimaru, *Wave Propagation in Scattering and Random Media* (Academic, New York, 1978), Chaps. 7 and 9.

[9] B. C. Wilson and G. Adam, 1983,"A Monte Carlo model for the absorption and flux distribution of light in tissue," Med. Phys. 10, 824-830.

[10] M. S. Patterson, B. Chance, and B. C. Wilson, 1989, "Time resolved reflectance and transmission for the non-invasive measurement of tissue optical properties," Appl. Opt. 28, 2331-2336.

[11] H. C. van de Hulst and R. Graff, 1996,"Aspects of similarity in tissue optics with strong forward scattering," Phys. Med. Biol. 41, 2519-2531.

[12] R. C. Haskell, L. O. Svaasand, T. T. Tsay, T. C. Feng, M. S. McAdams, and B. J. Tromberg, 1994,"Boundary conditions for the diffusion equation in radiative transfer," J. Opt. Soc. Am. A 11, 2727-2741.

[13] S. R. Arridge and J. C. Hebden, 1997,"Optical imaging in medicine: II. Modelling and reconstruction," Phys. Med. Biol. 42, 841-853.

[14] S. R. Arridge, "Why optical tomography is hard," in *Biomedical Optics: New Concepts in Therapeutic Laser Applications, Novel Biomedical Optical Spectroscopy, Imaging, and Diagnostics, Advances in Optical Imaging, Photon Migration, and Tissue Optics, OSA Technical Digest Series* (Optical Society of America, Washington, D.C., 1999), paper AMB1-1.

[15] W. H. Press, S. A. Teukolsky, W. T. Vetterling, and B. P. Flannery, Numerical Recipes—The Art of Scientific Computing, 2nd edition, (Cambridge U. Press, NY, 1996).

[16] R. F. Bonner, R. Nossal, S. Havlin, and G. S. Weiss, "Model for photon migration in turbid biological media, 1987," J. Opt. Soc. Am. A 4, 423-432.

[17] R. Nossal, J. Kiefer, G. H. Weiss, R. Bonner, H. Taitelbaum, and H. Havlin, 1988,"Photon migration in layered media," Appl. Opt. **27**, 3382-3391.

[18] A. F. Grünbaum, 1992,"Diffuse tomography: the isotropic case," Inv. Prob. **8**, 409-419.

[19] T. Durduran, A. G. Yodh, B. Chance, and D. A. Boas, 1997,"Does the photon-diffusion coefficient depend on absorption?," J. Opt. Soc. Am. A **14**, 3358-3365.

[20] D. J. Durian, 1998,"The diffusion coefficient depends on absorption," Opt. Lett. **23**, 1502-1504.

[21] R. Aronson, and N. Corngold, 1999,"Photon diffusion coefficient in an absorbing medium," J. Opt. Soc. Am. A **16**, 1066-1071.

[22] M. S. Patterson, B. C. Wilson, and D. R. Wyman, 1991,"The propagation of optical radiation in tissue I. Models of radiation transport and their application," Las. Med. Sci. **6**, 155-169.

[23] S. L. Jacques, 1997,"Path integral description of light transport in tissue," in *Proceedings of the Society for Photo – Optical Instumentation Engineers*, **2979**, San Jose, CA.

[24] L. T. Perelman, T. J. Wu, I. Itzkan and M. S. Feld, 1994,"Photon migration in turbid media using Feynman path integrals," Phys. Rev. Lett. **72**, 1341-1344.

[25] M. C. Case and P. F. Zweifel, *Linear Transport Theory*, (New York, Addison-Wesley, 1967).

[26] A. H. Hielscher, R. E. Alcouffe, and R. L. Barbour, 1998,"Comparisons of finite-difference transport and diffusion calculations for photon migration in homogeneous and heterogeneous tissues," Phys. Med, Biol. **43**, 1285-1302.

[27] S. T. Flock, B. C. Wilson, and M. S. Patterson, 1988,"Hybrid Monte Carlo-diffusion theory modelling of light distributions in tissue," in *Laser Interaction with Tissue,* Proc. SPIE **908**, 20-28.

[28] L. Wang, and S. L. Jacques, 1993,"Hybrid model of Monte Carlo simulation and diffusion theory for light reflectance by turbid media," J. Opt. Soc. Am. A **10**, 1746-1752.

[29] L. Wang, 1998,"Rapid modeling of diffuse reflectance of light in turbid slabs," J. Opt. Soc. Am. A **15**, 936-944.

[30] G. Alexandrakis, T. J. Farrell, M. S. Patterson, 2000,"Monte Carlo diffusion hybrid model for photon migration in a two-layer turbid medium in the frequency domain," Appl. Opt. **39**, 2235-2244.

[31] W. C. Goffe, G. D. Ferrier, and J. Rodgers, 1994,"Global optimization with statistical functions using simulated annealing," J. Economet. **60**, 65-100.

[32] J. C. Hebden, S. A. Arridge, and D. T. Delpy, 1997,"Optical imaging in medicine: I. Experimental techniques," Phys. Med. Biol. **42**, 825-840.

[33] M. S. Patterson, J. D. Moulton, B. C. Wilson, K. W. Berndt, and J. R. Lakowicz, 1991,"Frequency-domain reflectance for the determination of the scattering and absorption properties of tissue," Appl. Opt. **30**, 4474-4476.

[34] T. J. Farrell and M. S. Patterson, 1992,"A diffusion theory model of spatially resolved, steady state diffuse reflectance for the non-invasive determination of tissue optical properties *in vivo*," Med. Phys. **19**, 879-888.

[35] A. Kienle and M. S. Patterson, 1997,"Improved solutions of the steady-state and time-resolved diffusion equations for reflectance from a semi-infinite turbid medium," J. Opt. Soc. Am. A **14**, 246-254.

[36] A. Kienle, M. S. Patterson, N. Utke, R. Bays, G. Wagnières, and H. van den Bergh, 1998,"Determination of the optical properties of two-layer turbid media," Appl. Opt. **37**, 779-791.

[37] F. Bevilacqua, D. Piguet, P. Marquet, J. D. Gross, B. J. Tromberg, and C. Depeursinge, 1999,"*In vivo* local determination of tissue optical properties: applications to human brain," Appl. Opt. **38**, 4939-4950.

[38] B. W. Pogue and G. Burke, 1998,"Fiber-optic bundle design for quantitative fluorescence measurement from tissue," Appl. Opt. **37**, 7429-7436.

[39] D. E. Hyde, T. J. Farrell, and M. S. Patterson,"A diffusion theory model of spatially resolved fluorescence from depth dependent fluorophore concentrations," Accepted for publication, Phys. Med. Biol. (submitted August 2000).

[40] G. A. Wagnières, W. M. Star, and B. C. Wilson,1998,"*In vivo* fluorescence spectroscopy and imaging for oncological applications," Photochem. Photobiol. **68**, 603-632. Lilge,1997,"Implicit

[41] R. M. P. Doornbos, R. Lang, M. C. Aalders, F. W. Cross, and H. J. C. M. Sterenborg, 1999,"The determination of *in vivo* human tissue optical properties and absolute chromophore concentrations using spatially resolved steady-state diffuse reflectance spectroscopy," Phys. Med. Biol. **44**, 967-981.

[42] G. W. Faris, personal communication, June 2000.

[43] A. Kienle and T. Glanzmann, 1999,"*In vivo* determination of the optical properties of muscle with time-resolved reflectance using a layered model,"Phys. Med. Biol. **44**, 2689-2702.

[44] R. A. Weersink, and M. S. Patterson, 1998,"Spatially resolved diffuse reflectance measurements of two-layered samples in the frequancy-domain," in *Biomedical Optical Spectroscopy and Diagnostics*, OSA TOPS, **22**, 15-19.

[45] B. W. Pogue, and M. S. Patterson, "Error assessment of a wavelength tunable frequency domain system for noninvasive tissue spectroscopy," J. Biomed. Opt. **1**, 311-323 (1996).

[46] J. R. Lakowicz, H. Szmacinski, K. Nowaczyk, and M. L. Johnson, "Fluorescence lifetime imaging of free and protein-bound NADH," Proc. Nat. Acad. Sci. U.S.A. **89**, 1271-1275 (1992).